DOCTORAL DISSERTATION

Antimicrobial effect - decomposition of biological phenomena into physical approach - a theoretical model

Mateusz Rzycki

Supervisors:

Marta Gładysiewicz-Kudrawiec

Sebastian Kraszewski

Department of Experimental Physics

The important thing in science is not so much to obtain new facts as to discover new ways of thinking about them.

William Lawrence Bragg

European Funds
Knowledge Education Development

Wrocław University
of Science and Technology

European Union
European Social Fund

Acknowledgments

At the very beginning, I would like to acknowledge the immense amount of gratitude to my supervisors prof. Marta Gładysiewicz-Kudrawiec and prof. Sebastian Kraszewski for their intense and helpful discussions, sharing great knowledge from multiple disciplines, and any advice concerning private and scientific life. It was a real pleasure to collaborate with you.

I would like to massively thank my parents and my fiancee for your patience, faith, and support in moments of uncertainty.

Last but not least, I would like to thank my lab colleagues and collaborators, especially Dominik Drabik for the great teamwork and long discussions, especially those after hours.

Financial support

A series of thematically coherent publications constitute this doctoral dissertation. Articles included in the thesis:

- Paper 1 - **Rzycki M.**, Drabik D., Szostak-Paluch K., Hanus-Lorenz B., Kraszewski S., *Unraveling the mechanism of octenidine and chlorhexidine on membranes: does electrostatics matter?*, Biophysical Journal 2021, vol. 120, nr 16, s. 3392-3408.

- Paper 2 - **Rzycki M.**, Kaczorowska A., Kraszewski S., Drabik D., *A Systematic Approach: Molecular Dynamics Study and Parametrisation of Gemini Type Cationic Surfactants*, Int. J. Mol. Sci. 2021, 22, 10939.

- Paper 3 - **Rzycki M.**, Kraszewski S., Drabik D., *Towards Mimetic Membrane Systems in Molecular Dynamics: Characteristics of E. Coli Membrane System*, ICCS 2021, LNCS 12743, pp.551-563, 2021.

- Paper 4 - **Rzycki, M.**, Kraszewski S., Gładysiewicz-Kudrawiec M., *Diptool – a novel numerical tool for membrane interactions analysis, applying to antimicrobial detergents and drug delivery aids*, Materials 2021, 14, 6455.

Contents

Abstract

The widespread problem of antibiotic resistance in bacteria requires the application of many interdisciplinary approaches. An example of that approach is to reduce it to the form of appropriate interactions. The principal aim of this dissertation became to develop physical and numerical models of biological membranes that allow the evaluation of the antimicrobial activity of Gemini-structured molecules. In this thesis, the approaches from physics, as well as chemistry and biology, have been combined in order to create probabilistic and numerical bacterial membrane models that enable the assessment of the surfactants' effects on physicochemical and thermodynamic bilayer properties. One of the proposed concepts assumes the description of the activity of the compound on the cell membrane through dipole-dipole interactions in a non-conservative field due to the viscosity of the medium. An employed strategy that reduces the problem to physical interactions aims toward providing a broader perspective and knowledge in the uneven fight against antibiotic-resistant bacteria.

The widespread antimicrobial resistance in bacteria was identified in 2015 as one of the top 10 global threats to human health by the World Health Organization. Unless new drugs are discovered by 2050, millions of people will become victims to drug-resistant bacteria every year. Especially overwhelming is the constant expansion of so-called superbugs, such as *Klebsiella pneumoniae*, which cause a wide spectrum of infections and exhibit ongoing acquisition of drug resistance even to antibiotics of last resort. There are many factors why microorganisms become resistant, including constant mutations, *i.e.* modification of genetic material, acquisition of resistance genes from other organisms (lateral transfer). The human factor also has a strong influence on bacterial resistance by frequent overuse of antibiotics, insufficient doses, or too short antibiotic therapy duration. Over the years, bacteria are escaping from the lethal activity of antibiotics by developing their own adaptive mechanisms. A promising approach to solve that issue is to focus on antiseptics that do not have a well-defined molecular target in bacterial cells, unlike current antibiotics, but target bacteria structures, in general. It has been reported that some of these agents selectively attack cell membranes inducing their destruction by emulsification. Several commonly used antimicrobial agents from the cationic surfactants (Gemini surfactants) family are commercially available. The most well-known are octenidine (OCT) and chlorhexidine (CHX), which are effective against both Gram-positive and Gram-negative bacteria. In addition, new compounds within the Gemini structures are synthesized each year and present potential antimicrobial activity. The comparison of the antibacterial efficacy of given compounds becomes problematic due to various protocols used by research groups. Therefore the selection of potential precursors that can substitute currently used antibiotics becomes challenging.

The first work in the thesis (Paper 1 - Section 6) was focused on delivering insights into the molecular interactions of OCT and CHX on negatively charged (*i.e* bacterial) and zwitterionic (*i.e.* eukaryotes) membranes. The use of numerical and experimental methods allowed to determine the preferential location of these compounds, their formation of aggregates, their destructive effect on membranes, and to describe the changes in membrane mechanical parameters under the analyzed molecules' activity. The in-depth analysis allowed to propose a novel mechanism of the selective antibacterial compounds' action, especially for OCT - based on differences between emerging mechanical properties of bacterial and eukaryotic membranes, respectively.

In the further research stage (Paper 2 - Section 7), other Gemini-structured compounds with strong antibacterial activity were investigated. Since different protocols and bacterial strains are used in experimental studies, comparison of the antimicrobial efficiency remained unfeasible. Therefore we decided to provide a systematic theoretical approach, hence we collected a database of over 250 Gemini molecules

with potential antibacterial activity. The performed quantum calculations allowed to optimize the force fields of all the collected molecules. Employing a standardized protocol based on molecular dynamics simulations, 25 molecules with estimated potential antibacterial activity were tested on three-component model of bacterial membrane. The analysis of membrane parameters allowed to define a pre-emulgation stage, and to select the 8 most promising precursors with possible strongest antimicrobial activity.

Computational studies often address questions regarding the accuracy and reliability of presented models to real biological structures. The models may differ significantly from real or experimental analogs, thus resulting in inaccurate conclusions. Therefore, in the following research (Paper 3 - Section 8), a comprehensive numerical model, reflecting the detailed (multicomponent) lipid structure of *Escherichia coli* bacteria was proposed. It was also determined whether the complexity may significantly affect the conclusions drawn from numerical analyses of simplified models. An in-depth analysis of structural, dynamic, and mechanical properties revealed that the complexity and composition of the bacterial membrane model are crucial. The potential lack of complexity in current numerical bacterial membrane models undoubtedly affects the fundamental origins of interactions, so that some biological phenomena may remain elusive or suppressed.

The awareness of the limitations in experimental and well-established numerical methods has inspired me to the development of a dedicated methodology and original simulation software for the rapid evaluation of antibacterial potential in Gemini surfactants (Paper 4 - Section 9). Molecular dynamics simulations allow to assess the compound behavior on membranes with the potential structure interactions. The free energy calculation methods enable to precisely determine the behavior of antibacterial molecules in contact with the membrane, indicating the location of energy barriers or preferential agent location. Construction of an accurate energy profile for Gemini-type molecule acting on the membrane is computationally demanding and time-consuming process. Simplification of the interaction scheme and limitation of redundant parameters allowed to develop a unique software called *Diptool*, a tool for rapid screening the membrane-agent interactions and for potential antimicrobial candidate selection. *Diptool* is primarily based on the dipole interactions of lipids and antimicrobial compounds, whereas a modified Verlet algorithm is responsible for the integrating equations of motion. Using an experimental set of Gemini surfactants we provided quantitative structure-activity relationship (QSAR) studies, which in the end allowed to select the most significant parameters that influence the agent antimicrobial activity. Implementation of those identified parameters within the *Diptool* allowed to assess whether the molecule penetrates the membrane and what the free energy distribution looks like. This, in the end, allows for a direct estimation of the agent's antibacterial potential. The tool was validated with the Adaptive Biasing Force approach, well-known from molecular dynamics. The greatest advantage of the *Diptool* software is its speed, since can provide results comparable to full-atom MD simulations but in a matter of minutes.

To summarize, in this dissertation a selective activity molecular mechanism of widely used antibacterial compounds OCT and CHX was proposed. Subsequently, a Gemini molecule database was developed and a unified numerical protocol to study antimicrobial compounds was proposed. Further, an improved and comprehensive numerical model of *E. coli* bacteria was delivered. Finally, an original methodology and software for the analysis of the antibacterial potential of Gemini-structured molecules were developed. The core of the dissertation consists of four scientific publications (Paper 1-4), in which the above achievements were described, covering methodology, implementation stage, and verification of assumptions.

List of Abbreviations

Abbreviations	
ABF	Adaptive Biasing Force
BacM	Bacterial membrane
CAMP	Cationic antimicrobial peptides
CHX	Chlorhexidine
CXF	Carboxyfluorescein
DPH	Diphenylhexatriene
FEP	Free energy perturbation
GLASS	Global Antimicrobial Resistance and Use Surveillance System
GS	Gemini surfactant
IM	Inner membrane
logP	Partition coefficient
LPS	Lipopolysaccharide
MD	Molecular dynamics
MDR	Multidrug resistance
MIC	Minimal inhibitory concentration
NegM	Negative lipid membrane
NLM	Neutral lipid membrane
OCT	Octenidine
OM	Outer membrane
OMP	Outer membrane protein
QAS	Quaternary ammonium salts
QM	Quantum mechanics
QSAR	Quantitative structure–activity relationship
TMA-DPH	Trimethylammonium-diphenylhexatriene
US	Umbrella sampling
WHO	World Health Organization

Chapter 1

Introduction and description of dissertation

1.1 Antibiotic resistance – a crucial problem of the mankind

Antibiotics are undoubtedly one of the finest inventions of modern medicine. Their usage resulted in the effective elimination of pathogens and a great reduction in mortality. Previously abundant in everyday life and during most surgeries microbes are currently manageable. Primary insights into the 'antibiotic era' are usually associated with the inhibition of cells proliferation by Paul Ehrlich and penicillin discovery by Alexander Fleming in the 20th century [1–3]. From that time, the mode of action of various antimicrobial compounds has been revealed. There are several mechanisms and targets for antimicrobial agents, each one focuses on various vulnerabilities leading to cell death:

- inhibition of cell wall synthesis - bacteria cell walls are composed of peptidoglycan. Several antibiotics such as penicillins and cephalosporins destroy the cell wall integrity inhibiting the peptidoglycans synthesis. Since human host cells lack cellular walls they remain unaffected [4],

- inhibition of metabolism - reaction rates catalyzed by bacterial enzymes are affected. Drugs may influence the synthesis of metabolic complexes competitively. Thus, structural analogs (medicaments) of enzyme activators substitute the biological ones in metabolic reactions. Sulfonamides are an example of the molecules acting in that manner [5, 6],

- interactions with plasma membranes – cellular membranes are selective barriers that contribute to the transport of micro and macromolecules in and out of the cell. Some of the antimicrobial agents are able to damage the selective permeability, leading to the cell death. Cationic peptides like valinomycin, polymyxin B, or gramicidin disrupt the membrane in that manner however, lack of selectivity presents high toxicity toward host cells [7, 8],

- interruption of protein synthesis – protein synthesis employs numerous biological organelles like ribosomes, nucleic acids, and enzymes. The antibacterial agents disturb the ribosomal activity restricting the synthesis process, which at the final stage results in the cell death. Drugs like rifamycin, chloramphenicol or tetracyclines represent that mechanism by inhibiting the transcription or translation process [9–11].

Over time the bacteria mutated forming several mechanisms to avoid the lethal activity of antibiotics. It was possible due to the classical bullet-target concept of antibiotic activity, which appeared not as straightforward as stated [3]. The 'golden era' of delivering antibiotics slowed down since researchers

were incapable of providing a sufficient amount of agents to face novel emerging resistant microbes [12]. The growth in the number of antibiotics was also accompanied by a growth of new immune pathogens. Initially, those antibiotics saved hundreds of thousands lives but taking into account the current bacteria mutation rate a return to the pre-antibiotic age is a real concern [13]. Different organisms developed their own defensive system to escape from fatal antimicrobial action by preventing drug access and distribution, mutations of the target site, or antibiotic degradation by new enzymes. In the literature, intrinsic and acquired resistance are mostly highlighted types of bacterial defense mechanisms [14, 15]. Intrinsic resistance is associated with the presence of antibacterial resistance genes or efflux pump genes. A good example are *Pseudomonas* - Gram-positive bacteria (further explained), which suppressed a susceptible target site, therefore, they become resistant to triclosan activity, which is usually effective against Gram-positives [16]. Acquired resistance is accompanied by horizontal gene transfer or mutations in the chromosomal genes, which results in the development of new resistance genes. Plasmids of *E. coli* bacteria with acquired resistance were discovered in poultry farms, dogs and humans [17, 18].

The World Health Organization recognized multidrug-resistant (MDR) pathogens as a critical problem of the current times [19]. In their reports, it has been classified in the top ten global health threats, which affect millions of people and absorb billions of dollars annually [13, 20]. The worst-case scenario presented by Research and Development Corporation assumes that in the near future the whole of mankind may lack any effective antibacterial compounds. If that horrific forecast makes happen, the worldwide financial burden might reach even 3 trillion dollars annually, which is close to the total health care budget in the USA, and by 2050 almost 440 million people succumb to pathogens [21, 22]. Additionally, the global overuse and misuse of drugs significantly affect the resistance evolution making the treatment much more difficult. According to published reports in the USA, in 30-50% of the cases the antibiotic therapies were inappropriately conducted [23, 24], while in Pakistan or Ghana strike up to 85% of improper usage events [25, 26]. The WHO experts clearly state that unless the way that drugs are used now will not change, every novel antibiotic finally becomes ineffective like many currently used. Insufficient hygienic prophylaxis and lack of clean water combined with human travels and migration additionally boost the distribution of pathogens. In the global priority list of antibiotic-resistant bacteria published by WHO, three importance classes (with critical, high and medium tags) were assigned to several bacteria species, where *Acinetobacter baumannii*, *Pseudomonas aeruginosa*, and *Enterobacteriaceae* (*i.e. Klebsiella pneumoniae*, *Escherichia coli*) were flagged with critical priority [27, 28]. Moreover, listed microbes are resistant to 3rd generation cephalosporins or carbapenems and so-called last-resort antibiotics. *K. pneumoniae* exists globally and may induce lethal bloodstream infections, pneumonia, meningitis, or liver abscess. Similarly, *E. coli* occurs all over the world and may cause respiratory problems or diarrhea. Currently, the only effective antibiotic against *Enterobacteriaceae* is colistin however, recent papers [29, 30] report the presence of colistin-resistant microbes, thus mankind may become vulnerable to diseases related to them.

Worth emphasizing that the clinical pipeline of promising antimicrobials is limited. In 2019 from 32 developed antibiotics addressed to fight against pathogens listed by WHO only 6 were recognized as innovative, but only two showed activity spectrum against MDR pathogens classified with the critical flag [31]. Novel antimicrobial compounds are instantly required to face carbapenem-resistant, vancomycin-resistant, fluoroquinolone-resistant bacteria flagged with critical priority [27, 28, 32].

Since MDR is a multisectoral issue, only complex and well-coordinated activities may limit the distribution of that phenomenon. Hence Global Antimicrobial Resistance and Use Surveillance System (GLASS) was set up by WHO that collect the data from all over the world and deliver a consistent strategy and improve global awareness [33]. As stated, well-performed diagnostics may significantly reduce imprudent antibiotics usage, especially in developing countries, since outdated microbiological

instruments are often used for bacteria identification. Employing novel and adequate molecular diagnosis only the selected patients undergo antibiotic therapy within the personalized medicine approach. GLASS delivers a normalized procedure for data analysis, classification, and distribution by countries and supervises domestic surveillance systems, with special attention to the quality of gathered information [19,33]. Countries that progressively implement national programs with controlled antibiotic prescriptions, developed health care systems, regulated disease control setups succeed in limiting MDR [34]. Those strategies remain consistent with the 'One Health' program concentrating on public health, food production, and agriculture sectors to cooperate during the preparation and realization of policies, procedures and research to achieve the best possible healthcare outcomes. Every known and possible branch should be activated to find a comprehensive solution focused on the MDR problem. Novel and innovative research methods in drug discovery, vaccines, or alternative antimicrobial agents should be launched to fight especially against resistant Gram-negative pathogens. Massive fund injection is provided by various organizations and funds *i.e.* Antimicrobial Resistance Multi Partner Trust Fund or the Global Antibiotic Research & Development Partnership to bridge the financial gap while searching for lasting scenarios in the resistant microbes battle.

1.2   Surfactants as alternative compounds struggling against bacteria

Faced with the emerging need to deliver innovative approaches to the antibiotic resistance problem, researchers from various fields have proposed several means addressed to that issue. Despite the publications that propose and raise the prevention and control strategies, ones are focused on the ways of combining well-known drug therapies to maximize the effort [35] and others are focused on the development of small antimicrobial peptides and amphiphiles [36–38] or novel antibiotics discovering [39, 40]. Regardless which pathway is represented by the authors of the given paper, the further need for knowledge exploration is emphasized to effectively overcome the MDR problem.

One of the most promising activities is presented by compounds with the ability to selectively bind to fundamental bacterial structures. Such agents often exhibit a broad spectrum of activity and are targeted on slowly evolving elements such as cell walls or lipid membranes. That kind of activity exposes nonspecific interactions thus the development of resistance mechanisms is much more complex and difficult. Those properties are frequently observed in novel classes of compounds such as cationic antimicrobial peptides (CAMPs) and cationic Gemini surfactants (GS).

The former are or are based on, naturally existing compounds in various organisms, playing a crucial role in the innate immune system functions [41]. They present a broad spectrum of activity against Gram-positive and negative bacteria, fungi, and viruses. Taking into account CAMPS structure, they may be divided into several groups such as α-helices, β-sheets, cyclics, and with prolonged conformation [42,43]. Despite structural and sequence differences between the groups, CAMPs have an extensive hydrophobic core, the positive charge and pose amphiphilic nature. Additionally, it is supposed that due to positive charge they can anchor to the negatively charged bacterial membranes and expose hydrophobic residues to penetrate the bilayer. Overall, the structure, amino acid arrangement, net charge or oligomerization influence peptides activity. The general model of action remains elusive however, several approaches have been proposed. The most common are barrel stave, toroidal and carpet models and are presented in Figure 1.1. The latter assumes the extensive distribution of CAMPs on bilayer surface increasing the surface tension resulting in membrane disorder. If the critical peptide concentration is exceeded, cell death occurs. The peptide hydrophilic residues disturb the polar lipid headgroup integrity causing the micellization [44–46]. The barrel-stave model assumes interactions of CAMPs hydrophobic region

Barrel-stave model
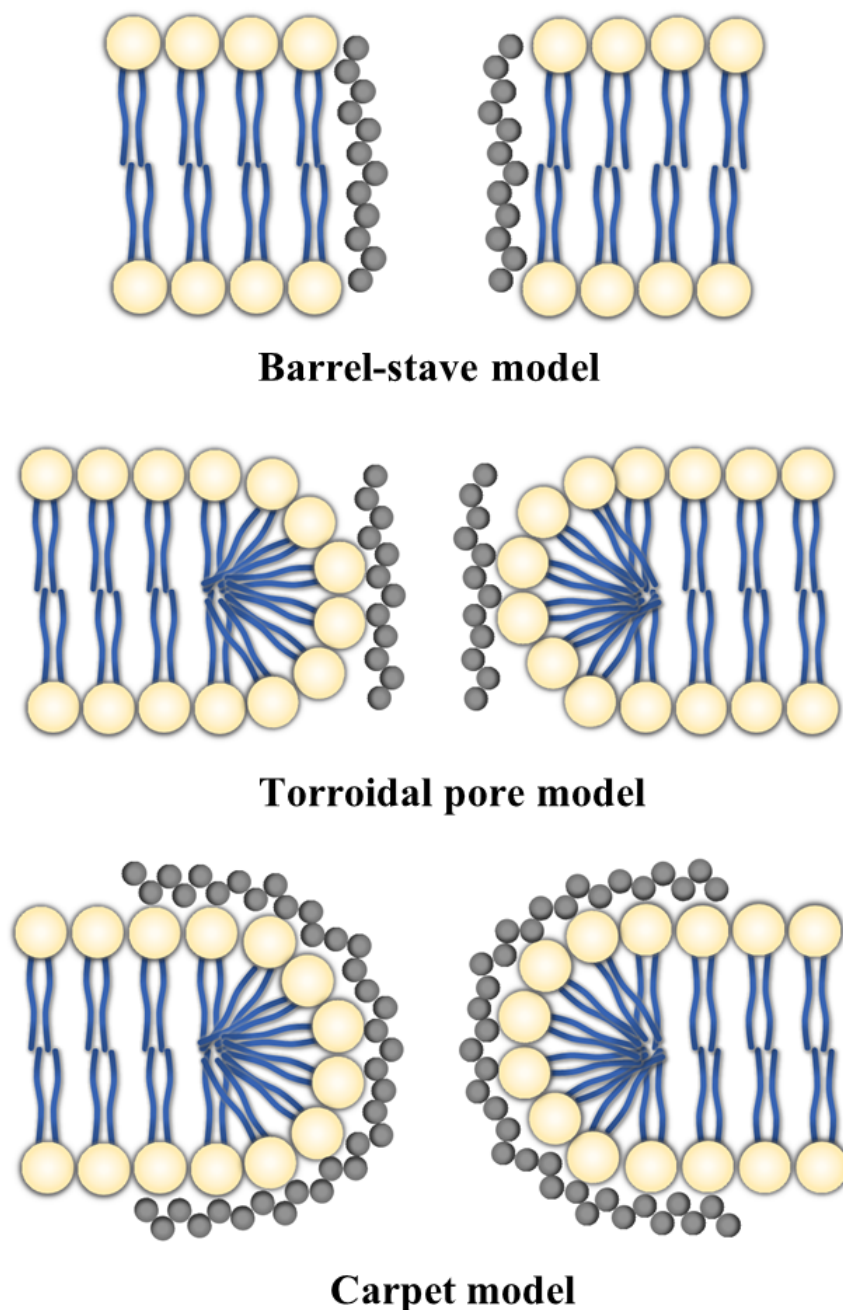
Torroidal pore model

Carpet model

Figure 1.1: Three means of pore-formation by antimicrobial molecules on membranes, inducing leakage of the cell interior.

with cell bilayer leading to conformational changes in membrane composition and transmembrane pore formation. This results in leakage from the cell interior and finally its death [45, 47]. The toroidal model is related to a barrel-stave since the pore formation also occurs. The CAMPs anchored to the membrane intercalate with bilayer lipids creating a torus pore. The bend of the lipid monolayer results in pore formation hence the lipid headgroups and CAMPs face the core of the pore [45, 47].

GS similarly to CAMPs also present strong antimicrobial properties, especially against both Gram-positive and negative bacteria as well as fungi and algae. In the previous three years, GS have been heavily explored, because 921 articles were published whereas 427 discussed antimicrobial properties of agents. Gemini compounds are composed of two monomeric surfactants linked by a spacer in various configurations (see Figure 1.2). The monomers are amphiphiles, thus hydrophobic and hydrophilic

moieties may be noticed [48]. The hydrophilic core is in general a polar or ionic headgroup, while a hydrophobic tail is usually a hydrocarbon chain with 6-18 carbons length [49].
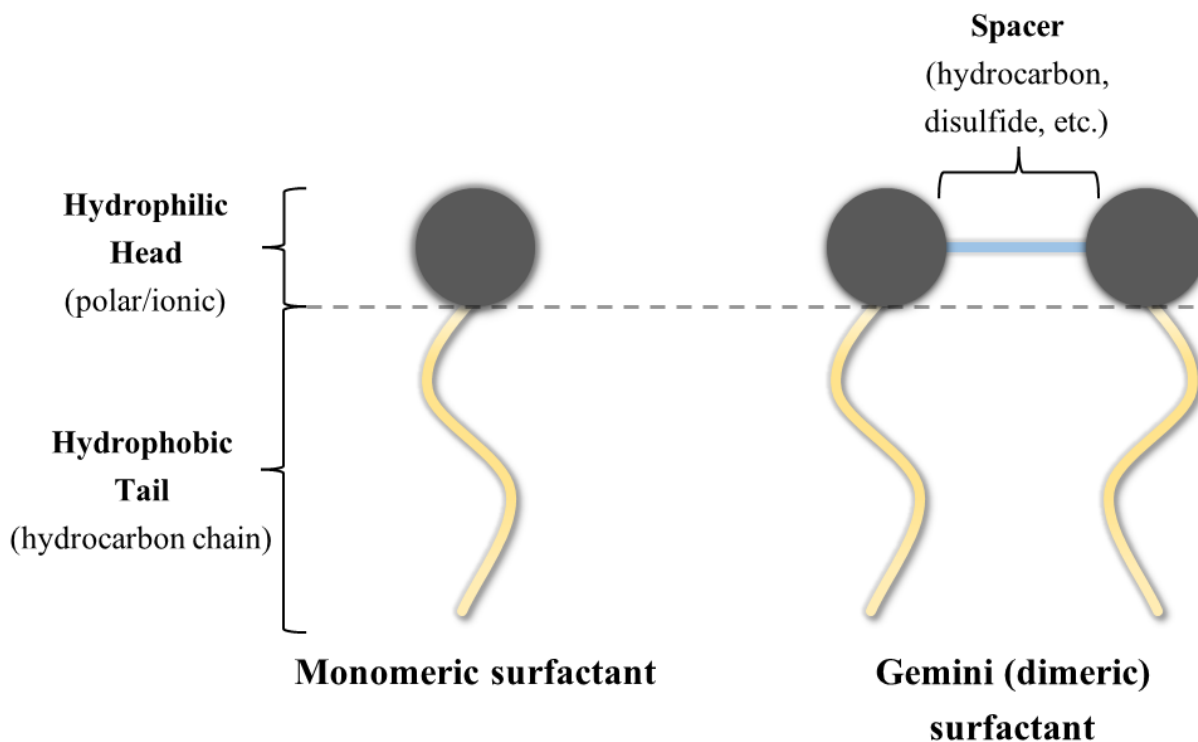

Figure 1.2: The overall structure of mono and dimeric surfactants [48].

GS are also characterized by various types of spacers, more rigid or flexible, longer or shorter, however, usually are represented by several methylene groups, sometimes accompanied by oxygen or nitrogen atoms. Concerning surfactant structures, they may be divided into cationic, anionic, non-ionic and amphoteric groups, while the former ones are most often identified with antistatic and antimicrobial properties [49]. Quaternary ammonium salts (QAS) are commonly used cationic surfactants with proven antimicrobial activity [49–52]. Dimerization of monomeric cationic surfactants has become very beneficial and fruitful since their antimicrobial properties increased significantly. It has been proven that Gemini analogs may indicate even 70 times smaller minimal inhibitory concentration (MIC) value – which quantifies the antimicrobial activity – compared to the monomers [51, 53]. The exact mode of action is still unclear [51] however, the proposed ones assume similarities to CAMPs and biocidal action, *i.e.* GS adsorbs on the membrane surface and penetrate the monolayer using long alkyl chains. This results in the outer cell barrier damage and leakage of cytoplasm, cellular components and ions leading to pathogen death. GS have several unique properties that distinguish them from other groups, present great antimicrobial properties, are less toxic than monomers, especially QAS, and are mostly effective against antibiotic-resistant bacteria. Several approaches to relate the compound structure with antimicrobial activity have been proposed. It is suggested that the type of headgroup and the positive charge of the molecule [51], the length and type of spacer [54, 55] or the length of the alkyl chain may affect the antibacterial effectiveness. The latter case is most often reported in the literature and the strongest antimicrobial activity against bacteria is assigned to the presence of 10-14 carbon atoms in the alkyl chain [49, 56, 57]. It is suspected that the shorter substituents fail to disturb the hydrophobic core

order or cannot efficiently penetrate the membrane, while the longer ones tend to coil, and anchoring to the membrane remain unfeasible [49].

Some of the commonly used and commercially available cationic surfactants are octenidine and chlorhexidine applied in Octanisept® and Eludril®, respectively.

Octenidine dihydrochloride (OCT) is a cationic agent from the bispyridine group and presents a broad antiseptic activity against fungi, Gram-positive and negative bacteria. It is remarkably effective even in lower concentrations compared with other antiseptics and exhibits long-lasting activity [58]. In contrast to well-known QAS, it presents reduced toxicity, since a lack of amide and ester components are present, so 4-nitroaniline metabolite will not be formed. The common OCT usage and published experimental data state that pathogens are susceptible to antimicrobial OCT action. Additionally, the scientific data collected during the COVID-19 pandemic indicate that the compound is effective not only against bacteria but also against SARS-CoV-2 [59, 60]. Several approaches to unravel selective OCT mechanism have been proposed, wherein the most recent published by Rzycki *et al.* [61] delivered molecular insights into OCT interaction with neutral and negatively charged membranes. They also emphasized that the mode of action is far more sophisticated than straightforward electrostatic interactions as stated in the literature and lies in the differences in mechanical membranes properties. They suggested that further disordering of mechanical features results in mechanical damage and loss of bilayer integrity [61].

Another commonly used and broadly studied cationic agent is chlorhexidine. Chlorhexidine digluconate is bioactive biguanidine extensively applied in infection prevention usually against Gram-positive and negative bacteria however, the activity against the latter is reduced. Additionally, several groups described limited susceptibility to CHX [62–64], especially Copin *et al.* [64] reported limited CHX activity due to resistance genes acquisition. Chlorhexidine activity results in destabilizing the membrane by calcium and magnesium cations displacement, resulting in potassium ions and protons leakage and finally integrity disorder and cell death [65].

Many more Gemini-structured compounds are reported as effective against resistant bacteria strains and give hope for success in the resistance battle however, the effectiveness comparison of compounds is often unfeasible. Antimicrobial activity is evaluated using several protocols of diffusion and dilution methods, time-kill tests or cytofluorometric methods [66]. Additionally, the bacteria strain selection for antimicrobials testing often varies significantly. This results in the limited outcome of the research in the antimicrobial aspect since novel synthesized agents usually cannot be compared with others or the well-known ones [67], especially delivered by other research groups.

1.3   Bacterial cell envelope – is this fortification unbreakable?

One of the most fundamental units in all living organisms is the cell. The cell border is called the lipid membrane, which apart from the protective role, controls the transport of nutrients toward the cell core and removes toxins outside. Membrane permeability is limited especially for ions, thus different distribution on both sides may be maintained, which is an essential regulatory property [68]. Overall, membranes are composed of proteins and self-assembling lipids maintained by electrostatics and hydrophobic effect. Bacteria, unlike other higher organisms, created their own cell envelope consisting of membranes, proteins and sugars that act as protection against invasive and unpredictable environmental conditions. The bacterial cell envelope may differ significantly between the species. Christian Gram in 1884 discovered that in general bacteria may be divided into two distinct classes, one which absorbs Gram stain and another which does not [69]. That experiment allowed to distinguish Gram-positive and negative bacteria, respectively,

and reveal the structural distinction in the bacterial cell envelope. The organization of Gram-positive and negative bacteria is presented in Figure 1.3.

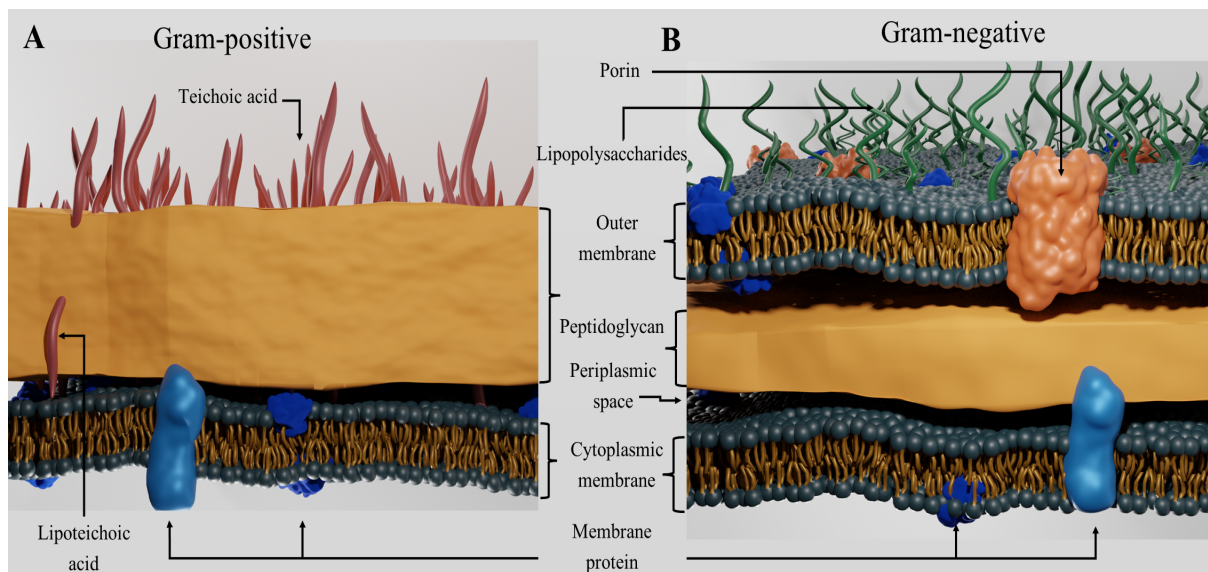In Gram-negative bacteria three fundamental layers may be highlighted, the outer membrane (OM),

Figure 1.3: The general structure of Gram-positive (A) and Gram-negative (B) bacterial membranes.

peptidoglycan cell wall and inner membrane (IM). The most external part is the outer membrane, which is present only in Gram-negatives. OM composition may vary significantly between other bilayers since the phospholipid layer appears only in the inner leaflet, close to the peptidoglycan layer, while the outer one is formed by lipopolysaccharides (LPS) [70]. LPS acts as a major protective barrier in OM and Gram-negatives in general, selectively limiting the membrane permeability. It is initially made of lipid A, a polysaccharide core and the O-antigen region at the end [71]. If the human immune system detects the LPS presence it may result in endotoxic shock or may even end with necrosis of the tissues [68, 72]. Several types of proteins are suspended in OM film, the most commonly occurring are lipoproteins and outer membrane proteins (OMPs) like porins. Lipoproteins are unique structures embedded in the inner leaflet of OM. Two fractions may be highlighted in their composition, the lipid and protein one, linked together by cysteine in N-terminus. Their functions are still discussed however, maintaining the stability and durability of the bacterial cell envelope is the most feasible [73, 74]. The second most abundant group of proteins anchored in the OM are OMPs. These cylindrical biopolymers have a β-barrel structure and create pores that control the passive diffusion of small nutrients and signaling compounds, toxins or antibiotics through the OM [75]. OmpA, OmpC and OmpF functions and their disorder are broadly studied in the literature since they are involved in antibiotic resistance and bacterial virulence in bacteria. Choi *et al.* reported in their studies that OmpA supports membrane integrity, while OmpF is responsible for antimicrobial agent transport and bilayer permeability [76]. Association OmpF functionality with the transport of the antibiotics *i.a.* β-lactam drugs toward bacteria core has become a goal of many scientists to unravel the bacteria resistance mechanism [76–78].

Another layer closer to the bacterial core is peptidoglycan. It appears in both Gram-positive and Gram-negative bacteria but its structure between the species may vary significantly. Peptidoglycan is a mesh-like framework composed of glycan chains cross-linked by peptide side chains [79]. In Gram-negative, it forms thin (up to 10nm thick) and rigid monolayer, which affects the overall bacterial cell shape [80]. Additionally, peptidoglycan interacts with placed above OM by lipoproteins, substantially strengthening

the mechanical properties of the cell envelope [74]. The lack of protective OM in Gram-positive bacteria induced a need to surround the cell core with a much thicker coating. Similar to Gram-negative the positive ones also occupy severe surroundings, thus peptidoglycan layer is almost 100nm thick [72]. Cell wall polymers like teichoic acids are embedded in glycan strands and play important role in cation homeostasis. These are long anionic moieties that often stick out above the peptidoglycan surface and constitute even 60% of the total cell wall mass. Two types of that acids may be found: lipoteichoic and wall teichoic which are embedded in membrane and peptidoglycan, respectively. Their presence combined with a slight shift in the location allows to preserve a constant spectrum of negative charge starting from IM toward peptidoglycan and further beyond. The absence of any of them may result in cell growth disorders or cell division issues [72].

In Gram-negative bacteria a cellular structure called periplasm space may be found between inner and outer membrane. It contains a peptidoglycan layer and a fluid segment where binding, transport proteins occur as well as several types of enzymes [81].

The innermost barrier in bacteria that separate the periplasm and cell wall from the cytoplasm is the IM. It is responsible for the selective transport of small molecules, detection of external signals, and energy management [82, 83]. Bacterial bilayers, in general, may be found as structural analogs to eukaryotic ones, since both are composed of phospholipids and proteins. Nevertheless, plenty of functions accomplished by intracellular organelles in eukaryotes is carried out in the bacterial IM. Since bacteria lack mitochondria, endoplasmic reticulum, or complex transport framework; the energy generation, protein manufacture or folding, and toxins removal functionality are performed by appropriate proteins embedded in IM [72, 84]. Several differences may be highlighted in bilayer composition between both bacteria species, due to the presence of teichoic and lipoteichoic acids anchored to the membrane in the latter ones. The proteins anchored in IM are usually typical secondary structures *i.a.* with α-helical segments. Depending on their functions may be localized on the peripheral surface or cross the membrane and act as transmembrane channels. ABC transporters are well-known sugars, ions and peptides importers related to lipoproteins [85]. Another large multiprotein is SecYEG which is major translocation machinery that assists and transfers proteins over the monolayer [86]. Tat is another protein-conducting machinery providing similar facilities to Sec however, it focuses on folded proteins passage [87].

As already mentioned lipids are the fundamental constituent forming the membranes. These amphiphilic structures are equipped with a polar head and hydrophobic tails and compose IM and an inner leaflet of OM in bacteria. Phospholipids may vary between the groups *i.e.* in the type of headgroup and distribution of the charge, as well as length and number of the hydrophobic tails [88]. The most abundant glycerophospholipids in bacteria are phosphatidylethanolamine (PE), phosphatidylglycerol (PG), and cardiolipin (CL), whereas phosphatidylserine (PS), phosphatidic acid (PA) appear in minority. Depending on the bacterial strains zwitterionic PE constitutes around 80%, negatively charged PG and CL 15% and 5%, respectively [89, 90]. Unlike eukaryotic cells, bacteria, in general, lack zwitterionic phosphatidylcholine (PC) and cholesterol, which affect the membrane fluidity and permeability [88]. The major role of phospholipids is to maintain the structural integrity of the membrane and cell envelope at all. In addition proteins' presence or microdomain formation affect the membrane curvature resulting in monolayer asymmetry, thus the distribution of the lipids is not equal on both bilayer sides. That membrane properties influence bacteria's selectivity to toxic molecules like drugs, contributing to antibiotic resistance [91]. Due to the synthesis of almost every bacterial component in the cytoplasmic space or at the inner leaflet of IM, disordering that membrane often becomes a target for antimicrobial compounds. The whole bacterial cell envelope is a complex facility equipped with sophisticated molecular machinery composed of lipid, proteins, and saccharides derivatives. Therefore investigation of membrane properties and protein impact

on bacteria well-being remains problematic on a large scale.

1.4 Numerical approaches in antimicrobial assessment

The American physicist and Nobel laureate Richard Feynman stated that one of the most powerful assumptions in life understanding involves conceiving reality as a set of atoms, thus processes in living structures reflect the sway and movement of those atoms. A vast of biophysical society has devoted the last 50 years for understanding the nature of atoms' movement. The proper awareness of molecular motions is absolutely crucial in drug discovery or investigating biological processes [92]. Taking into account the complexity of the physical, biological, or chemical phenomena, computer science and the development of computational methods have become essential to constantly progress in given fields. The consistent technological improvement resulted in the development of dedicated and accurate numerical approaches such as computer modeling or simulations in a large timescale. Numerical studies have become widespread and are a great linker of pure theory and experiments. That gives a great opportunity to combine both techniques provide less drastic approximations, improve existing models and finally deliver a better and more accurate nature representation.

Molecular dynamics become one of the pioneering numerical methods applied to biological systems [93, 94]. Nowadays, this method turned into a gold standard during drug discovery or biological machinery studies [95]. MD is most often used during antimicrobial agents studies in various approaches. It allows studying the interaction and motions of atoms based on solving Newtonian physics. Additionally, an appropriate force field is applied to calculate the forces among interacting molecules as well as evaluate the total energy in the system. Integration of Newton's equation through further MD steps delivers new atoms' positions and their velocities, resulting in a novel system arrangement in simulation time. Collecting the subsequent particle positions forms the system trajectory, from which further calculations or analyses can be performed. One of the fundamental concepts in MD or general numerical simulations is to investigate the time-dependent activity of a set of *i*-th particles constituting the system. Solving the Newtons eq. 1.1:

$$F_i(t) = m_i a_i(t) = m_i \frac{d^2 r_i(t)}{dt^2} \tag{1.1}$$

Where $F_i(t)$ is the force acting on *i*-th atom with given mass *m* at time *t*, and $r_i(t) = (x_i(t), y_i(t), z_i(t))$ represent atoms position vector at time *t* in Cartesian space. The atoms may be easily replaced by particles or their dipole moments etc. though adopting appropriate interaction law terms. The issue of reflecting a realistic potential lead to huge computational simplifications. In computer studies molecular mechanics statements are often used, to deliver the approximations of nuclei electrons' motion. To address this issue the empirical potential functions were introduced and atomic force field models were proposed. Many various force fields were proposed so far [96–105] however, mainly the overall formula remains consistent and includes bonded, non-bonded energy terms (see eq.1.2) sometimes supported with additional specific force field conditions.

$$U = \sum_{bonds} K_b (l_i - l_{i0})^2 + \sum_{angles} K_\theta (\alpha_i - \alpha_{i0})^2 + \sum_{dihedrals} K_\phi [1 + cos(n\phi_i - \gamma_i)]$$

$$+ \sum_{atompairs} \varepsilon_{ij} \left[\left(\frac{\sigma_{ij}}{r_{ij}} \right)^{12} - 2 \left(\frac{\sigma_{ij}}{r_{ij}} \right)^6 \right] + \sum_{atompairs} \frac{q_i q_j}{4\pi\varepsilon r_{ij}} \tag{1.2}$$

The eq. 1.2 may be divided into two parts according to type of interactions, the first three summation terms refers to covalent energy variations in bond length, angles, and dihedrals, while the last two refer to non-covalent, van der Waals and electrostatic interactions. The changes in bond length (l_i) and angle (α_i) are characterized by harmonic potentials with the equilibrium values (l_{i0}) and (α_{i0}), and force constant K_b and K_θ respectively. The last covalent term – torsions, denote the bond rotations described by periodic energy where K_ϕ is energy barrier, ϕ_i, γ_i is the phase angle, and n is periodicity. The last two terms represent nonbonded and distanced atoms (r_{ij}), where the first denote repulsion and attraction from the Lennard-Jones 12-6 potential and σ_{ij} describe the depth of energy well. In the last electrostatic energy term the Coulombic potential is applied with q_i and q_j atom partial charges and ε relate to permittivity. The usage of defined force fields allowed to accelerate the computation efficiency in contrast to quantum mechanics (QM). QM on the other hand is a very sophisticated method based on solving the Schrödinger equation. The complexity of the calculations usually limits the application horizon to extended systems. QM is extensively used in the molecule parametrization process, delivering appropriate calculations for further force field formation [91].

System evolution is described by velocity and position vectors, hence trajectories are generated by solvation of the equation of motion using numerical integrators. Integration to discrete and small-time intervals named time steps is necessary to preserve reliable forces over the simulation time. Verlet algorithm is a common and widely used integrator MD as well as in other numerical approaches, that allow the calculation of the following positions ($t + \delta t$) based on the current position, velocity and acceleration (see eq. 1.3).

$$r_i(t + \delta t) = r_i + v_i(t)\delta t + \frac{1}{2}a(t)\delta t^2 \tag{1.3}$$

Taking into account relation in eq. 1.4 between force F_i and potential energy U gradient:

$$F_i = -\nabla r_i U = -\left(\frac{\partial U}{\partial x_i}, \frac{\partial U}{\partial y_i}, \frac{\partial U}{\partial z_i}\right) \tag{1.4}$$

Additionally, taking into account combination of the forces definition from eq. 1.1 and 1.4, accelerations may be calculated, hence (see eq. 1.5):

$$v_i(t + \delta t) = v_i(t) + \frac{a_i(t) + a_i(t + \delta t)}{2}\delta t \tag{1.5}$$

To reconstruct the accurate trajectories infinitesimal integration step should be applied. On the other hand in practical approaches, longer ones are expected. To ensure appropriate time steps the light atom vibrations are taken into account, hence femtosecond scale (1-2 fs) preserves reliable integration. Some protocols were proposed to increase the timestep and result in simulation acceleration *i.a* hydrogen mass repartitioning (4 fs) [106].

In numerical studies, appropriate timescale and technique selection are crucial in observing modeled phenomena. Mentioned QM methods, are accurate and computationally demanding calculations however, the quantum character of electrons is taken into account. Density functional theory (DFT) calculations have been extensively applied to study the biomolecules at surfaces [107, 108]. Such accuracy allows for calculating the electronic structure of atoms and molecules, thus bond formation and chemical reactions may be observed. QM methods are broadly employed in antimicrobial agent force field determination [109, 110]. Further up to the microsecond scale, molecular mechanics including all-atom

MD, and coarse grain MD are used to reflect biological phenomena. This branch is the mainstream since allows for modeling and observing the protein conformational changes, complex interactions, agent binding, membrane dynamics and self-assembly. In all-atom systems, atom representation of bilayers, proteins and ligands are employed and simulated over hundreds of nanoseconds. If modeled membrane interactions or protein binding occur in a higher order of time magnitude *i.e.* microseconds the coarse-grain modeling (CG) is applied. The CG concept assumes a different structure representation since groups of atoms are described by beads (pseudoatoms), which limits the degrees of freedom and number of particles and accelerates the computation time. CG modeling is often used to observe large-scale events such as lipid microdomains or rafts formation or protein structure predictions [111]. Unless atomistic detail scope is not required and large-time scales are expected, CG models act as a sensible alternative to AA ones. Hybrid models such as united-atoms (UA) are still worth noting. In UA carbon atoms are grouped with their hydrogens and form pseudoatoms. They are often called hybrids, providing better performance than AA and also a deeper level of description compared to CG. It remains a reasonable approximation if intermolecular interactions are more crucial the intramolecular ones [112]. Over the years, several force fields have been proposed and improved [96–105] however, the imperfection issue and bias in the interpretation of numerical results due to various simplifications should be still taken into account.

From MD simulations several various parameters *i.a.* energy may be extracted. The total system energy state may be in general described by Hamiltonian $H(x, p)$, containing the potential and kinetic energy K based on molecules' coordinates and momenta (see eq. 1.6).

$$H(x, p) = U(x) + K(p) \tag{1.6}$$

In antimicrobial assays, the thermodynamic aspect were proven to be particularly important [113]. One of the crucial thermodynamic element in drug discovery and membrane interactions is free energy. It is expressed by Helmholtz (A) function under NVT ensemble (constant Number, Volume, and Temperature) and by Gibbs (G) function under NPT ensemble (constant Number, Pressure, and Temperature). Helmholtz potential can be defined from fundamental thermodynamic relation (see eq. 1.7),

$$A = U - TS \tag{1.7}$$

or linked with partition function (eq. 1.8).

$$A = -k_b T \ln Q = -k_b T \ln \left\langle e^{\frac{H(x,p)}{k_b T}} \right\rangle \tag{1.8}$$

where S denote the entropy, T - temperature, k_b - Boltzmann constant and Q is a partition function. Under NPT ensemble free energy is determined according to Gibbs potential (eq. 1.9).

$$G = H - TS \tag{1.9}$$

where H denote the system enthalpy. Free energy determination is particularly important in proteins studies and bridges the numerical and experimental approaches. Determining the free energy of two stable or meta-stable thermodynamic states of the protein allows for describing the system behavior. Especially convenient is the use of simplified approach and determine the difference between the states (ΔG) according to transition state theory [114, 115].

However, due to the inherent Boltzmann sampling limitations, several theoretical approaches called enhanced sampling methods have been proposed for the appropriate states distribution. Some of them are

based on the introduction of a biasing force into the system to accelerate the calculations. On the other hand, the unbiased ones present smooth system evolution however, may take much longer even up to hundreds of microseconds if interactions are weak.

One of the well-known theories is a free energy perturbation (FEP), where free energy is considered as a state function, thus free energy is based on differences between initial state A and target state B, instead of the actual system pathway. That approach usually employs Monte Carlo or MD sampling and is also called alchemical transformation and delivers differences in the binding affinities of smoothly mutating molecule A to its analog B (*e.g.* ethane to methanol) [116–118].

Another well-established method is umbrella sampling (US) with in contrast to FEP is based on the system pathways. In US method sampling procedure is passed along an established reaction coordinate or collective variables (CV) through conducting a set of simulations with additional bias potential, which is in the form of a harmonic interaction (umbrella). Consequently, the sampling through high-energy regions may be proceeded thoroughly and the potential of mean force (PMF) is calculated afterward using the weighted histogram analysis method [118, 119]. Providing the overlapping simulations windows is crucial in the sampling aspect as well as the determination of appropriate force constants [119].

Steered MD is a further method, to assess the free energy change. In this approach, an external potential is applied to the ligand to pull it along a pathway in conformation space, so that performed work is calculated. This method is mainly applied to drug design studies, where the ligand is undocked from the target protein [120]. This technique is comparable to experimental atomic force microscopy studies, where also external forces occur [118].

Another group of enhanced sampling methods is metadynamics. In this method, a rapid inspection of the free energy surface occurs and can exceed two dimensions, which is the biggest difference from other techniques. The reaction coordinate is reflected by a variety of order parameters. In the literature metadynamics main idea is often compared to covering up explored energy wells with the sand moving toward energy barriers and then to the further energy wells, covering them up with sand again, and further on [121]. This method is often called a history-dependent, since biasing Gaussian-shaped potential (sand) is added to the actual CV location to prevent repeated exploration of the same area. When the potential is high enough to cross the energy barrier it may move to another local minimum, build up the potential and move another barrier, and so on [121–123]. In the end, PMF can be easily estimated from the created biasing potential by reversing the sign [118]. Metadynamics evolved over the years as well as been combined with other methods *i.e.* machine learning [124].

On the other hand, unbiased MD simulations are still in the research scope since several accelerations were introduced. One of the most successful is the Replica Exchange, where simultaneously several copies of the system are simulated in various temperature conditions (T-REMD) [118, 125]. Afterward, in the given replica pair the exchange of the temperature occurs periodically. Hence the random walk in temperature space promote crossing the energy barriers and allow to sample a broad conformational space of the tested compound [125, 126]. However, to effectively use this technique large replica collections are needed.

The last commonly used method is Adaptive biasing force (ABF). The main purpose of this technique is to improve the MD simulations performance, in which the presence of free energy barriers leads to insufficient potential energy surface sampling. The mean force applied along the reaction coordinate ξ follow the relation from eq. 1.10 [127, 128]:

$$\frac{dA}{d\xi} = -\langle F \rangle_\xi \tag{1.10}$$

Taking into account Jacobian (J) correction delivered by Carter *et al.* [127, 129] (see eq. 1.11) which regard to geometric transformation from Cartesian to generalized coordinate:

$$\left\langle -\frac{\partial U}{\partial \xi} + k_b T \frac{\partial ln|J|}{\partial \xi} \right\rangle_{\xi} = \langle F \rangle_{\xi} \tag{1.11}$$

Where U represents the energy potential k_b is Boltzmann constant T is temperature. The major idea behind ABF is to calculate the mean force along the reaction coordinate, which is afterward balanced by an equivalent and opposite biasing force. This approach allows to cross the energy barriers and prevents settling in a local minimum of the free energy surface. During the simulation time, the ξ is discretized into small $d\xi$ bins. Samples of the applied force F_{ξ} are computed in appropriate $d\xi$ bins. Afterward, the opposite biasing force act on the system, which results in a consistent sampling process by the whole ξ [127, 130]. Taking into account the relation of biasing force and free energy from eq.1.10 and 1.11 the integration of the biasing force determines free energy evolution along ξ. The ABF method comprises accurate and reliable calculations in a sufficient timescale, its approach is intuitive and postprocessing like in US is not necessary [118]. Additionally, it is well suited to membrane applications and is user-friendly [130–132].

Free energy calculations are extensively used in assessing membrane barriers. Sharma *et al.* [133] applied the US method to provide free energy graphs for thymol, penetrating both OM and IM bacterial membrane models of *E. coli.* Similarly, Bonhenry *et al.* [130] performed both alchemical transformations and applied the ABF method in transferring small cationic peptide across the bilayer model.

Discussed simulation methods are extensively applied in antimicrobial agent evaluation. The membrane rupture often is not noticeable in simulations however, such parameters as lateral diffusion, order parameter, system energy, area per lipid, membrane thickness and surface tensions are affected [61, 134–137]. Apart from Gemini structured agents plenty of other antibiotics, antiviral and antifungal agents are tested in similar manner *i.a.* kanamycin A [138], cholic acid-derived amphiphile [139], daunorubicin [140], amantadine [141–143]. In the review paper, Róg *et al.* [121] collected hundreds of most recent articles, where molecular dynamics studies were employed to evaluate the membrane-drug interactions. The collection of almost 1100 references, mostly discussing the inducing of bilayer disorders clearly indicates that the numerical approach represents an essential branch in antimicrobial assays [121].

Chapter 2

Hypotheses

The major aim of the dissertation assumes the development of biophysical and numerical approaches to fast evaluate the antimicrobial activity in prominent Gemini-structured agents, supporting an alternative branch in antimicrobial-resistant bacteria battle. With respect to the objectives, the following theses were proposed:

1. The antimicrobial activity of amphiphilic particles is possible to evaluate using physical and numerical approaches.

2. The origin of the cationic agents' mode of action is more sophisticated than pure and straightforward electrostatic interactions.

3. The composition and complexity of bacteria membrane numerical model play significant role in accurate reflection of biological and biophysical phenomena.

4. Employing structural, molecular parameters of Gemini agents it is possible to assess their behavior and activity on physical models of membranes.

Chapter 3

Summary of results

3.1 Core information

The thesis consists of 4 papers published in international peer-reviewed journals indexed in Scopus. In this chapter, essential results are outlined in the following four sections. In the first paper two commonly used antibacterial agents OCT and CHX were studied referring to the molecules' mode of action and antimicrobial properties [61]. In the second paper, a slightly different perspective on Gemini-structured agents was provided. An extensive and standardized database of 250 Gemini surfactants was created and the antimicrobial activity of selected compounds was further assessed [135]. In the third paper novel and complex numerical model of *E. coli* bacteria was proposed, indicating how the structure of the model may affect the outcome, biasing the biological conclusions [144]. In the last article, a problem with assessing the antimicrobial activity of Gemini surfactants was addressed. To solve that issue numerical approach was proposed in an original software called *Diptool*. The origins, methodology, and procedure of the tool were included in that article [113]. In the collection of presented papers, agents' antimicrobial activity was assessed based on the evolution of membrane parameters as well as variation of system energy. Mainly numerical and computational methods were employed, nevertheless in the first article experimental verification of *in silico* results was also included. The calculations were performed: on a local computational node hosted by the Department of Biomedical Engineering at Wrocław University of Science and Technology; at the Centre of Informatics Tricity Academic Supercomputer and Network; and on a computational node hosted by Laboratoire de Physique et Chimie Théoriques at University of Lorraine.

3.2 Unraveling the mechanism of octenidine and chlorhexidine on membranes: Does electrostatic matter?

The antimicrobial resistance issue has been raised and discussed several times so far (see Section 1.1). One of the approaches in the fight against MDR assumes the selective attack on slowly evolving bacterial membranes leading to its disruption and cell death [145]. Commonly used cationic agents, OCT and CHX are effective against Gram-positive and Gram-negative bacteria however, their selective mechanism was unclear, thus often attributed to electrostatic interactions [58, 146, 147]. Since eukaryotic membranes are in general made of zwitterionic PC lipids, and the bacterial are enriched in negatively charged PG and CL, it was suggested that the mechanism is based on charge attraction. In this paper, we

17

decided to verify that proposal and describe a molecular model of disintegration using highly negative membranes (NegM) neutral ones (NLM) and bacteria mimicking (BacM – only computationally). To deliver a comprehensive point of view we combined a series of experiments with MD studies. To achieve defined objectives zeta potential measurements in the function of agent concentration, fluorescence studies with trimethylammonium-diphenylhexatriene (TMA-DPH) and DPH probes, carboxyfluorescein leakage (CXF) test and bending rigidity measurements were conducted. In the MD studies two aspects were tested, the effect of the highly ionized solvent versus neutral one on agent interaction with the membranes, and higher and lower agent to lipid ratio in the systems.

Firstly we delivered data on OCT and CHX location in the membrane using TMA-DPH probes and molecular dynamics simulations. The numerical approach allowed to find out major differences in OCT behavior in low and high concentrations. Single OCT molecule bind to all types of membrane in a staple shape, penetrating it by the alkyl chains, while in higher concentrations OCT tends to form aggregate and anchor to bilayer afterward. Depending on the system, the exact shape of aggregate varied starting from a typical balloon where only one OCT chain was embedded in the membrane leaving the rest of OCTs 'bubble' above NLM, to a more spread 'spider' form, where OCTs penetrated heavily BacM surface. Interestingly, limited OCT and NLM interactions were observed in a neutral solvent. That may suggest slight prevention in agent self-aggregation and result in stronger affinity to bilayers. Regarding CHX behavior no differences were observed in interaction with various membranes and concentrations. CHX constantly anchored in staple shape to all membranes, which remains consistent with other reports [136, 148]. Minor reduction in CHX and NLM contact was observed in the neutral solvent since six of seven chains were incorporated into the bilayer. Further, the fluorescence assay with TMA-DPH probes allowed to confirm that both OCT and CHX locate at the edge of a carbonyl-glycerol region which stays in line with MD studies [136].

Subsequently, zeta-potential studies allowed to evaluate the behavior of charge close to membrane surface in agent concentration function. Taking into account the results, in our opinion, OCT is prone to form aggregates on the bilayer face than penetrate and anchor, thus slower kinetics may be observed in NegM.

Disordering properties of studied agents were noticed during the membrane self-assembly approach. Unless detergents were present the phospholipids suspended in solvent tend to form a model bilayer. Nevertheless, OCT or CHX presence effectively disrupted that process, resulting in an abnormal doughnut structure. On the other hand, the destructive activity of molecules was confirmed during CXF leakage tests. Leakage experiments revealed that at lower OCT concentrations, more damage is observed in NLM than NegM, implying a lack of selectivity through pure electrostatic interactions. CHX results were not so clear, since CXF release was barely visible and almost constant however, based on obtained results it is not certain that the CHX mode of action involves bilayer fluidity disorder.

In the end, the mechanical properties of NegM and NLM were tested using bending rigidity measurements. The results indicated that pure NegM is several times more rigid than NLM and OCT activity distinctly affects the membrane mechanics, especially in lower concentrations. Taking into account the collection of results, the OCT mechanism was proposed. We postulated that the OCT mode of action is selective based on mechanical membrane properties, OCT primary induces structural changes, ripping the membrane at a sufficiently large concentration afterward. This remains consistent with the finding that NegMs are stiffer than NLMs [149]. Furthermore, in other studies, *E. coli* enhanced the membrane stiffness against external forces *i.e.* stress-induced by ZnO nanorods [150], which may indicate the bacteria's potential defensive mechanism. Delivered data and literature review allowed to suggest that CHX antibacterial activity corresponds with membrane stiffness variation, which can lead to disorders in

microdomains organization or loss in proteins homeostasis [151].

Results and conclusions included in Rzycki *et al.* article [61] allowed to confirm the 1st and 2nd hypothesis as well as expand the knowledge of the antibacterial activity of commonly used compounds.

Publication details: M. Rzycki, D. Drabik, K. Szostak-Paluch, B. Hanus-Lorenz, S. Kraszewski, *Unraveling the mechanism of octenidine and chlorhexidine on membranes: does electrostatics matter?*, Biophysical Journal, vol. 120 (16), s. 3392-3408 (2021)

Contribution: conceptualization of numerical approach, providing the MD calculations, conducting the experiments, literature review, results analysis, data visualization, conclusions formation, manuscript writing and editing.

3.3 A Systematic Approach: Molecular Dynamics Study and Parametrisation of Gemini Type Cationic Surfactants

Over the recent years, Gemini surfactants (see Section 1.2) have gained the attraction of scientists from all over the world. Within the last 5 years, many articles have been released, where the synthesis process, potential application, or antimicrobial properties were introduced and discussed. Despite the increasing number of novel synthesized compounds, the general knowledge and outcome are limited. The antibacterial effectiveness essays are usually restricted to MIC determination, which results are sensitive toward the protocol applied [67, 152, 153]. More comprehensive analysis with several types of various agents targeted for disordering and destruction of bacterial barriers is rather exceptional.

In this work, we decided to provide a systematic and universal theoretical approach over a large set of Gemini molecules. To this end, we reviewed the literature and collected a database of 250 Gemini molecules, which were divided into appropriate subgroups based on their structure. To maintain the systematic comparison of agents' antimicrobial activity on membranes, each molecule has been optimized and parametrized to deliver a valid force field for MD studies. From classified subgroups, 25 representants were selected and placed over the surface of the bacterial inner membrane model. Based on the 10 most informative membrane parameters used to evaluate the antimicrobial activity we selected the four most affected and significant ones, which may reflect the agent impact. The detergents significantly influenced the mechanical and dynamic membrane parameters such as compressibility, bending rigidity, lateral diffusion, and surface tension. Eight most prominent and vital candidates which severely affected at least two membrane parameters were collected and discussed. The obtained results correspond well with the general mode of Gemini's action [154] and also relate to the mechanical mode of action revealed during OCT studies [61]. In our opinion, besides the theoretical outcome, experimental verification plays a key role to confirm provided predictions.

The problem with the comparison of experimental data is common and often affects many branches. Conducting complex and systematic studies remain challenging and costly. In this study, the theoretical approach to ensure a unified protocol in antimicrobial activity evaluation was proposed. Additionally, the outcome of the research allowed to confirm the 1st hypothesis. Apart from that, provided classification with relevant structure characteristics and force fields may inspire other experimental or theoretical groups to extend studies on Gemini molecules.

Contribution: design and conceptualization of the research, numerical modeling, providing the MD calculations, literature review, results analysis, data visualization, conclusions formation, manuscript writing and editing.

3.4   Towards Mimetic Membrane Systems in Molecular Dynamics: Characteristics of *E. Coli* Membrane System

In computational studies the questions concerning the accuracy and reliability of presented models often appear. Is the presented model good enough? Whether the biological phenomena will be correctly reflected? That issues often bothered and inspired me simultaneously to verify the complexity of commonly used bacterial models. The biological structure has been presented in detail in Section 1.3, nonetheless, three fundamental layers may be highlighted in Gram-negative bacteria: the outer membrane (OM), inner membrane (IM), and periplasm. In general, the planar membrane models are commonly used mimicking bacterial OM or IM [155–158]. That usually may reflect and correspond well with Giant Unilamellar Vesicles or Large Unilamellar Vesicles known from experiments [159]. However, presented models may in fact vary significantly from the real ones or from experimental analogs, which sometimes result in inaccurate conclusions.

In that work, we wanted to emphasize that issue and present a complex *E. coli* membrane model that reflects the biological structure and assess the impact of structural complexity on the mainstream membrane parameters. For that purpose double membrane system (IM+OM) features were compared with the same features of pure IM and OM. In addition, the presence of the O-antigen region in the OM was evaluated and discussed.

The presence of the O-antigen region in pure OM models significantly affected in membrane thickness, mobility as well as mechanics. Most visible changes are noticed between the lateral pressure profiles since the presence of the additional saccharide region impact greatly on pressure reduction. Our studies reflected significant changes among complex and separate membrane systems, especially in the reduction of mobility, significant mechanical changes and even various pressure distributions between leaflets.

In that paper, we delivered a comprehensive means to highlight, that membrane complexity and composition matter. Simultaneously it allowed to confirm 3rd hypothesis. The variation of studied parameters changed progressively with the systems complexity. Due to the essential origins of interactions and potential lack of complexity in numerical models some biological phenomena may remain elusive or suppressed.

Contribution: design and conceptualization of the research, numerical modeling, providing MD calculations, literature review, results analysis, data visualization, conclusions formation, manuscript writing and editing.

3.5 *Diptool* – a novel numerical tool for membrane interactions analysis, applying to antimicrobial detergents and drug delivery aids

Limited efficiency benchmarks concerning different protocols and distinct bacterial strains applied in MIC experimental studies have been already mentioned in Section 3.3. Considering the experimental shortcomings and the universality of the MD approach led to the development of own methodology and software called *Diptool*.

The beauty of numerical simulations especially MD, lies in the universality of the tool however, on the other hand is also its victim. As proven in previous sections and published papers, the MD approach provides a wide range of means in antimicrobial activity assessment, starting from the agent attraction or repulsion toward membrane up to complex interaction analysis. Performing free energy calculations, allow precisely to determine agent sweet-spot in the membrane and visualize the high energy barriers from lipid headgroups or hydrophobic core region. Delivering well-sampled free energy profiles is quite time-consuming and computationally demanding.

Limitation of redundant parameters in the universality of MD or providing alternative and targeted solutions may influence the calculation time scales without a drastic reduction of outcome significance. That was the major idea behind the design of *Diptool* – a software for rapid screening the membrane-agent interactions and potential antimicrobial candidate selection. Using an experimental set of Gemini surfactants we provided quantitative structure-activity relationship (QSAR) studies, which in the end allowed to select the most significant and overlapping parameters such as dipole moment, partition coefficient (logP), and length/width (agent size). In that approach, the *Diptool* acts as a specific probabilistic membrane modeler, based on the Gaussian distribution of lipid dipole moments.

The greatest difference between other computational methods is that *Diptool* is based on dipole interactions, thus each structure in the system such as lipid or Gemini molecule is identified as dipoles. In the calculation core of *Diptool* the provided parameters, as well as Gibbs energy conditions, have been employed. For Newton's equation integration a modified Verlet algorithm has been applied with an additional description of the medium suppression. Thus the *Diptool* has become a powerful tool for physical modeling of given biological phenomena. The software outcome was verified with the results from the ABF approach from MD as well as our previous study [61]. The trajectories obtained from *Diptool* for both tested agents (OCT and CHX), despite the different core of motion, corresponded with the others acquired by the MD approach. The energy profiles from *Diptool* and ABF were further compared and the presented results on PC and PG membranes were a bit underestimated but fairly reflected. In the end, the performance tests have been provided, where million-fold times acceleration of *Diptool* has been highlighted.

In this paper, we presented *Diptool*, a novel software for rapid evaluation of the antimicrobial Gemini agents on various types of lipid membranes. Despite various calculation theories behind the software and MD, substantial similarities were found in the trajectories as well as in the free energy profiles. To be clear *Diptool* is an effective screening tool enabling the high-throughput for antimicrobials studies and may also find application in drug-delivery aids. Taking into account the total outcome from this work, the first (1st) and the last (4th) hypothesis - that the use of structural parameters of Gemini agents enables the evaluation of their behavior and activity on membranes, was confirmed.

Contribution: design and conceptualization of the research and methodology, software development and implementation, numerical modeling, providing the MD calculations, literature review, results analysis, data visualization, conclusions formation, manuscript writing and editing.

Chapter 4

Summary and conclusions

The major aim of the dissertation was focused on the development of biophysical and numerical approaches to evaluate the antimicrobial activity in prominent Gemini-structured agents. To this end, various methods were employed to look at the antimicrobial resistance problem from different angles and to propose adequate and fast solution. Therefore four hypotheses were addressed related to the main dissertation objective.

The presented introduction clearly indicates that antimicrobial resistance issue can be considered on various levels. In this work, one of the most promising branches *i.e.* analysis of potent antimicrobial agents, which attack the slowly evolving bacterial membranes was followed. Selected agents belong to the amphiphilic Gemini family however, their main advantage lies in limited bacterial immunity to their activity. In addition, some of them present a selective mode of action, thus are lethal for pathogens and harmless for humans.

In my first study, referred in Section 6, the antimicrobial effectiveness of OCT and CHX were tested. In this work, one of the most important conclusions has been proposed, that the fundaments of selective activity mechanism also lay in the mechanical properties of bacterial membranes. It is a prominent outcome since most of the previous studies debated only electrostatic interactions. In this study, molecular insights into agents' activity were repeatedly reported as well as resulting membrane disorders. Considering the results from this research, the first hypothesis - *The antimicrobial activity of amphiphilic particles is possible to evaluate using physical and numerical approaches*, and the second hypothesis - *The origin of the cationic agents' mode of action is more sophisticated than pure and straightforward electrostatic interactions*, were confirmed.

In my second research, referred in Section 7, the problem with the comparison of antimicrobial effectiveness of Gemini agents was addressed. Unless the relative activity of agents remains unknown, how one may conclude about enhanced antibacterial properties? The major benefit of this study is a systematic protocol for the evaluation of several antimicrobial agents and a unified database of 250 Gemini agents. Classified agents according to their structure with appropriate force fields, may be used by anyone in computational studies about testing antimicrobial properties, adsorption on surfaces, or even in general in material sciences. Finally, 8 Gemini surfactants that activity significantly affected membrane parameters were selected and labeled as promising ones and recommended for further experimental confirmation. Taking into account the results from that work, the first hypothesis, *The antimicrobial activity of amphiphilic particles is possible to evaluate using physical and numerical approaches*, was re-confirmed.

23

In the further study, referred in Section 8, the complexity of bacterial numerical models was examined. The main message from that work assumed that great emphasis should be placed on the correct reflection of experimental or real models since it matters significantly. In theoretical modeling simplifications often occurs however, it has to be highlighted that it may result in suppressed or elusive biological phenomena. Considering delivered findings from that work, the third hypothesis, *The composition and complexity of the bacteria membrane numerical model play a significant role in the accurate reflection of biological and biophysical phenomena*, was confirmed.

In the last work, referred in Section 9, the assessment of antimicrobial effectiveness issue was raised. The most important outcome from that work is *Diptool* release, a novel and original software for rapid evaluation of the antimicrobial Gemini agents on lipid membranes and potential candidate selection. Implementation of significant structural parameters of Gemini agents resulted in software convergence with MD, since substantial similarities in trajectories, as well as free energy profiles, were found. The greatest advantage of the software is its speed, which can provide results comparable to all-atom MD simulations in a matter of minutes. It is well suited for screening large databases in search of prominent molecules (manuscript in preparation: data not yet published, neither included in dissertation). Taking into account the results from that work, the first, *The antimicrobial activity of amphiphilic particles is possible to evaluate using physical and numerical approaches*, and the fourth hypothesis, *Employing structural molecular parameters of Gemini agents it is possible to assess their behavior and activity on physical models of membranes*, were confirmed.

To sum up, all provided hypotheses were confirmed in the course of achieving the main aim. The numerical simulations and computational approaches play an important role in antimicrobial-resistance assays. They can deliver a molecular insight into the interaction types or induced disorders. Moreover, they often set the paths for experiments to follow by delivering atomistic evidence, and this dissertation proves that.

Chapter 5

Streszczenie w j.polskim

Szerzący się problem antybiotykooporności bakterii wymusza zastosowanie wielu podejść interdyscyplinarnych. Przykładem takiego podejścia może być sprowadzenie go do postaci odpowiednich oddziaływań. Głównym celem tej rozprawy stało się opracowanie fizycznych i numerycznych modeli błon biologicznych, aby umożliwić ocenę aktywności przeciwdrobnoustrojowej cząsteczek o strukturze Gemini. W niniejszej pracy połączono podejścia w głównej mierze z fizyki oraz chemii i biologii celem stworzenia probabilistycznych oraz numerycznych modeli błon bakteryjnych pozwalających na ocenę wpływu związków powierzchniowo czynnych na fizykochemiczne i termodynamiczne parametry błon. Jedna z proponowanych koncepcji zakłada opis interakcji związku z błoną komórkową poprzez oddziaływania dipol-dipol w polu nie będącym polem zachowawczym ze względu na lepkość ośrodka. Zastosowana strategia sprowadzająca problem do oddziaływań fizycznych ma na celu dostarczenie szerszej perspektywy oraz wiedzy w nierównej walce z bakteriami opornymi na antybiotyki.

Szeroki wzrost oporności bakterii na środki przeciwdrobnoustrojowe został uznany w 2015r. przez Światową Organizację Zdrowia za jeden z 10 największych globalnych zagrożeń dla zdrowia ludzkości. Jeżeli do 2050 roku nie zostaną odkryte nowe leki, miliony osób będą ofiarami bakterii lekoopornych każdego roku. Szczególnie przytłaczająca jest ciągła ekspansja tak zwanych superbakterii, takich jak *Klebsiella pneumoniae*, powodująca szerokie spektrum infekcji i wykazująca ciągłe nabywanie oporności na leki nawet na te nazywane antybiotykami ostatniej szansy. Przyczyn uodparniania się mikroorganizmów jest wiele, m.in. ciągłe mutacje, czyli modyfikacje materiału genetycznego, nabywanie genów odporności od innych organizmów (transfer lateralny) czy nawet nieprawidłowo prowadzone antybiotykoterapie. Czynnik ludzki również silnie wypływa na uodparnianie się bakterii poprzez częste nadużywanie antybiotyków, przyjmowanie zbyt małych dawek lub zbyt krótki czas trwania antybiotykoterapii. Z biegiem czasu bakterie uciekają przed zabójczym działaniem antybiotyków, wykształcając swój własny mechanizm adaptacyjny. Obiecującym podejściem do rozwiązania tego problemu jest skupienie się na substancjach antyseptycznych, które nie mają dobrze zdefiniowanego celu molekularnego w komórkach bakteryjnych. Doniesiono, że niektóre z nich są środkami selektywnie atakującymi błony komórkowe poprzez oddziaływanie wywołujące jej destrukcję na drodze emulsyfikacji. Na rynku dostępnych jest kilka powszechnie stosowanych środków przeciwdrobnoustrojowych z rodziny kationowych środków powierzchniowo czynnych (surfaktantów Gemini). Jednymi z najbardziej znanych są oktenidyna (OCT) oraz chlorheksydyna (CHX), które skutecznie zwalczają bakterie Gram-dodatnie oraz Gram-ujemne. Dodatkowo każdego roku syntezowane są nowe związki o podwójnej (lustrzanej) strukturze Gemini, które wykazują potencjalne działanie antybakteryjne. Ze względu na różne protokoły stosowane przez grupy badawcze przy ocenie

skuteczności antybakteryjnej danych związków, problematyczne staje się porównanie wprost ich efektywności, czy wybranie potencjalnych prekursorów mogących w przyszłości zastąpić obecnie używane antybiotyki.

W ramach pracy dostarczono wgląd w molekularne oddziaływania OCT oraz CHX na błony ujemnie naładowane (np. bakteryjne) oraz neutralne (np. eukariontów). Wykorzystanie modeli biofizycznych wspartych metodami numerycznymi oraz eksperymentami pozwoliło na określenie preferencyjnego miejsca lokowania się związków, tworzonych przez nich agregatów, destrukcyjnego działania na błony, czy ocenę zmian parametrów mechanicznych błon pod wpływem działania analizowanych cząsteczek. Przeprowadzona analiza pozwoliła zaproponować nowatorski mechanizm selektywnego oddziaływania związków antybakteryjnych - zwłaszcza OCT, oparty o różnice emergentnych własności mechanicznych błon bakteryjnych i zwierzęcych.

W dalszym etapie badań poszukiwano innych związków o budowie Gemini, które wykazują silne działanie antybakteryjne. Poprzez stosowanie różnych protokołów oraz szczepów bakteryjnych przy określaniu aktywności biobójczej surfaktantów, niemożliwym stało się porównanie ich efektywności. W związku z tym utworzono bazę ponad 250 cząsteczek Gemini o potencjalnym działaniu bakteriobójczym, w której cząsteczki zaklasyfikowano do odpowiednich grup uwzględniając ich strukturę. Wykonane obliczenia kwantowe pozwoliły na zoptymalizowanie pól siłowych (ang. force fields) wszystkich zebranych molekuł. Stosując ujednolicony protokół oraz symulacje dynamiki molekularnej przetestowano wpływ 25 związków o potencjalnym działaniu bakteriobójczym na trójkomponentowych modelach błon bakteryjnych. Analiza parametrów biofizycznych i mechanicznych błon pozwoliła na wybranie 8 najlepiej rokujących prekursorów o możliwym najsilniejszym działaniu przeciwbakteryjnym.

W podejściach teoretycznych i badaniach obliczeniowych często pojawiają się pytania dotyczące dokładności i rzetelności prezentowanych modeli struktur biologicznych. Modele mogą znacznie odbiegać od rzeczywistych lub od eksperymentalnych analogów, co może skutkować nieprecyzyjnymi wnioskami. W związku z tym ramach kolejnych prac badawczych zaproponowano kompleksowy model numeryczny odzwierciedlający szczegółową (wielokomponentową) strukturę lipidową bakterii *Escherichia coli* oraz oceniono czy jego złożoność może istotnie wpływać na wnioski płynące z analiz numerycznych takiego modelu. Dogłębna analiza parametrów strukturalnych, dynamicznych oraz własności mechanicznych wykazała, że złożoność i skład modelu błony bakteryjnej ma kluczowe znaczenie i nie może być przybliżane przez dowolne, ujemnie naładowane lipidy. Potencjalny brak złożoności obecnych modeli numerycznych błon bakteryjnych bez wątpienia wpływa na zasadnicze źródła interakcji, przez co niektóre zjawiska biologiczne mogą pozostać nieuchwytne lub stłumione.

Świadomość ograniczeń metod eksperymentalnych oraz ugruntowanych metod numerycznych stała się inspiracją do stworzenia dedykowanej metodologii oraz autorskiego narzędzia symulacyjnego do szybkiej oceny potencjału antybakteryjnego surfaktantów Gemini. Symulacje dynamiki molekularnej pozwalają na ocenę zachowania związku względem błony oraz potencjalnego oddziaływania struktur. Metody szacowania energii swobodnej układu w precyzyjny sposób pozwalają na określenie zachowania cząsteczek antybakteryjnych w kontakcie z błoną, w tym zlokalizowanie barier energetycznych czy ocenę preferowanej lokacji molekuły w błonie. Stworzenie dokładnego profilu energetycznego cząsteczki typu Gemini w kontakcie z membraną jest procesem dość wymagającym obliczeniowo oraz czasochłonnym. Uproszczenie schematu oddziaływań i ograniczenie redundantnych parametrów pozwoliło na stworzenie autorskiego narzędzia *Diptool* do szybkiej analizy cząsteczek o potencjalnym działaniu antybakteryjnym. *Diptool* został oparty w głównej mierze na oddziaływaniach dipolowych lipidów oraz związków antybakteryjnych, a za całkowanie równań ruchu odpowiada zmodyfikowany algorytm Verleta. Korzystając z zależności struktura-funkcja (ang. quantitive structure-activity relationship) stworzono wzorzec is-

totnych statystycznie parametrów cząsteczek Gemini wpływających na ich aktywność czyli skuteczne działanie przeciwbakteryjne. Stworzenie probabilistycznego modelu błon biologicznych oraz implementacja wybranych parametrów w narzędziu *Diptool* pozwoliła w szybki sposób uzyskać odpowiedz na wystarczająco dokładnym poziomie czy cząsteczka penetruje błonę oraz jak wygląda rozkład energii swobodnej w procesie translokacji cząsteczki w poprzek błony. W efekcie końcowym pozwala to wprost oszacować jej potencjał antybakteryjny. Narzędzie zostało zwalidowane z użyciem metody Adaptive Biasing Force znanej z dynamiki molekularnej. Największą zaletą narzędzia jest jego szybkość działania, która pozwala w ciągu kilku minut otrzymać wyniki porównywalne z pełno-atomowymi symulacjami dynamiki molekularnej.

Podsumowując, w ramach pracy doktorskiej zaproponowano mechanizm selektywnego działania związków antybakteryjnych - OCT oraz CHX stosowanych na szeroką skalę. Następnie stworzono bazę cząsteczek Gemini i zaproponowano ujednolicony numeryczny protokół badania związków o charakterze bakteriobójczym. Dalej, zaproponowano ulepszony i kompleksowy model bakterii *E. coli* do zastosowań numerycznych. Na koniec stworzono autorskie narzędzie bazujące na zjawiskach fizycznych w układach biologicznych do analizy potencjału antybakteryjnego cząsteczek o strukturze Gemini. Rdzeniem pracy doktorskiej są cztery publikacje naukowe, w których powyższe osiągnięcia zostały opisane, uwzględniając metodykę, etap wdrażania oraz weryfikację założeń.

Bibliography

[1]   Fleming, A. (1929) On the Antibacterial Action of Cultures of a Penicillium, with Special Reference to their Use in the Isolation of B. influenzæ. *Br J Exp Pathol* 10, 226–236.

[2]   Ehrlich, P & Hata, S. (1910) *Die experimentelle Chemotherapie der Spirillosen.* (Springer, Berlin, Heidelberg).

[3]   Aminov, R. I. (2010) A Brief History of the Antibiotic Era: Lessons Learned and Challenges for the Future. *Frontiers in Microbiology* 1.

[4]   Enany, S & Alexander, L. (2017) in *The Rise of Virulence and Antibiotic Resistance in Staphylococcus aureus.* (IntechOpen).

[5]   Tortora, G. J, Berdell, F. R, & Case, C. L. (2015) *Microbiology : an introduction.* (Pearson), 12th edition, pp. 1–960.

[6]   Kirmusaoğlu, S, Gareayaghi, N, & Kocazeybek, B. S. (2019) *Antimicrobials, Antibiotic Resistance, Antibiofilm Strategies and Activity Methods* ed. Kirmusaoğlu, S. (IntechOpen), pp. 1–152.

[7]   Bian, X, Liu, X, Hu, F, Feng, M, Chen, Y, Bergen, P. J, Li, J, Li, X, Guo, Y, & Zhang, J. (2022) Pharmacokinetic/Pharmacodynamic Based Breakpoints of Polymyxin B for Bloodstream Infections Caused by Multidrug-Resistant Gram-Negative Pathogens. *Frontiers in Pharmacology* 12, 3747.

[8]   Takada, Y, Itoh, H, Paudel, A, Panthee, S, Hamamoto, H, Sekimizu, K, & Inoue, M. (2020) Discovery of gramicidin A analogues with altered activities by multidimensional screening of a one-bead-one-compound library. *Nature Communications 2020 11:1* 11, 1–10.

[9]   Feklistov, A, Mekler, V, Jiang, Q, Westblade, L. F, Irschik, H, Jansen, R, Mustaev, A, Darst, S. A, & Ebright, R. H. (2008) Rifamycins do not function by allosteric modulation of binding of Mg2+ to the RNA polymerase active center. *Proceedings of the National Academy of Sciences of the United States of America* 105, 14820–14825.

[10]   Marks, J, Kannan, K, Roncase, E. J, Klepacki, D, Kefi, A, Orelle, C, Vázquez-Laslop, N, & Mankin, A. S. (2016) Context-specific inhibition of translation by ribosomal antibiotics targeting the peptidyl transferase center. *Proceedings of the National Academy of Sciences of the United States of America* 113, 12150–12155.

[11]   Chopra, I & Roberts, M. (2001) Tetracycline Antibiotics: Mode of Action, Applications, Molecular Biology, and Epidemiology of Bacterial Resistance. *Microbiology and Molecular Biology Reviews* 65, 232.

[12] Nathan, C & Cars, O. (2014) Antibiotic Resistance — Problems, Progress, and Prospects. *New England Journal of Medicine* 371, 1761–1763.

[13] Aslam, B, Wang, W, Arshad, M. I, Khurshid, M, Muzammil, S, Rasool, M. H, Nisar, M. A, Alvi, R. F, Aslam, M. A, Qamar, M. U, Salamat, M. K. F, & Baloch, Z. (2018) Antibiotic resistance: a rundown of a global crisis. *Infection and Drug Resistance* 11, 1645.

[14] Sandner-Miranda, L, Vinuesa, P, Cravioto, A, & Morales-Espinosa, R. (2018) The genomic basis of intrinsic and acquired antibiotic resistance in the genus Serratia. *Frontiers in Microbiology* 9, 828.

[15] Impey, R. E, Hawkins, D. A, Sutton, J. M, & Soares da Costa, T. P. (2020) Overcoming Intrinsic and Acquired Resistance Mechanisms Associated with the Cell Wall of Gram-Negative Bacteria. *Antibiotics* 9, 623.

[16] Zhu, L, Lin, J, Ma, J, Cronan, J. E, & Wang, H. (2010) Triclosan resistance of Pseudomonas aeruginosa PAO1 is due to FabV, a triclosan-resistant enoyl-acyl carrier protein reductase. *Antimicrobial agents and chemotherapy* 54, 689–698.

[17] Mohsin, M, Raza, S, Roschanski, N, Guenther, S, Ali, A, & Schierack, P. (2017) Description of the First Escherichia coli Clinical Isolate Harboring the Colistin Resistance Gene mcr-1 from the Indian Subcontinent. *Antimicrobial Agents and Chemotherapy* 61.

[18] Poirel, L, Madec, J.-Y, Lupo, A, Schink, A.-K, Kieffer, N, Nordmann, P, & Schwarz, S. (2018) Antimicrobial Resistance in Escherichia coli. *Microbiology Spectrum* 6.

[19] World Health Organization. (2021) Global Antimicrobial Resistance and Use Surveillance System (GLASS) Report: 2021 (https://www.who.int/publications/i/item/9789240027336). Online; accessed 09 March 2022.

[20] Landers, T & Kavanagh, K. T. (2016) Is the Presidential Advisory Council on Combating Antibiotic Resistance missing opportunities? *AJIC: American Journal of Infection Control* 44, 1356–1359.

[21] Gould, I & Bal, A. (2013) New antibiotic agents in the pipeline and how they can help overcome microbial resistance. *Virulence* 4, 185–191.

[22] Bartlett, J. G, Gilbert, D. N, & Spellberg, B. (2013) Seven Ways to Preserve the Miracle of Antibiotics. *Clinical Infectious Diseases* 56, 1445–1450.

[23] Fleming-Dutra, K. E, Hersh, A. L, Shapiro, D. J, Bartoces, M, Enns, E. A, File, T. M, Finkelstein, J. A, Gerber, J. S, Hyun, D. Y, Linder, J. A, Lynfield, R, Margolis, D. J, May, L. S, Merenstein, D, Metlay, J. P, Newland, J. G, Piccirillo, J. F, Roberts, R. M, Sanchez, G. V, Suda, K. J, Thomas, A, Woo, T. M, Zetts, R. M, & Hicks, L. A. (2016) Prevalence of Inappropriate Antibiotic Prescriptions Among US Ambulatory Care Visits, 2010-2011. *JAMA* 315, 1864–1873.

[24] Lushniak, B. D. (2014) Surgeon General's Perspectives. *Public Health Reports* 129, 314.

[25] Saleem, Z, Saeed, H, Hassali, M. A, Godman, B, Asif, U, Yousaf, M, Ahmed, Z, Riaz, H, & Raza, S. A. (2019) Pattern of inappropriate antibiotic use among hospitalized patients in Pakistan: A longitudinal surveillance and implications. *Antimicrobial Resistance and Infection Control* 8, 1–7.

[26] Afari-Asiedu, S, Oppong, F. B, Tostmann, A, Ali Abdulai, M, Boamah-Kaali, E, Gyaase, S, Agyei, O, Kinsman, J, Hulscher, M, Wertheim, H. F, & Asante, K. P. (2020) Determinants of Inappropriate Antibiotics Use in Rural Central Ghana Using a Mixed Methods Approach. *Frontiers in Public Health* 8, 90.

[27] Tacconelli, E, Carrara, E, Savoldi, A, Kattula, D, & Burkert, F. (2017) Global priority list of antibiotic-resistant bacteria to guide research, discovery, and development of new antibiotics. (`https://www.who.int/medicines/publications/global-priority-list-antibiotic-resistant-bacteria/en/`). Online; accessed 09 March 2022.

[28] Tacconelli, E, Carrara, E, Savoldi, A, Harbarth, S, Mendelson, M, Monnet, D. L, Pulcini, C, Kahlmeter, G, Kluytmans, J, Carmeli, Y, Ouellette, M, Outterson, K, Patel, J, Cavaleri, M, Cox, E. M, Houchens, C. R, Grayson, M. L, Hansen, P, Singh, N, Theuretzbacher, U, Magrini, N, Aboderin, A. O, Al-Abri, S. S, Awang Jalil, N, Benzonana, N, Bhattacharya, S, Brink, A. J, Burkert, F. R, Cars, O, Cornaglia, G, Dyar, O. J, Friedrich, A. W, Gales, A. C, Gandra, S, Giske, C. G, Goff, D. A, Goossens, H, Gottlieb, T, Guzman Blanco, M, Hryniewicz, W, Kattula, D, Jinks, T, Kanj, S. S, Kerr, L, Kieny, M. P, Kim, Y. S, Kozlov, R. S, Labarca, J, Laxminarayan, R, Leder, K, Leibovici, L, Levy-Hara, G, Littman, J, Malhotra-Kumar, S, Manchanda, V, Moja, L, Ndoye, B, Pan, A, Paterson, D. L, Paul, M, Qiu, H, Ramon-Pardo, P, Rodríguez-Baño, J, Sanguinetti, M, Sengupta, S, Sharland, M, Si-Mehand, M, Silver, L. L, Song, W, Steinbakk, M, Thomsen, J, Thwaites, G. E, van der Meer, J. W, Van Kinh, N, Vega, S, Villegas, M. V, Wechsler-Fördös, A, Wertheim, H. F. L, Wesangula, E, Woodford, N, Yilmaz, F. O, & Zorzet, A. (2018) Discovery, research, and development of new antibiotics: the WHO priority list of antibiotic-resistant bacteria and tuberculosis. *The Lancet Infectious Diseases* 18, 318–327.

[29] Gogry, F. A, Siddiqui, M. T, Sultan, I, & Haq, Q. M. R. (2021) Current Update on Intrinsic and Acquired Colistin Resistance Mechanisms in Bacteria. *Frontiers in Medicine* 8, 1250.

[30] Hamel, M, Rolain, J. M, & Baron, S. A. (2021) The History of Colistin Resistance Mechanisms in Bacteria: Progress and Challenges. *Microorganisms 2021, Vol. 9, Page 442* 9, 442.

[31] World Health Organization. (2019) 2019 Antibacterial Agents in Clinical Development an analysis of the antibacterial clinical development pipeline (`https://apps.who.int/iris/bitstream/handle/10665/330420/9789240000193-eng.pdf`). Online; accessed 09 March 2022.

[32] Doi, Y. (2019) Treatment Options for Carbapenem-resistant Gram-negative Bacterial Infections. *Clinical Infectious Diseases* 69, S565–S575.

[33] WHO Antimicrobial Resistance Division. (2020) Global antimicrobial resistance and use surveillance system (GLASS) report (`http://www.who.int/glass/resources/publications/early-implementation-report-2020/en/`). Online; accessed 09 March 2022.

[34] Laxminarayan, R, Duse, A, Wattal, C, Zaidi, A. K, Wertheim, H. F, Sumpradit, N, Vlieghe, E, Hara, G. L, Gould, I. M, Goossens, H, Greko, C, So, A. D, Bigdeli, M, Tomson, G, Woodhouse, W, Ombaka, E, Peralta, A. Q, Qamar, F. N, Mir, F, Kariuki, S, Bhutta, Z. A, Coates, A, Bergstrom, R, Wright, G. D, Brown, E. D, & Cars, O. (2013) Antibiotic resistance—the need for global solutions. *The Lancet Infectious Diseases* 13, 1057–1098.

[35]   Schmid, A, Wolfensberger, A, Nemeth, J, Schreiber, P. W, Sax, H, & Kuster, S. P. (2019) Monother-
       apy versus combination therapy for multidrug-resistant Gram-negative infections: Systematic
       Review and Meta-Analysis. *Scientific Reports 2019 9:1* 9, 1–11.

[36]   Huan, Y, Kong, Q, Mou, H, & Yi, H. (2020) Antimicrobial Peptides: Classification, Design,
       Application and Research Progress in Multiple Fields. *Frontiers in Microbiology* 11, 2559.

[37]   Huang, T, Qian, Y, Fu, X, Huang, S, Li, Y, & Zhou, C. (2020) De Novo Design of Triblock
       Amphiphilic Short Antimicrobial Peptides. *ACS Applied Polymer Materials* 2, 3988–3992.

[38]   Stachurski, O, Neubauer, D, Małuch, I, Wyrzykowski, D, Bauer, M, Bartoszewska, S, Kamysz,
       W, & Sikorska, E. (2019) Effect of self-assembly on antimicrobial activity of double-chain short
       cationic lipopeptides. *Bioorganic Medicinal Chemistry* 27, 115129.

[39]   Pieroni, M, Wan, B, Cho, S, Franzblau, S. G, & Costantino, G. (2014) Design, synthesis and
       investigation on the structure–activity relationships of N-substituted 2-aminothiazole derivatives as
       antitubercular agents. *European Journal of Medicinal Chemistry* 72, 26–34.

[40]   Azzali, E, Machado, D, Kaushik, A, Vacondio, F, Flisi, S, Cabassi, C. S, Lamichhane, G, Viveiros,
       M, Costantino, G, & Pieroni, M. (2017) Substituted N-Phenyl-5-(2-(phenylamino)thiazol-4-
       yl)isoxazole-3-carboxamides Are Valuable Antitubercular Candidates that Evade Innate Efflux
       Machinery. *Journal of Medicinal Chemistry* 60, 7108–7122.

[41]   Fox, J. L. (2013) Antimicrobial peptides stage a comeback. *Nature Biotechnology* 31, 379–382.

[42]   Wilmes, M, Stockem, M, Bierbaum, G, Schlag, M, Götz, F, Tran, D. Q, Schaal, J. B, Ouellette, A. J,
       Selsted, M. E, & Sahl, H. G. (2014) Killing of Staphylococci by θ-Defensins Involves Membrane
       Impairment and Activation of Autolytic Enzymes. *Antibiotics 2014, Vol. 3, Pages 617-631* 3,
       617–631.

[43]   Omardien, S, Brul, S, & Zaat, S. A. (2016) Antimicrobial activity of cationic antimicrobial
       peptides against gram-positives: Current progress made in understanding the mode of action and
       the response of bacteria. *Frontiers in Cell and Developmental Biology* 4, 111.

[44]   Bechinger, B & Gorr, S. U. (2017) Antimicrobial Peptides: Mechanisms of Action and Resistance.
       Journal of Dental Research 96, 254–260.

[45]   Kunda, N. K. (2020) Antimicrobial peptides as novel therapeutics for non-small cell lung cancer.
       Drug Discovery Today 25, 238–247.

[46]   Swithenbank, L & Morgan, C. (2017) The Role of Antimicrobial Peptides in Lung Cancer Therapy.
       Journal of Antimicrobial Agents 03.

[47]   Silva, J. P, Appelberg, R, & Gama, F. M. (2016) Antimicrobial peptides as novel anti-tuberculosis
       therapeutics. *Biotechnology Advances* 34, 924–940.

[48]   Neubauer, D, Jaśkiewicz, M, Bauer, M, Olejniczak-Kęder, A, Sikorska, E, Sikora, K, & Kamysz,
       W. (2021) Biological and Physico-Chemical Characteristics of Arginine-Rich Peptide Gemini
       Surfactants with Lysine and Cystine Spacers. *International Journal of Molecular Sciences* 22,
       3299.

[49] Brycki, B. E, Kowalczyk, I. H, Szulc, A, Kaczerewska, O, & Pakiet, M. (2017) *Multifunctional Gemini Surfactants: Structure, Synthesis, Properties and Applications.* (IntechOpen).

[50] Gerba, C. P. (2015) Quaternary Ammonium Biocides: Efficacy in Application. *Applied and Environmental Microbiology* 81, 464.

[51] Kwaśniewska, D, Chen, Y. L, & Wieczorek, D. (2020) Biological Activity of Quaternary Ammonium Salts and Their Derivatives. *Pathogens* 9, 1–12.

[52] Cole, E. C, Addison, R. M, Rubino, J. R, Leese, K. E, Dulaney, P. D, Newell, M. S, Wilkins, J, Gaber, D. J, Wineinger, T, & Criger, D. A. (2003) Investigation of antibiotic and antibacterial agent cross-resistance in target bacteria from homes of antibacterial product users and nonusers. *Journal of applied microbiology* 95, 664–676.

[53] Koziróg, A & Brycki, B. (2015) Monomeric and gemini surfactants as antimicrobial agents - influence on environmental and reference strains. *Acta biochimica Polonica* 62, 879–883.

[54] Muslim, A. A, Ayyash, D, Gujral, S. S, Mekhail, G. M, Rao, P. P, & Wettig, S. D. (2017) Synthesis and characterization of asymmetrical gemini surfactants. *Physical chemistry chemical physics : PCCP* 19, 1953–1962.

[55] Zhang, S, Ding, S, Yu, J, Chen, X, Lei, Q, & Fang, W. (2015) Antibacterial Activity, in Vitro Cytotoxicity, and Cell Cycle Arrest of Gemini Quaternary Ammonium Surfactants. *Langmuir* 31, 12161–12169.

[56] Black, J. W, Jennings, M. C, Azarewicz, J, Paniak, T. J, Grenier, M. C, Wuest, W. M, & Minbiole, K. P. (2014) TMEDA-derived biscationic amphiphiles: An economical preparation of potent antibacterial agents. *Bioorganic Medicinal Chemistry Letters* 24, 99–102.

[57] Kowalczyk, I, Pakiet, M, Szulc, A, & Koziróg, A. (2020) Antimicrobial Activity of Gemini Surfactants with Azapolymethylene Spacer. *Molecules* 25.

[58] Malanovic, N, Ön, A, Pabst, G, Zellner, A, & Lohner, K. (2020) Octenidine: Novel insights into the detailed killing mechanism of Gram-negative bacteria at a cellular and molecular level. *International Journal of Antimicrobial Agents* 56, 106146.

[59] Steinhauer, K, Meister, T. L, Todt, D, Krawczyk, A, Paßvogel, L, Becker, B, Paulmann, D, Bischoff, B, Pfaender, S, Brill, F. H, & Steinmann, E. (2021) Comparison of the in-vitro efficacy of different mouthwash solutions targeting SARS-CoV-2 based on the European Standard EN 14476. *Journal of Hospital Infection* 111, 180–183.

[60] Clanner-Engelshofen, B. M, French, L. E, & Reinholz, M. (2020) Octenidine disinfection during the SARS-CoV-2 pandemia. *European Journal of Dermatology* 30, 613.

[61] Rzycki, M, Drabik, D, Szostak-Paluch, K, Hanus-Lorenz, B, & Kraszewski, S. (2021) Unraveling the mechanism of octenidine and chlorhexidine on membranes: Does electrostatics matter? *Biophysical Journal* 120, 3392–3408.

[62] Cieplik, F, Jakubovics, N. S, Buchalla, W, Maisch, T, Hellwig, E, & Al-Ahmad, A. (2019) Resistance toward chlorhexidine in oral bacteria-is there cause for concern? *Frontiers in Microbiology* 10.

[63] Leshem, T, Gilron, S, Azrad, M, & Peretz, A. (2022) Characterization of reduced susceptibility to chlorhexidine among Gram-negative bacteria. *Microbes and Infection* 24, 104891.

[64] Copin, R, Sause, W. E, Fulmer, Y, Balasubramanian, D, Dyzenhaus, S, Ahmed, J. M, Kumar, K, Lees, J, Stachel, A, Fisher, J. C, Drlica, K, Phillips, M, Weiser, J. N, Planet, P. J, Uhlemann, A. C, Altman, D. R, Sebra, R, van Bakel, H, Lighter, J, Torres, V. J, & Shopsin, B. (2019) Sequential evolution of virulence and resistance during clonal spread of community-acquired methicillin-resistant Staphylococcus aureus. *Proceedings of the National Academy of Sciences of the United States of America* 116, 1745–1754.

[65] Horner, C, Mawer, D, & Wilcox, M. (2012) Reduced susceptibility to chlorhexidine in staphylococci: is it increasing and does it matter? *Journal of Antimicrobial Chemotherapy* 67, 2547–2559.

[66] Balouiri, M, Sadiki, M, & Ibnsouda, S. K. (2016) Methods for in vitro evaluating antimicrobial activity: A review. *Journal of Pharmaceutical Analysis* 6, 71.

[67] Schuurmans, J. M, Nuri Hayali, A. S, Koenders, B. B, & ter Kuile, B. H. (2009) Variations in MIC value caused by differences in experimental protocol. *Journal of Microbiological Methods* 79, 44–47.

[68] Salton, M. R & Kim, K.-S. (1996) *Structure* ed. Baron, S. (University of Texas Medical Branch at Galveston, Galveston (TX)), 4th edition.

[69] Gram, C. (1884) Ueber die isolirte Farbung der Schizomyceten in Schnitt-und Trockenpraparaten. *Fortschritte der Medicin* pp. 185–189.

[70] Kamio, Y & Nikaido, H. (1976) Outer membrane of Salmonella typhimurium: accessibility of phospholipid head groups to phospholipase c and cyanogen bromide activated dextran in the external medium. *Biochemistry* 15, 2561–2570.

[71] Murzyn, K & Pasenkiewicz-Gierula, M. (2015) Structural properties of the water/membrane interface of a bilayer built of the E. coli Lipid A. *Journal of Physical Chemistry B* 119, 5846–5856.

[72] Silhavy, T. J, Kahne, D, & Walker, S. (2010) The Bacterial Cell Envelope. *Cold Spring Harbor Perspectives in Biology* 2.

[73] Gonzalez, T, Gaultney, R. A, Floden, A. M, & Brissette, C. A. (2015) Escherichia coli lipoprotein binds human plasminogen via an intramolecular domain. *Frontiers in Microbiology* 6, 1095.

[74] Mathelié-Guinlet, M, Asmar, A. T, Collet, J. F, & Dufrêne, Y. F. (2020) Lipoprotein Lpp regulates the mechanical properties of the E. coli cell envelope. *Nature Communications* 11, 1–11.

[75] Kefala, G, Ahn, C, Krupa, M, Esquivies, L, Maslennikov, I, Kwiatkowski, W, & Choe, S. (2010) Structures of the OmpF porin crystallized in the presence of foscholine-12. *Protein Science : A Publication of the Protein Society* 19, 1117.

[76] Choi, U & Lee, C. R. (2019) Distinct Roles of Outer Membrane Porins in Antibiotic Resistance and Membrane Integrity in Escherichia coli. *Frontiers in Microbiology* 10, 953.

[77] Cama, J, Bajaj, H, Pagliara, S, Maier, T, Braun, Y, Winterhalter, M, & Keyser, U. F. (2015) Quantification of Fluoroquinolone Uptake through the Outer Membrane Channel OmpF of Escherichia coli. *Journal of the American Chemical Society* 137, 13836–13843.

[78] Ziervogel, B. K & Roux, B. (2013) The Binding of Antibiotics in OmpF Porin. *Structure* 21, 76–87.

[79] Vollmer, W. (2015) Peptidoglycan. *Molecular Medical Microbiology: Second Edition* 1-3, 105–124.

[80] Gan, L, Chen, S, & Jensen, G. J. (2008) Molecular organization of Gram-negative peptidoglycan. *Proceedings of the National Academy of Sciences of the United States of America* 105, 18953–18957.

[81] Miller, S. I & Salama, N. R. (2018) The gram-negative bacterial periplasm: Size matters. *PLoS Biology* 16.

[82] Jacob-Dubuisson, F, Mechaly, A, Betton, J. M, & Antoine, R. (2018) Structural insights into the signalling mechanisms of two-component systems. *Nature Reviews Microbiology 2018 16:10* 16, 585–593.

[83] Kuhn, A, Koch, H.-G, & Dalbey, R. E. (2017) Targeting and Insertion of Membrane Proteins. *EcoSal Plus* 7.

[84] Hobot, J. A. (2015) Bacterial Ultrastructure. *Molecular Medical Microbiology: Second Edition* 1-3, 7–32.

[85] Durmort, C & Brown, J. S. (2015) Streptococcus pneumoniae Lipoproteins and ABC Transporters. *Streptococcus Pneumoniae: Molecular Mechanisms of Host-Pathogen Interactions* pp. 181–206.

[86] Oswald, J, Njenga, R, Natriashvili, A, Sarmah, P, & Koch, H. G. (2021) The Dynamic SecYEG Translocon. *Frontiers in Molecular Biosciences* 8, 248.

[87] Sueki, A, Stein, F, Savitski, M. M, Selkrig, J, & Typas, A. (2020) Systematic Localization of Escherichia coli Membrane Proteins. *mSystems* 5.

[88] Pasenkiewicz-Gierula, M, Baczynski, K, Markiewicz, M, & Murzyn, K. (2016) Computer modelling studies of the bilayer/water interface. *Biochimica et Biophysica Acta (BBA) - Biomembranes* 1858, 2305–2321.

[89] Sohlenkamp, C & Geiger, O. (2016) Bacterial membrane lipids: diversity in structures and pathways. *FEMS Microbiology Reviews* 40, 133–159.

[90] Epand, R. M & Epand, R. F. (2009) Lipid domains in bacterial membranes and the action of antimicrobial agents. *Biochimica et Biophysica Acta (BBA) - Biomembranes* 1788, 289–294.

[91] Tang, X, Chang, S, Qiao, W, Luo, Q, Chen, Y, Jia, Z, Coleman, J, Zhang, K, Wang, T, Zhang, Z, Zhang, C, Zhu, X, Wei, X, Dong, C, Zhang, X, & Dong, H. (2020) Structural insights into outer membrane asymmetry maintenance in Gram-negative bacteria by MlaFEDB. *Nature Structural Molecular Biology 2020 28:1* 28, 81–91.

[92] Durrant, J. D & McCammon, J. A. (2011) Molecular dynamics simulations and drug discovery. *BMC Biology* 9, 1–9.

[93] McCammon, J. A, Gelin, B. R, & Karplus, M. (1977) Dynamics of folded proteins. *Nature* 267, 585–590.

[94] Levitt, M & Warshel, A. (1975) Computer simulation of protein folding. *Nature 1975 253:5494* 253, 694–698.

[95] Schlick, T. (2015) in *Encyclopedia of Applied and Computational Mathematics.* (Springer, Berlin, Heidelberg), pp. 940–951.

[96] Zhang, C, Lu, C, Jing, Z, Wu, C, Piquemal, J. P, Ponder, J. W, & Ren, P. (2018) AMOEBA Polarizable Atomic Multipole Force Field for Nucleic Acids. *Journal of Chemical Theory and Computation* 14, 2084–2108.

[97] Thompson, A. P, Aktulga, H. M, Berger, R, Bolintineanu, D. S, Brown, W. M, Crozier, P. S, in 't Veld, P. J, Kohlmeyer, A, Moore, S. G, Nguyen, T. D, Shan, R, Stevens, M. J, Tranchida, J, Trott, C, & Plimpton, S. J. (2022) LAMMPS - a flexible simulation tool for particle-based materials modeling at the atomic, meso, and continuum scales. *Computer Physics Communications* 271, 108171.

[98] Doherty, B, Zhong, X, Gathiaka, S, Li, B, & Acevedo, O. (2017) Revisiting OPLS Force Field Parameters for Ionic Liquid Simulations. *Journal of Chemical Theory and Computation* 13, 6131–6135.

[99] Jorgensen, W. L, Maxwell, D. S, & Tirado-Rives, J. (1996) Development and testing of the OPLS all-atom force field on conformational energetics and properties of organic liquids. *Journal of the American Chemical Society* 118, 11225–11236.

[100] Li, H, Chowdhary, J, Huang, L, He, X, MacKerell, A. D, & Roux, B. (2017) Drude Polarizable Force Field for Molecular Dynamics Simulations of Saturated and Unsaturated Zwitterionic Lipids. *Journal of Chemical Theory and Computation* 13, 4535–4552.

[101] Marrink, S. J, Risselada, H. J, Yefimov, S, Tieleman, D. P, & De Vries, A. H. (2007) The MARTINI Force Field: Coarse Grained Model for Biomolecular Simulations. *Journal of Physical Chemistry B* 111, 7812–7824.

[102] Vanommeslaeghe, K, Hatcher, E, Acharya, C, Kundu, S, Zhong, S, Shim, J, Darian, E, Guvench, O, Lopes, P, Vorobyov, I, & Mackerell, A. D. (2010) CHARMM general force field: A force field for drug-like molecules compatible with the CHARMM all-atom additive biological force fields. *Journal of Computational Chemistry* 31, 671–690.

[103] Pastor, R. W & MacKerell, A. D. (2011) Development of the CHARMM force field for lipids. *Journal of Physical Chemistry Letters* 2, 1526–1532.

[104] Wang, J, Wolf, R. M, Caldwell, J. W, Kollman, P. A, & Case, D. A. (2004) Development and testing of a general amber force field. *Journal of Computational Chemistry* 25, 1157–1174.

[105] Reif, M. M, Hünenberger, P. H, & Oostenbrink, C. (2012) New interaction parameters for charged amino acid side chains in the GROMOS force field. *Journal of Chemical Theory and Computation* 8, 3705–3723.

[106] Hopkins, C. W, Le Grand, S, Walker, R. C, & Roitberg, A. E. (2015) Long-time-step molecular dynamics through hydrogen mass repartitioning. *Journal of Chemical Theory and Computation* 11, 1864–1874.

[107] Ozboyaci, M, Kokh, D. B, Corni, S, & Wade, R. C. (2016) Modeling and simulation of protein–surface interactions: achievements and challenges. *Quarterly Reviews of Biophysics* 49.

[108] Van Mourik, T, Bühl, M, & Gaigeot, M. P. (2014) Density functional theory across chemistry, physics and biology. *Philosophical transactions. Series A, Mathematical, physical, and engineering sciences* 372.

[109] Yesylevskyy, S, Cardey, B, Kraszewski, S, Foley, S, Enescu, M, da Silva, A. M, Santos, H. F, & Ramseyer, C. (2015) Empirical force field for cisplatin based on quantum dynamics data: case study of new parameterization scheme for coordination compounds. *Journal of Molecular Modeling* 21, 1–9.

[110] Mayne, C. G, Saam, J, Schulten, K, Tajkhorshid, E, & Gumbart, J. C. (2013) Rapid parameterization of small molecules using the force field toolkit. *Journal of Computational Chemistry* 34, 2757–2770.

[111] Singh, N & Li, W. (2019) Recent Advances in Coarse-Grained Models for Biomolecules and Their Applications. *International Journal of Molecular Sciences* 20, 3774.

[112] Chen, C, Depa, P, Sakai, V. G, Maranas, J. K, Lynn, J. W, Peral, I, & Copley, J. R. (2006) A comparison of united atom, explicit atom, and coarse-grained simulation models for poly(ethylene oxide). *The Journal of Chemical Physics* 124, 234901.

[113] Rzycki, M, Kraszewski, S, & Gładysiewicz-Kudrawiec, M. (2021) Diptool—A novel numerical tool for membrane interactions analysis, applying to antimicrobial detergents and drug delivery aids. *Materials* 14, 6455.

[114] Bolhuis, P. G, Chandler, D, Dellago, C, & Geissler, P. L. (2002) Tranition Path Sampling: Throwing Ropes Over Rough Mountain Passes, in the Dark. *Annual Review of Physical Chemistry* 53, 291–318.

[115] Laidler, K. J & King, M. C. (1983) Development of transition-state theory. *Journal of Physical Chemistry* 87, 2657–2664.

[116] Zwanzig, R. W. (2004) High-Temperature Equation of State by a Perturbation Method. I. Nonpolar Gases. *The Journal of Chemical Physics* 22, 1420.

[117] Song, L. F & Merz, K. M. (2020) Evolution of alchemical free energy methods in drug discovery. *Journal of Chemical Information and Modeling* 60, 5308–5318.

[118] De Vivo, M, Masetti, M, Bottegoni, G, & Cavalli, A. (2016) Role of Molecular Dynamics and Related Methods in Drug Discovery. *Journal of Medicinal Chemistry* 59, 4035–4061.

[119] Kästner, J. (2011) Umbrella sampling. *Wiley Interdisciplinary Reviews: Computational Molecular Science* 1, 932–942.

[120] Do, P. C, Lee, E. H, & Le, L. (2018) Steered Molecular Dynamics Simulation in Rational Drug Design. *Journal of Chemical Information and Modeling* 58, 1473–1482.

[121] Róg, T, Girych, M, & Bunker, A. (2021) Mechanistic Understanding from Molecular Dynamics in Pharmaceutical Research 2: Lipid Membrane in Drug Design. *Pharmaceuticals* 14, 1062.

[122] Valsson, O, Tiwary, P, & Parrinello, M. (2016) Enhancing Important Fluctuations: Rare Events and Metadynamics from a Conceptual Viewpoint. *Annual Review of Physical Chemistry* 67, 159–184.

[123] Bussi, G & Laio, A. (2020) Using metadynamics to explore complex free-energy landscapes. *Nature Reviews Physics* 2, 200–212.

[124] Tribello, G. A, Ceriotti, M, & Parrinello, M. (2010) A self-learning algorithm for biased molecular dynamics. *Proceedings of the National Academy of Sciences of the United States of America* 107, 17509–17514.

[125] Sugita, Y & Okamoto, Y. (1999) Replica-exchange molecular dynamics method for protein folding. *Chemical Physics Letters* 314, 141–151.

[126] Oshima, H, Re, S, & Sugita, Y. (2019) Replica-Exchange Umbrella Sampling Combined with Gaussian Accelerated Molecular Dynamics for Free-Energy Calculation of Biomolecules. *Journal of Chemical Theory and Computation* 15, 5199–5208.

[127] Hénin, J, Fiorin, G, Chipot, C, & Klein, M. L. (2009) Exploring Multidimensional Free Energy Landscapes Using Time-Dependent Biases on Collective Variables. *Journal of Chemical Theory and Computation* 6, 35–47.

[128] Darve, E, Rodríguez-Gómez, D, & Pohorille, A. (2008) Adaptive biasing force method for scalar and vector free energy calculations. *The Journal of Chemical Physics* 128, 144120.

[129] Carter, E. A, Ciccotti, G, Hynes, J. T, & Kapral, R. (1989) Constrained reaction coordinate dynamics for the simulation of rare events. *Chemical Physics Letters* 156, 472–477.

[130] Bonhenry, D, Tarek, M, & Dehez, F. (2013) Effects of phospholipid composition on the transfer of a small cationic peptide across a model biological membrane. *Journal of Chemical Theory and Computation* 9, 5675–5684.

[131] Kraszewski, S, Bianco, A, Tarek, M, & Ramseyer, C. (2012) Insertion of Short Amino-Functionalized Single-Walled Carbon Nanotubes into Phospholipid Bilayer Occurs by Passive Diffusion. *PLOS ONE* 7, e40703.

[132] Comer, J, Gumbart, J. C, Hénin, J, Lelievre, T, Pohorille, A, & Chipot, C. (2015) The adaptive biasing force method: Everything you always wanted to know but were afraid to ask. *Journal of Physical Chemistry B* 119, 1129–1151.

[133] Sharma, P, Parthasarathi, S, Patil, N, Waskar, M, Raut, J. S, Puranik, M, Ayappa, K. G, & Basu, J. K. (2020) Assessing Barriers for Antimicrobial Penetration in Complex Asymmetric Bacterial Membranes: A Case Study with Thymol. *Langmuir* 36, 8800–8814.

[134] Kholina, E. G, Kovalenko, I. B, Bozdaganyan, M. E, Strakhovskaya, M. G, & Orekhov, P. S. (2020) Cationic Antiseptics Facilitate Pore Formation in Model Bacterial Membranes. *Journal of Physical Chemistry B* 124, 8593–8600.

[135] Rzycki, M, Kaczorowska, A, Kraszewski, S, & Drabik, D. (2021) A systematic approach: Molecular dynamics study and parametrisation of gemini type cationic surfactants. *International Journal of Molecular Sciences* 22, 10939.

[136] Van Oosten, B, Marquardt, D, Komljenović, I, Bradshaw, J. P, Sternin, E, & Harroun, T. A. (2014) Small molecule interaction with lipid bilayers: A molecular dynamics study of chlorhexidine. *Journal of Molecular Graphics and Modelling* 48, 96–104.

[137] Van Oosten, B, Marquardt, D, & Harroun, T. A. (2017) Testing High Concentrations of Membrane Active Antibiotic Chlorhexidine Via Computational Titration and Calorimetry. *Journal of Physical Chemistry B* 121, 4657–4668.

[138] John, T, Thomas, T, Abel, B, Wood, B. R, Chalmers, D. K, & Martin, L. L. (2017) How kanamycin A interacts with bacterial and mammalian mimetic membranes. *Biochimica et Biophysica Acta (BBA) - Biomembranes* 1859, 2242–2252.

[139] Kumar, S, Thakur, J, Yadav, K, Mitra, M, Pal, S, Ray, A, Gupta, S, Medatwal, N, Gupta, R, Mishra, D, Rani, P, Padhi, S, Sharma, P, Kapil, A, Srivastava, A, Priyakumar, U. D, Dasgupta, U, Thukral, L, & Bajaj, A. (2019) Cholic Acid-Derived Amphiphile which Combats Gram-Positive Bacteria-Mediated Infections via Disintegration of Lipid Clusters. *ACS Biomaterials Science and Engineering* 5, 4764–4775.

[140] Matyszewska, D. (2020) The influence of charge and lipophilicity of daunorubicin and idarubicin on their penetration of model biological membranes – Langmuir monolayer and electrochemical studies. *Biochimica et Biophysica Acta (BBA) - Biomembranes* 1862, 183104.

[141] Khurana, E, Devane, R. H, Dal Peraro, M, & Klein, M. L. (2011) Computational study of drug binding to the membrane-bound tetrameric M2 peptide bundle from influenza A virus. *Biochimica et Biophysica Acta (BBA) - Biomembranes* 1808, 530–537.

[142] Konstantinidi, A, Chountoulesi, M, Naziris, N, Sartori, B, Amenitsch, H, Mali, G, Čendak, T, Plakantonaki, M, Triantafyllakou, I, Tselios, T, Demetzos, C, Busath, D. D, Mavromoustakos, T, & Kolocouris, A. (2020) The boundary lipid around DMPC-spanning influenza A M2 transmembrane domain channels: Its structure and potential for drug accommodation. *Biochimica et Biophysica Acta (BBA) - Biomembranes* 1862, 183156.

[143] Konstantinidi, A, Naziris, N, Chountoulesi, M, Kiriakidi, S, Sartori, B, Kolokouris, D, Amentisch, H, Mali, G, Ntountaniotis, D, Demetzos, C, Mavromoustakos, T, & Kolocouris, A. (2018) Comparative Perturbation Effects Exerted by the Influenza A M2 WT Protein Inhibitors Amantadine and the Spiro[pyrrolidine-2,2-adamantane] Variant AK13 to Membrane Bilayers Studied Using Biophysical Experiments and Molecular Dynamics Simulations. *Journal of Physical Chemistry B* 122, 9877–9895.

[144] Rzycki, M, Kraszewski, S, & Drabik, D. (2021) Towards Mimetic Membrane Systems in Molecular Dynamics: Characteristics of Membrane System. *ICCS 2021, Lecture Notes in Computer Science* 12743, 551–563.

[145] Ferreira, R. L, Da Silva, B. C, Rezende, G. S, Nakamura-Silva, R, Pitondo-Silva, A, Campanini, E. B, Brito, M. C, Da Silva, E. M, De Melo Freire, C. C, Da Cunha, A. F, & Da Silva Pranchevicius, M. C. (2019) High prevalence of multidrug-resistant klebsiella pneumoniae harboring several virulence and β-lactamase encoding genes in a brazilian intensive care unit. *Frontiers in Microbiology* 10, 3198.

[146] Banerjee, D, Sarkar, U, & Roy, D. (2013) Multicomponent adsorption of chlorhexidine gluconate in presence of a cationic surfactant: Role of electrostatic interactions and surface complexation. *Journal of Environmental Chemical Engineering* 1, 241–251.

[147] Strakhovskaya, M. G, Lukashev, E. P, Korvatovskiy, B. N, Kholina, E. G, Seifullina, N. K, Knox, P. P, & Paschenko, V. Z. (2021) The effect of some antiseptic drugs on the energy transfer in chromatophore photosynthetic membranes of purple non-sulfur bacteria Rhodobacter sphaeroides. *Photosynthesis Research* 147, 197–209.

[148] Komljenović, I, Marquardt, D, Harroun, T. A, & Sternin, E. (2010) Location of chlorhexidine in DMPC model membranes: a neutron diffraction study. *Chemistry and Physics of Lipids* 163, 480–487.

[149] Faizi, H. A, Frey, S. L, Steinkühler, J, Dimova, R, & Vlahovska, P. M. (2019) Bending rigidity of charged lipid bilayer membranes. *Soft Matter* 15, 6006–6013.

[150] Matuła, K, Richter, Ł, Janczuk-Richter, M, Nogala, W, Grzeszkowiak, M, Peplińska, B, Jurga, S, Wyroba, E, Suski, S, Bilski, H, Silesian, A, Bluyssen, H. A, Derebecka, N, Wesoły, J, Łoś, J. M, Łoś, M, Decewicz, P, Dziewit, L, Paczesny, J, & Hołyst, R. (2019) Phenotypic plasticity of Escherichia coli upon exposure to physical stress induced by ZnO nanorods. *Scientific Reports 2019 9:1* 9, 1–12.

[151] Giannelli, M, Chellini, F, Margheri, M, Tonelli, P, & Tani, A. (2008) Effect of chlorhexidine digluconate on different cell types: A molecular and ultrastructural investigation. *Toxicology in Vitro* 22, 308–317.

[152] Mouton, J. W, Meletiadis, J, Voss, A, & Turnidge, J. (2018) Variation of MIC measurements: the contribution of strain and laboratory variability to measurement precision. *Journal of Antimicrobial Chemotherapy* 73, 2374–2379.

[153] Catania, S, Bottinelli, M, Fincato, A, Gastaldelli, M, Barberio, A, Gobbo, F, & Vicenzoni, G. (2019) Evaluation of Minimum Inhibitory Concentrations for 154 Mycoplasma synoviae isolates from Italy collected during 2012-2017. *PLOS ONE* 14, e0224903.

[154] Brycki, B. E, Szulc, A, Kowalczyk, I, Koziróg, A, & Sobolewska, E. (2021) Antimicrobial Activity of Gemini Surfactants with Ether Group in the Spacer Part. *Molecules 2021* 26, 5759.

[155] Wu, E. L, Engström, O, Jo, S, Stuhlsatz, D, Yeom, M. S, Klauda, J. B, Widmalm, G, & Im, W. (2013) Molecular dynamics and NMR spectroscopy studies of E. coli lipopolysaccharide structure and dynamics. *Biophysical Journal* 105, 1444–1455.

[156] Hwang, H, Paracini, N, Parks, J. M, Lakey, J. H, & Gumbart, J. C. (2018) Distribution of mechanical stress in the Escherichia coli cell envelope. *Biochimica et Biophysica Acta (BBA) - Biomembranes* 1860, 2566–2575.

[157] Piggot, T. J, Holdbrook, D. A, & Khalid, S. (2013) Conformational dynamics and membrane interactions of the E. coli outer membrane protein FecA: A molecular dynamics simulation study. *Biochimica et Biophysica Acta (BBA) - Biomembranes* 1828, 284–293.

[158] Chen, J, Zhou, G, Chen, L, Wang, Y, Wang, X, & Zeng, S. (2016) Interaction of Graphene and its Oxide with Lipid Membrane: A Molecular Dynamics Simulation Study. *Journal of Physical Chemistry C* 120, 6225–6231.

[159] Drabik, D, Chodaczek, G, Kraszewski, S, & Langner, M. (2020) Mechanical Properties Determination of DMPC, DPPC, DSPC, and HSPC Solid-Ordered Bilayers. *Langmuir* 36, 3826–3835.

Chapter 6

Paper 1

Unraveling the mechanism of octenidine and chlorhexidine on membranes: Does electrostatics matter?

Unraveling the mechanism of octenidine and chlorhexidine on membranes: Does electrostatics matter?

Mateusz Rzycki,[1,2,*] Dominik Drabik,[2,3] Kamila Szostak-Paluch,[2,4] Beata Hanus-Lorenz,[2] and Sebastian Kraszewski[2]

[1]Department of Experimental Physics and [2]Department of Biomedical Engineering, Faculty of Fundamental Problems of Technology, Wroclaw University of Science and Technology, Wroclaw, Poland; [3]Laboratory of Cytobiochemistry, Faculty of Biotechnology, University of Wroclaw, Wroclaw, Poland; and [4]Research and Development Center, Regional Specialized Hospital, Wroclaw, Poland

ABSTRACT   The increasing problem of antibiotic resistance in bacteria requires the development of new antimicrobial candidates. There are several well-known substances with commercial use, but their molecular mode of action is not fully understood. In this work, we focus on two commonly used antimicrobial agents from the detergent family—octenidine dichloride (OCT) and chlorhexidine digluconate (CHX). Both of them are reported to be agents selectively attacking the cell membrane through interaction inducing membrane disruption by emulsification. They are believed to present electrostatic selectivity toward charged lipids. In this study, we tested this hypothesis and revised previously proposed molecular mechanisms of action. Employing a variety of techniques such as molecular dynamics, ζ potential with dynamic light scattering, vesicle fluctuation spectroscopy, carboxyfluorescein leakage measurement, and fluorescence trimethylammonium-diphenylhexatriene- and diphenylhexatriene-based studies for determination of OCT and CHX membrane location, we performed experimental studies using two model membrane systems—zwitterionic PC and negatively charged PG (18:1/18:1):PC (16:0/18:1) 3:7, respectively. These studies were extended by molecular dynamics simulations performed on a three-component bacterial membrane model system to further test interactions with another negatively charged lipid, cardiolipin. In summary, our study demonstrated that detergent selectivity is far more complicated than supposed simple electrostatic interactions. Although OCT does disrupt the membrane, our results suggest that its primary selectivity was more linked to mechanical properties of the membrane. On the other hand, CHX did not disrupt membranes as a primary activity, nor did it show any sign of electrostatic selectivity toward negatively charged membranes at any stage of interactions, which suggests membrane disruption by influencing more discrete membrane properties.

SIGNIFICANCE   The common abuse of antibiotics caused bacteria to develop effective drug resistance over the years. The World Health Organization states that it is one of the biggest threats nowadays. An approach to address this problem is to focus on antiseptic substances that do not have a well-defined molecular target in bacterial cells. As a result, the development of resistance is reduced or even prevented. However, although the substances are commonly used, the knowledge of their mechanism and behavior is limited. Hence, there is a need for more study of these compounds to enable further development. In this work, we employed advanced experimental and computational methods to study the mechanism and selectivity of two commonly used antiseptics, octenidine and chlorhexidine.

INTRODUCTION

The rapidly spreading antibiotic resistance of bacteria has been recognized as a potentially catastrophic threat over the next few years. Because of the common abuse of antibi-

otics, through genetic adaptation bacteria have developed effective drug resistance (1), and the forecast is not optimistic. The World Health Organization states that it is one of the biggest threats to global health, food security, and development nowadays (2). Millions more people will start dying every year unless new antimicrobial substances are discovered by 2050. This phenomenon is accelerating because of the constant mutations, horizontal gene transfer between the microorganisms, improperly conducted

antibiotic therapies, and overuse of antibiotics in animal production (3). As a result, substances previously known to save lives will not fulfill their function. A well-known example is the story of penicillin and β-lactam antibiotic resistance (4). One approach to address this problem is to focus on antiseptic substances with a broad spectrum of activity. Such substances do not have a well-defined molecular target in bacterial cells. Interaction with different cellular structures simultaneously makes it harder to develop resistance based on suitable mutations in genetic material. A further advantage is the potential for local application with higher concentration, directly on the skin, mucous membranes, or wounds (5). Another approach is the use of agents with understood and designed molecular selectivity toward the most slowly evolving bacterial structures such as their lipid membrane. Numerous widely used antiseptics belong to the cationic surfactants class. Two of them— chlorhexidine digluconate (CHX) and octenidine dihydrochloride (OCT)—are known for their broad-spectrum activity with a not completely understood molecular mode of action. They are commonly used in various antimicrobial products available on the market, such as Octenisept (Schülke & Mayr, Germany) or Eludril (Pierre Fabre, French), for skin and oral applications (6).

Octenidine dihydrochloride is an antiseptic agent originally described in the 1980s. It is a cationic surfactant that belongs to the bispyridine class (7). Its structure consists of two noninteracting cationic rings separated by a hydrocarbon chain. It exhibits activity against both Gram-positive and Gram-negative bacteria (7,8). A concentration of octenidine less than 1.5 μM (0.94 μg/mL) was reported to decrease the population of tested organisms by more than 99% within 15 min of application (9). It differs from other well-known compounds such as quaternary ammonium compounds because of the lack of an amide and ester component within the structure. As a result, OCT toxicity is lower, and a common quaternary ammonium compound toxic metabolite known as 4-nitroaniline cannot be formed during structural changes (7). OCT is stable over the whole pH range 1.6–12.2, which is particularly important considering varying conditions of healing wounds (10). The wide use of OCT as an antiseptic agent and a number of research articles indicate the incapability of microorganisms to adapt to the presence of this molecule (11). However, the exact mechanism of octenidine action is not well understood. Kodevova et al. noted that OCT creates nontoxic complexes at the site of action (12) It was also indicated that there is strong binding to the negatively charged elements of the yeast cell membrane, leading to disintegration of the cell membrane. When the negatively charged membrane was used as a model and incubated with 3 μM OCT solution, a significant part of it was destroyed after 3 min (12). Selectivity of action was also reported. Recently, a different mode of action was proposed (13). Specifically, because of electrostatic interactions, OCT immediately at-

taches to the outer membrane, leading to neutralization of the bacterial surface charge. This is followed by OCT hydrocarbon interfering with fatty acyl chains in the outer membrane and inducing strong disorder, disturbing integrity, and causing depolarization and loss of packing order. The literature does not indicate any negative impact of this agent on human epithelial cells or the healing process. Both Brill et al. and Hubner et al. suggested strong adhesion of OCT to bacterial cell membrane components (e.g., cardiolipin) (14,15). It may suggest a selective mechanism of action, as no toxic effect was observed in human epithelial cells. Assadian suggested that the mechanism of OCT is based on interactions with glycerol phosphates present in the microorganism membrane and the enzymatic system, which results in cytoplasmic leakage and cell death (7). Based on available literature, the presumed mode of action is not associated with a specific metabolic pathway or target protein but acts more comprehensively. Most of the currently suggested mechanisms of action involve attack on cell or lipid membrane with electric charge dependency. Also, some works mention the possible occurrence of resistance to OCT (16–18). A significant change in shape, and possible change in membrane composition, was observed to counter the antimicrobial effect of OCT, which may be considered as the first steps in the development of an OCT resistance mechanism. Dopcea et al. reported that OCT exposure resulted in an increased minimal inhibitory concentration (MIC) in *Staphylococcus aureus* and *S. epidermidis* strains (17). In the same study, they reported that the minimal bactericidal concentration, which is the lowest concentration of an antibacterial agent required to kill a bacterium, had increased significantly in a clinical isolate of *S. aureus* (17). In another approach, Shepherd et al. exposed *Pseudomonas aeruginosa* strains to increased concentrations of OCT (18). Their results demonstrate that *P. aeruginosa* can resist great doses of in-use OCT formulations, and furthermore, it can adapt to OCT in a clinical setup, leading to increased OCT tolerance.

The second substance, chlorhexidine, is an antiseptic agent originally described in the 1950s. It is a divalent, cationic biguanidine that exists in three forms: gluconate, acetate, and hydrochloride salt (19). Its net charge is zero, but in solution it dissociates and becomes positively charged. It is most commonly used in concentrations of 0.5–4.0% in the form of gluconate. This compound has a wide spectrum of action against Gram-positive bacteria, but worse (20 times lower MIC value) results are achieved with Gram-negative bacteria (20–22) such as *P. aeruginosa* and *Providencia stuartii*. Some groups report solving this issue by using chelators. The antimicrobial properties of chlorhexidine have remained strong over the years, which suggests limited resistance development by bacteria (23,24). Any observed changes of MIC in the previous century were believed to be caused by composition modification of used model membranes but not increasing

bacteria resistance (23,25). However, Horner et al. draw attention to the increasing number of reports on the reduction in microbial susceptibility to CHX (19). Recently, Copin et al. reported that the spread of community-associated methicillin-resistant *S. aureus* was caused by the acquisition of resistance genes to chlorhexidine agents (26). Also noteworthy are reports collected by Cieplik et al. indicating the presence of CHX resistance at the genetic level in *P. stutzeri* and in different staphylococci (27). The authors also emphasize the need to standardize the concept of resistance in the context of CHX because the research was conducted mainly on Gram-negative bacteria (19). Nevertheless, a few studies investigating the effect of chlorhexidine on Gram-positive bacteria have been conducted. For instance, Cheung et al. concluded that *Bacillus subtilis* is more susceptible to CHX action because more proteins were lost from those cells compared with *Escherichia coli* cells (28). The mechanism of action remains unclear, despite several studies being carried out. Chawner et al. suggested that the mechanism of antimicrobial action of CHX is related to biguanidine structure. In detail, the biguanide group exhibits a strong association with exposed anionic centers on the membrane and negatively charged extracellular matrix's acid phospholipid groups and proteins (29,30). Binding of biguanides to these structures may cause displacement of bivalent Mg^{2+} and Ca^{2+} cations, bound to the cell bilayer, which leads to leakage of potassium cations and protons through the membrane. Therefore, CHX disrupts the osmotic balance of the cell (31). Additionally, CHX hydrophobic regions are not dissolved in the membrane core. As a result, a six-carbon chain linking (coupling) the rings in CHX cannot be incorporated sufficiently in the bilayer. Hence, CHX forms bridges between adjacent phosphate groups of phospholipids and displaces the associated divalent cation from the system (Mg^{2+} and Ca^{2+}). At lower concentrations, CHX causes membrane fluidity reduction and dysfunction both in osmoregulation and in metabolic efficiency of the membrane enzymes, causing leakage of potassium ions and protons from the microbial cell, inhibition of respiratory activity, and transport of dissolved substances (27,32–35). At high concentrations, membrane transition to the liquid crystal phase occurs, which is accompanied by integrity loss and rapid, massive leakage from the cell (29,30,36,37). Another suggestion was proposed by Banerjee et al. in 2013 (38). They examined CHX adsorption on the surface. It was determined that surface charge is one of the most important factors in CHX antimicrobial mechanism of action (38). These findings are consistent with the work by Freitas et al., in which electrostatic effects were emphasized and CHX had a reducing effect on the interfacial tension (39). Costalonga et al. (40) observed noticeable CHX activity in various dental surface models, showing that intrinsic interactions of the drug with the hydrophobic part of the lipid membrane led to disruption of the lipid organization at the interphase. Additionally, the

secondary structure of the polypeptide model was changed as a result of CHX action. Moreover, the described interactions between lipid and protein moieties are believed to be present in membranes and may have a specific implication for understanding how antiseptics act on the bacterial membrane (40). Based on the available literature, it can be assumed that the effect of CHX is comprehensive. It not only affects potassium ions, by disrupting osmotic balance, but also interacts with lipid membranes by creating bridges between lipid head molecules.

Despite numerous attempts to unravel the exact molecular mechanism of action for both CHX and OCT, it remains too comprehensive, unspecified, and elusive. However, as mentioned in the Introduction, most of the literature data partially suggest interactions with the membrane by electrostatic selectivity. Based on available knowledge, we have focused on those two aspects. By combining experimental and simulation methods, we attempt to verify the proposed molecular mechanism of action and establish the model action of membrane disintegration based on electrostatic interactions. To enable us to test the electrostatic selectivity hypothesis, we decided to mimic *E. coli* Gram-negative bacteria membrane rich in CL and PG lipids. Specifically, membrane composition was selected based on the negative charge of the outer surface of bacterial cells. Gram-negative bacteria have a negative surface charge because of the presence of phospholipids and lipopolysaccharides (rich in phosphate groups) in the outer membrane (41). We decided to use a model membrane with a highly negative mean ζ potential (-60 mV), which consists of PG (18:1/18:1; DOPG) and PC (16:0/18:1; POPC) in the 3:7 ratio, respectively. As a model of a neutral membrane (with mean surface charge equal to 0 mV), we used pure PC (16:0/18:1; POPC) membrane. In our research, we combined molecular dynamics simulations with various experimental approaches. The experimental models of the membrane were additionally enhanced with numerical simulations on bacteria mimicking membrane (8:1.5:0.5 ratio PE (16:0/16:1 PYPE):PG (16:0/16:1 PYPG):CL (16:0.18:1/16:0.18:1 PVCL2), respectively) (42,43). We studied membrane structure and stability as a function of OCT and CHX concentration by determination of the ζ potential and dynamic light scattering. The localization of the antimicrobial compounds in the lipid membrane was investigated by fluorescence studies with trimethylammonium-diphenylhexatriene (TMA-DPH) and DPH probes. These probes react to changes occurring in the inner part of the bilayer at the level of hydrophobic tails and hydrophilic heads. This allowed us to determine the preferential location of accumulation of the compounds in the lipid membrane. Mechanical changes, specifically bending rigidity, as a function of OCT and CHX concentration were measured using flicker-noise spectroscopy. Finally, we investigated the leakage of carboxyfluorescein (CXF) encapsulated in the liposomes to identify the potency of membrane-disrupting antibacterial

activity and selectivity of compounds. All these various aspects were verified using molecular dynamics simulations, which allowed the analysis of the system at the atomic level, as well as enabling us to overcome the limitations of the experiments. The main aim of our research was to verify the prevailing opinion that the interaction and antiseptic effect of OCT and CHX result from the electrostatic interactions of the molecules with negatively charged elements on the outer surface of bacterial cells. In our study, we managed to experimentally test the hypothesis of the electrostatic selectivity of two investigated agents, OCT and CHX. Through the use of molecular dynamics simulations, we were able to independently verify this hypothesis and to propose alternative mode of action.

MATERIALS AND METHODS

Materials

POPC and DOPG lipid powders were purchased from Avanti Polar Lipids (Alabaster, AL). Fluorescent dye Atto 488 DOPE was purchased from ATTO-TECH (Siegen, Germany), and both TMA-DPH and DPH were purchased from Sigma-Aldrich (Darmstadt, Germany). Octenidine dihydrochloride was purchased from Ferak (Berlin, Germany). Digluconian chlorhexidine was purchased from MP Biomedicals (Eschwege, Germany). CXF was purchased from Merck (Kenilworth, NJ).

Large unilamellar vesicle preparation procedure

The large unilamellar vesicles were formed using the extrusion method. Lipids were dissolved in chloroform and dried under a stream of argon, followed by 12-h vacuum treatment to ensure complete organic solvent removal. The resulting dry lipid film was hydrated with an aqueous solution and vortexed to obtain a milky suspension. The obtained mixture was extruded through polycarbonate filters with 100-nm pores (Whatman, Dassel, Germany). The quality of the liposomes was tested using the dynamic light scattering technique (Zetasizer Nano ZS; Malvern, Malvern, UK).

Giant unilamellar vesicles preparation procedure: electroformation

The modified method of model membrane formation for giant unilamellar vesicles (GUVs) was used. Briefly, 10 μL of 1 mM POPC and fluorescent probe mixture (1 m%) in chloroform was distributed equally along the platinum electrodes and dried under reduced pressure for 1 h. The electrodes were then submerged in aqueous nonconductive solution, and a square 1-Hz AC electric field was applied for 2 h with increasing voltage up to 4 V in a custom polytetrafluoroethylene electroformation chamber (44).

Vesicle fluctuation spectroscopy

Thermally induced shape fluctuations of GUVs can be used to determine the mechanical properties (bending rigidity). The series of images of GUVs were recorded using fluorescence confocal microscopy. A Stellaris confocal microscope (Leica, Wetzlar, Germany) was equipped with an HC PL APO 86×/1.20 water immersion objective (Leica). 256 × 256 pixel images were recorded with a hybrid (HyD; Leica) detector with pixel size ranging from 0.088 to 0.136 μm with video integration time ranging from 130 ms up to 190 ms depending on the zoom magnitude. Samples were illuminated with white laser set at 488 nm; emitted light was recorded from 500 up to 600 nm. The series usually consisted of 1200 images. The two-dimensional liposome images are transformed to the three-dimensional Helfrich model using both the average-based and statistical approaches. Then, the radial position of the bilayer, extracted from images, is used to construct angular autocorrelation curves. In the average-based approach, autocorrelation curves are decomposed into Legendre polynomial series and are plotted as a function of fluctuation mode so the bending rigidity coefficient can be determined. In the statistical approach, autocorrelation curves are decomposed into Fourier series, and a frequency histogram of amplitudes for each mode of fluctuation is calculated. The histogram is then used for determination of the bending rigidity coefficient as described in detail elsewhere (45). The radii of investigated vesicles ranged from 3.3 up to 12.8 μm. Selected videos of vesicles treated with investigated agents are presented in the Supporting material (Videos S1 and S2, POPC and POPC/DOPG vesicles; Videos S3 and S4, POPC and POPC/DOPG vesicles treated with 0.1 OCT/LIP.; Videos S5 and S6, POPC and POPC/DOPG vesicles with 0.1 CHX/LIP.).

ζ-potential determination and dynamic light scattering

ζ-potential and dynamic light scattering measurements were performed on 1 mM liposomes. Measurements were performed in 10 mM NaCl solution. Liposomes were titrated with 1.5 mM octenidine solution in the same buffer. Measurements were performed using Zetasizer Nano ZS (Malvern). Each sample was left for 15 min after adding a solution of octenidine to obtain equilibrium in the sample. ζ-potential measurements were used for partitioning coefficient determination using the established approach (46). However, this approach can only be applied if a net charge of the particle and the proportion and effective charge of the ionic phospholipids in the vesicles are known and are not equal to 0. All performed experiments were repeated three times unless specified differently in the particular Materials and methods section.

CXF leakage measurement and sample preparation

Encapsulation of CXF

60 mM pure POPC or a 3:7 ratio of DOPG/POPC liposomes, respectively, with 50 mM CXF in buffer (100 mM KCl, 10 mM Tris, 10 mM MES (2-(N-morpholino)ethanesulfonic acid) (pH 7.0)) were prepared. Solutions were extruded by 100-nm filters (Whatman, Dassel, Germany). The polydispersity of the population was checked and did not exceed 10%. Liposomes were purified by the dialysis method, based on Micro Float-A-Lyzer dialysis membranes (Sigma-Aldrich) with the threshold ∼50 kDa. Lipid concentration was determined using ammonium ferrothiocyanate colorimetric method to assess the loss after ultrafiltration. The final lipid concentration was equal to 20 mM. Kinetics of release of CXF was measured with a Horiba Fluoromax 4 spectrofluorometer (λ_{ex} 492 nm, slit, 1 nm; λ_{em} 517 nm, slit, 1 nm; Horiba, Piscataway, NJ) for ∼700 s with a time step of 1 s. 4 μL of liposome solution was added to 3 mL buffer in measuring cuvette. This corresponds to 27 μM final lipid concentration during the measurement.

Kinetics of CXF leakage

Kinetics lasted for 700 s with a time step of 1 s. For each measurement, the intensity of the reference detector was recorded to include light source fluctuation corrections. This correction has already been applied in the results below. The solution was injected with a Hamilton syringe to the bottom. A magnetic stirrer was present in the measuring cuvette to enable equal distribution of agents. After ∼100 s of signal recording, octenidine or chlorhexidine solution was added to obtain the appropriate ratio of tested particles and lipids. After 500 s of signal recording, 15 μL of 5% solution

of Triton-X100 was added (as a positive control), leading to complete micellization of the membrane and release of all CXF into the solution.

Localization study using TMA-DPH and DPH fluorescent probes

To investigate the incorporation of agents into membranes, the DPH and TMA-DPH fluorescence probes were selected. Liposomes were prepared with a probe concentration of 0.5 mol%. The concentration of all investigated lipid vesicles was equal to 1 mM in 10 mM NaCl solution. Either OCT or CHX was added to the liposomes and followed with incubation for 1 h to obtain equilibrium. The measurement was made using the SpectroFluoromax 4 spectrofluorometer (Horiba). The excitation wave λex was equal to 350 nm, and emission was in the range of λem 360–520 nm. Both slits were 2 nm wide.

Quantum mechanics

Quantum level calculations were performed using the Gaussian 2016 software package (47). The equilibrium geometry of OCT and CHX molecules was calculated at the HF/6–311+g level of theory. The solvent effect was taken into consideration using the integral equation formalism of the polarizable continuum model IEFPCM. Supplementary analysis based on the construction of the Hessian matrix (the matrix of second derivatives of the energy with respect to geometry) was also performed for further use in the force field parameterization for further molecular dynamics (MD) study. The specific geometric and electronic data such as bond lengths, angles, dihedrals, and charge distribution were extracted from a Hessian matrix. Those parameters are crucial for the construction of the force field used in MD simulations, as described below. The charge distribution was determined from the RESP charge calculations as being the most adapted to reproduce the molecular behavior with the subsequently used CHARMM force field. For logP determination, the octanol/water partitioning coefficient was calculated using SCIGRESS software (SCIGRESS, Molecular modeling software, FQS Poland, ver. FJ-3.3.3).

MD simulations

Several MD systems were constructed for studying the antiseptic agent and lipid membrane interactions and behavior. Three types of membrane systems were assembled in CHARMM-GUI (48) and investigated afterward: neutral (NLM), pure PC (16:0/18:1; POPC); negatively charged (NegM), 3:7 PG (18:1/18:1; DOPG):PC (16:0/18:1; POPC) lipid ratio, respectively; and bacteria mimicking (BacM), 8:1.5:0.5 PE (16:0/16:1; PYPE):PG (16:0/16:1; PYPG):CL (16:0.18:1/16:0.18:1; PVCL2) lipid ratio, respectively. Two different concentrations of antiseptic agents (OCT and CHX) were investigated: lower 1:80 agent/lipid (80 lipid system) and higher 1:26 agent/lipid (182 lipid system). A snapshot of the system's initial state is presented in Figs. S1 and S2. The lipid bilayers were solvated with 400 mM NaCl solution including 100 water molecules per lipid. Such a high ion concentration was selected given the fact that both substances, OCT and CHX, are antimicrobial agents and are often used on open wounds (blood) or in the mouth (saliva). Both blood and saliva are known for their buffering properties. Salt is present in much higher concentrations in the blood than in our simulations, and yet an antimicrobial effect is still present. Additionally, we performed simulations without additional ions to evaluate their impact on agent behavior. The TIP3P water model was employed. Finally, self-assembly of lipid systems was investigated. Systems with pure PC (16:0/18:1 POPC) lipid molecules (180 lipid particles) randomly distributed in space with or without the presence of an additional agent (240 OCT or CHX particles) were created. After brief minimization, they were hydrated as previously described.

MD simulations were performed using the GROMACS (version 2018.3) package with the CHARMM36 force field. Every system was first minimized using the steepest descent algorithm for energy minimization. Calculations were carried out in the NPT ensemble (constant number of particles, pressure and temperature) using a Berendsen thermostat and barostat including semi-isotropic coupling at T = 303.15 K and p = 1 bar. The initial part of the NPT calculations was performed using the leap-frog integrator with a 1-fs time step. Subsequently, for the further NPT ensemble at T = 303.15 K and p = 1 bar, a Nosé-Hoover thermostat and Parrinello-Rahman barostat were applied. The second part of long-run production was carried out for at least 400 ns using the leap-frog integrator. Chemical bonds between hydrogen and heavy atoms were constrained to their equilibrium values using the LINCS algorithm, and long-range electrostatic forces were evaluated using the particle mesh Ewald method, which allowed us to employ an integration time step of 2 fs. Based on simulated pure membranes, the action of antiseptic agents was investigated. Molecules were placed on average 2 nm above the membrane leaflet. The same procedure was employed for constructed lipid/agent systems. For visualization and analysis purpose we used GROMACS tools, Visual Molecular Dynamics (49), and Diffusion Coefficient Tool (50). Selected videos of numerical bilayers treated with investigated agents are presented in the Supporting material (Videos S7 and S8, NLM and BacM with OCT; Videos S9 and S10, NLM and NegM with CHX).

Statistics and data representation

To test for the significant difference between the parameters, the one-way analysis of variance test was used with the significance level at 0.05. The Tukey test was used as a post hoc test. All statistical analysis was performed using the OriginPro 2015 (OriginLabs) software. Average values are presented with standard deviation.

RESULTS AND DISCUSSION

OCT

Location and behavior

The general behavior of the OCT-membrane interaction was first assessed using MD. In control NLM, the OCT particle (Fig. 1 *A*) reached the surface and anchored after 140 ns. In BacM membrane (mimicking the bacterial one), the OCT particle reached the surface faster, which was followed by anchoring after 45 ns. The entire particle incorporation to the negative membrane (NegM) lasted the longest—220 ns. However, one acyl chain anchored after 120 ns, leaving the second one and the spacer above, and it took almost 100 ns more for the second one to attach. After incorporation in the membrane, OCT took the shape of a staple, penetrating the monolayer with two acyl chain ends (as shown in Fig. 1 *B*).

Clearly, the OCT interaction was strongest with the BacM, as both reaching the surface and anchoring were faster. Movement of incorporated particles in the lateral plane of the membrane was observed after incorporation in both membranes. Furthermore, in all simulated model membranes, OCT particle penetrated the membrane deeply inside, anchoring at the carbonyl-glycerol region. It is noteworthy that on the BacM, the hydrogen atoms from the agent's acyl chain statistically penetrated the deepest,
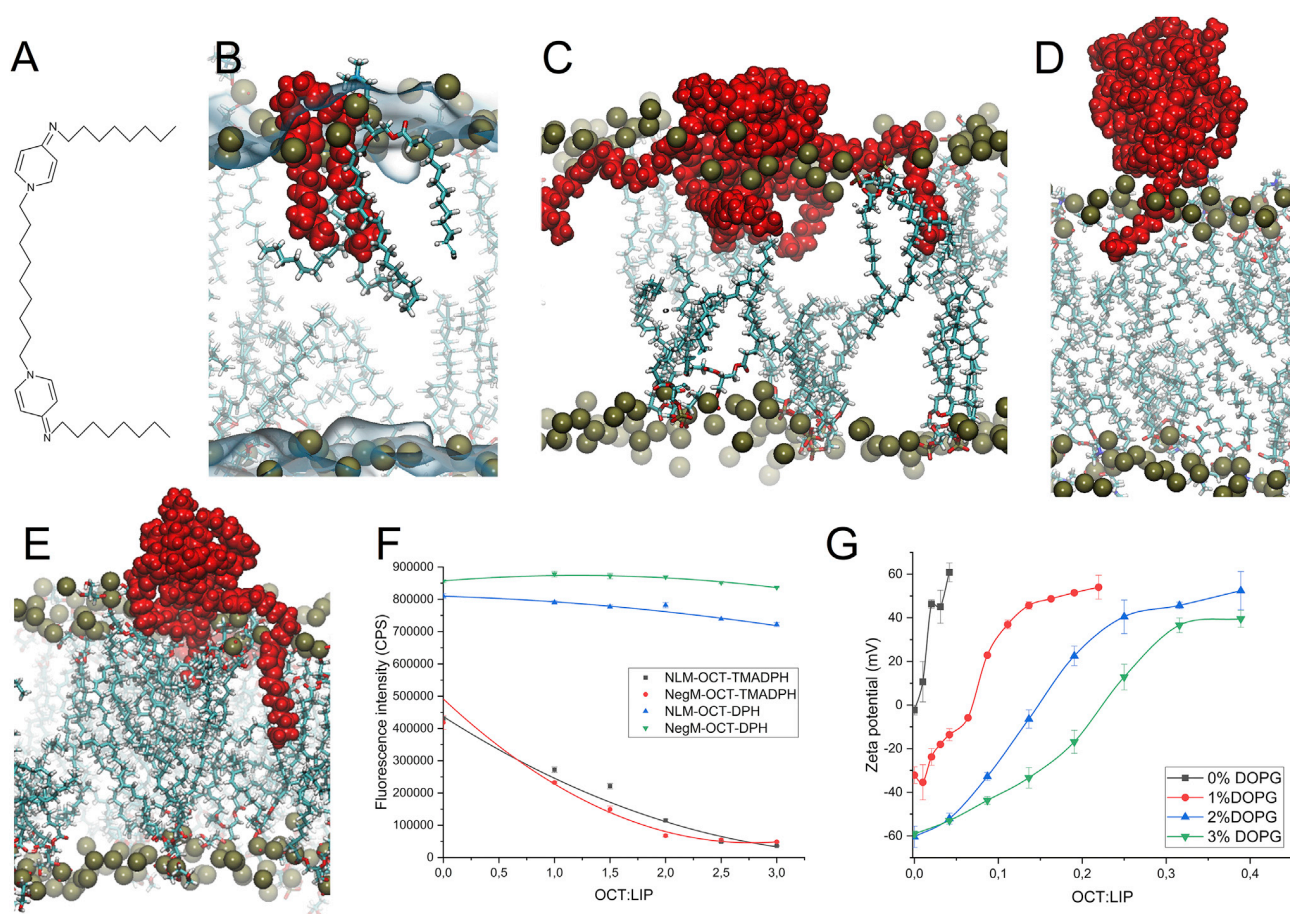
FIGURE 1 (A) Chemical structure of OCT, (B) single OCT molecule incorporated into BacM, (C) visualization of spread aggregate of OCT on BacM membrane, (D) visualization of balloon-shaped OCT aggregate on NLM, and (E) visualization of spread aggregate of OCT on NegM membrane; in all snapshots, several lipids have been hidden for clarity. OCT molecules, phosphorus atoms from lipid headgroups, and water surface have been colored in red, olive, and blue, respectively. (F) Fluorograms from DPH and TMA-DPH probes indicating OCT localization in carbonyl-glycerol region and (G) ζ-potential changes due to OCT titration for the POPC membranes with various DOPG composition. To see this figure in color, go online.

reaching 8.7 ± 2.9 Å level from bilayer center. In the case of the NLM and NegM, the OCT reached the 9.8 ± 2.9 and 9.9 ± 2.8 Å levels, respectively, from the bilayer center. Only the NLM and NegM pair was not statistically distinct. The detailed location of system components such as lipid fragments or agent molecules has been presented in the partial density charts in Figs. S3 and S4. The OCT particle directed its acyl chains toward the membrane, leaving the spacer above (as shown in Fig. 1 B). It could possibly be due to the distribution of the OCT positive charges on acyl chains. Almost all types of lipid membranes exposed to OCT action showed slight differences in thickness and area per lipid (APL) (see Table S1). A noticeable decrease after OCT incorporation was observed in the majority of cases. Only in the case of the PG lipid and the NegM system was an increase observed. Furthermore, the incorporation process did not differ between the NegM and NLM; hence, interaction between the positive chains and negatively charged heads of lipids could not be considered as a factor

influencing incorporation into the membrane when a single OCT molecule was simulated in the system. Similar OCT behavior was observed in systems without NaCl ions. OCT is anchored to the bilayer in a staple shape in all systems. Interestingly, the staple shape was more extensive compared to 400 mM NaCl systems and the process of incorporation was much faster—35, 20, and 120 ns in the NLM, BacM, and NegM, respectively. This was also followed by a significant increase of OCT's APL values compared with systems with ions (see Table S2). Similar incorporation was observed by Kholina et al. in PE-PG membranes (51).

Afterward, the simulations with an increased number of OCT particles were investigated to study aggregation behavior. A stable aggregate was formed at the initial phase of each of the systems. After several nanoseconds, it interacted with the membrane. Snapshots are presented in Fig. 1, C–E. In all of the investigated membrane systems, OCT interaction with the lipid headgroups could be

observed over ∼300 ns. On the NLM, the aggregate anchored inside the membrane purely by one tail, forming a balloon shape that does not interact with lipids. OCTs on the BacM behave differently; the aggregate settled down and spread on the membrane surface, penetrating it heavily with acyl tails. A hybrid model appeared in the NegM system, in which at the initial state OCT particles gathered together, forming a balloon-shaped aggregate similar to that in the NLM system. It settled down on the membrane surface and anchored inside the bilayer by two tails afterward. The NegM exhibits comparable behavior to the NLM, although the first molecule interaction with membrane was clearly faster. To this end, we focused on the incorporation of OCT into membrane systems. The provided phenomenon can be seen by comparing the thickness parameter, which illustrates the growth of lipid surface area in the BacM with greater agent concentration because of higher surfactant penetration (see Table S1). It is noteworthy that it is directly related to the change in the value of the area per molecule (APM) because of the incorporation of OCT aggregate. This indicates the level of interaction between the OCT aggregate and the lipid bilayer. The occupied OCT area in the BacM is equal to 50.1 ± 3.2 Å^2 and is almost twice as large as in the NLM, where it is 27.5 ± 6.1 Å^2. Additionally, the changes of APL, APM, and thickness for all model systems are presented in Table S1. Slightly different OCT dynamics were observed in the 0 mM NaCl NLM system. In this case, the agent formed a balloon-shaped aggregate; however, it did not incorporate into the bilayer. It stayed in the water phase, slipping on the membrane surface (see Fig. S7). The OCT aggregate completely ignored the membrane. Interestingly, when a system with one anchored OCT in the membrane was employed, the rest of the OCT particles partially followed that manner and incorporated into the membrane (see Fig. S8). This suggests that high salt concentration in solvent prevents OCT from self-aggregation and significantly increases the affinity toward membranes. On both the BacM and NegM, we did not observe substantial permutations such as in the NLM. OCT particles gathered and settled down on the membrane surface, penetrating it with a couple of acyl chains. Similar to before, on the BacM OCT aggregate was more spread and flattened, whereas on the NegM it was more soaring, in the shape of a balloon with a couple of chains anchored. Here, we also noticed a reduction trend in APM, especially in the NegM and BacM systems (see Table S2). Additionally, the lateral diffusion was calculated to check the possibility of OCT preferential interaction with a lipid type, as presented by Kholina et al. (51). In this hypothesis, the radial distribution and diffusion coefficient were used to estimate the level of the propensity for interaction with antiseptics. Our results did not show any strong affinity toward any type of lipid molecule (see Table S3). Our results revealed also that the presence of the agent directly affects the diffusion of

all lipids in the system. This is similar to Kholina et al.'s conclusions (51).

We used DPH and TMA-DPH fluorescence probes to experimentally confirm the location of OCT molecules in membranes obtained from MD studies. The location of OCTs in the membrane after incorporation is in the hydrophobic core, close to the heads of hydrophilic lipid membranes. Both of the selected probes are known to be strongly affected by the influence of environment polarity on fluorescent intensity. Therefore, the intensity of their quantum fluorescence in water is significantly lower compared to after localizing in the hydrophobic part of the membrane (52,53). Both probes are also sensitive to the spatial ordering of lipids. Specifically, the DPH probe's fluorescence is known to be a function of the acyl-chain region of the lipid membrane (54), whereas its modification, TMA-DPH, allows for determination of the carbonyl-glycerol region (54–56). Fig. 1 *F* illustrates fluorescence intensity changes at peak value for both probes as a function of the OCT/Lipid ratio for both the NLM and NegM. In both membranes, significant changes were observed for the TMA-DPH probe, whereas no major changes were observed in the case of the DPH probe. Detailed fluorograms for both probes are presented in Fig. S13. Such results suggest an accumulation of the OCT molecules in carbonyl-glycerol, which corresponds perfectly with our results from MD, in which preferential surfactant localization took place in the upper layers of the membrane. Such results could initially suggest a lack of disturbances in the alkyl-chain region. Poojari et al. (57) showed that DPH may not directly reflect information about acyl-chain region packing when additional molecules other than lipids are present. This is especially crucial when the molecule is large and amphipathic (like OCT). Furthermore, as suggested by Nazari et al. (58), the detergent molecules mix poorly with the lipid ones, resulting in segregation into detergent-rich clusters that disrupt the membrane locally, whereas the rest of the membrane with the majority of DPH is only a little affected. Malanovic et al. (13) showed by x-ray scattering on model membranes with PE that disruption in the hydrophobic region was observed. It is possible that OCT particles localized in the carbonyl-glycerol region are inducing acyl-chain packing changes that do not influence the DPH probe behavior. To this end, we performed analysis of order parameter on MD systems (see Fig. S11) containing PC and PE. We showed that differences in order parameter after OCT incorporation into the membrane were observed for PE lipids, but not for PC lipids, in the model membrane systems investigated here. Therefore, we may conclude that there is a high possibility of no direct interaction at the hydrophobic core level of the bilayer and preferential accumulation occurs in the membrane surface area in NegM and NLM membrane systems. In the case of the BacM system, an indirect influence of OCT on the

acyl-chain region was observed that is supported by the experimental results of Malanovic et al. (13).

ζ-potential measurements and partition coefficient

Subsequently, we decided to study membrane structure and stability in function of OCT concentration by determination of the ζ potential and dynamic light scattering and to evaluate the influence of membrane charge on interaction strength as well. The results presented in Fig. 1 G indicate a different, less rapid nature of the interaction between OCT and the NegM compared with the NLM. Specifically, the slope of the ζ-potential change was highest for the neutral membrane (16 mV/m%) and slowly decreased with an increase of DOPG in the membrane (7.5, 6.2, and 6.0 mV/m%, respectively). The average size of vesicles determined using dynamic light scattering remained unchanged (see Fig. S15). The ζ-potential changes are not correlated with pH, which remains steady in various agent concentrations (see Fig. S17).

The lipid/water partition coefficient determined from ζ-potential measurement (Fig. S18) was equal to 2.3 ± 0.2 in charged membrane (1, 2, and 3% DOPG) systems (46). Interestingly, this value is significantly smaller than the obtained logP value using the SCIGRESS calculation tool, where it was equal to 9.25. Such a difference highlights the complicated nature of interaction between the OCT and the membrane. Because membranes are much more complex structures than the octanol used in logP determination, the difference between the partition coefficients is not surprising. The magnitude of the difference can lead to the conclusion that interactions between OCT molecules are stronger than between OCT and membrane. This is also in agreement with MD simulations and literature data (59), as it has been reported that OCT tends to form aggregates in water. Nonetheless, OCT directly affects the liposome surface charge, leading to its continuous growth, suggesting that more OCT is located in the membrane than in water. However, that does not necessarily need to be the correct conclusion, because the ζ potential is located above the membrane and OCT particles tend to form aggregates above the membrane surface. The initial electrostatic effect could push OCT particles in the vicinity of the membrane, although particles tend to form aggregates on the membrane surface rather than incorporate into the membrane. This view is additionally supported when the evolution of ζ potential is taken into account in low concentrations of the antimicrobial agent. In the case of the NLM, the difference between 0 and 0.03 of OCT/LIP equals 63 mV, but with increasing DOPG content it decreases to 19, 8, and 6 mV, respectively. The initial conclusion suggests that the more negatively charged the membrane is, the lower the ability of OCT to incorporate into the membrane. However, it is also possible that aggregation is stronger on the negatively charged surface of the membrane, which increases its graininess. As a result, vesicle topology is changed by incorpo-

rated anchors, increasing its roughness and friction and hence influencing the outcome of ζ measurement. Moreover, we assume that OCT forms aggregates preferentially to minimize the entropy of the system. Because the ζ potential is located above the membrane interphase, it is possible that, as stated previously, the less rapid character of ζ-potential change means equal or more OCT on the membrane (but not necessarily in the membrane). It also could suggest a very sophisticated antiseptic mechanism of selectivity that is based on how the particle is incorporated into the membrane. This could be related to interaction with negatively charged lipid headgroups but also to membrane curvature and/or other macroscopic properties. Interestingly, results from TMA-DPH and DPH suggest that more rapid increase of ζ potential in the NLMs is not due to OCT incorporation, as for both the NegM and NLM, the incorporation in carbonyl-glycerol is not significantly different. This strengthens the conclusion that an increase in ζ potential for membranes, especially the NegM, is related to the formation of balloon aggregates rather than the rapid incorporation into the membrane of OCT in the first place—especially because, regardless of the charge and the amount of delivered OCT, we observe continuous linear changes in the probe's environment, which results in a decrease in fluorescence intensity.

Destructive effect of agent and selectivity

Finally, we examined the effect of OCT on membranes in terms of disruption of self-assembly. The idea of this simulation is to investigate inverse emulsification of the lipid molecules suspended randomly in water (see Fig. S12). We performed membrane self-assembly studies in the presence of OCT particles. Provided that OCT is not interacting with the membrane, the lipids should self-assemble without any problems. In the case of randomly distributed PC lipids without OCT, formation of a bilayer was observed after 60 ns with a 580 kcal/mol increase in van der Waal (VdW) energy from the initial system to the self-assembled one. Unlike the potential energy, VdW component does not decrease over time when aggregation of components that constitute a significant volume of the simulated particles system occurs. It is expected that aggregation will induce local crowding of particles. In the case of crowding, the VdW energy component will increase to a certain value, higher than the initial one. One can conclude that the electrostatic energy component, being much more negative than at the beginning of the simulation and lowering importantly over time, is the driving force of observed aggregation phenomenon. The entropic changes in MD systems are taken into account indirectly, which could be concluded as the electrostatic driving force. However, in reality, it may have its origins in hydrophobic forces driving the self-assembly of molecules even at the cost of a higher VdW energy component. During the simulation, because of the hydrophobic effect, lipids formed a bilayer, which is
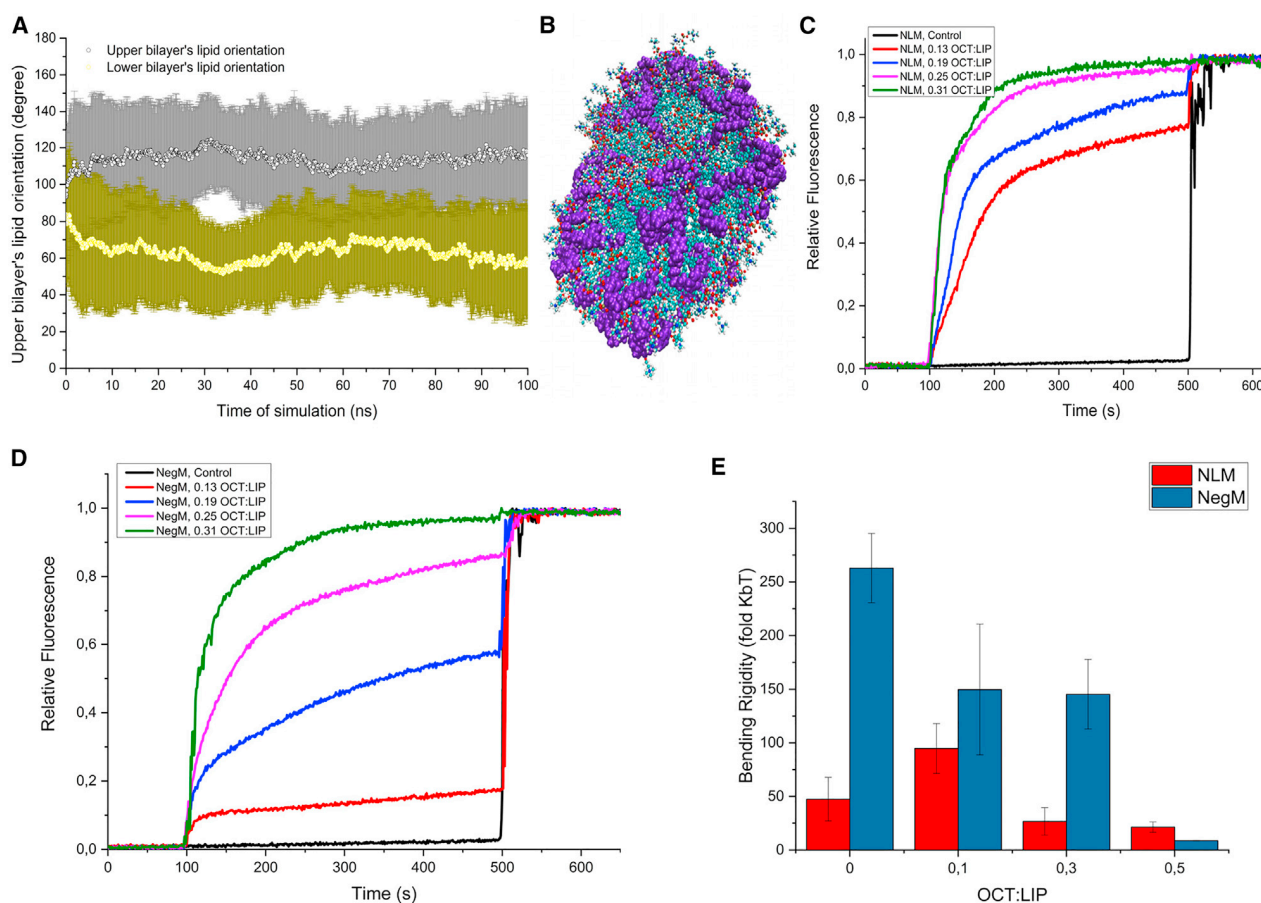
FIGURE 2 (A) Self-assembly MD simulation presenting individual lipid particles orientation during disrupted membrane formation by OCT particles, (B) visualization of doughnut-like membrane structure after self-assembly accompanied by OCT particles, (C) CXF leakage from NLM after OCT addition at 100 s, (D) CXF leakage from NegM after OCT addition at 100 s, and (E) bending rigidity analysis introduced by statistical approach; results obtained from vesicle fluctuation spectroscopy. To see this figure in color, go online.

associated with the displacement of a significant amount of water molecules from the core interior. However, in the case of the system with OCT molecules, formation of a bilayer did not occur. Evolution of the system is presented in Fig. 2 A. Instead, a doughnut-like structure covered with OCT was formed, which is presented in Fig. 2 B. The VdW energy increase equaled 435 kcal/mol. This suggests that OCT, as an agent influencing the self-assembly process of the membrane, has a significant impact on its structure and/or fluidity.

Furthermore, the destructive effect of the membrane was investigated experimentally by observing the leakage of CXF loaded inside the liposomes. CXF is a probe that has a self-quenching effect in high concentration; therefore, its fluorescence decreases with increasing concentration (60,61). This makes it commonly used as a tracer agent. Both the NLM and NegM systems were measured. The change in relative fluorescence is presented in Fig. 2, C and D. Increased volumes of OCT were added to the successive measurements, maintaining the same concentration of liposomes to study the effect of higher surfactant dose on

liposome damage. Based on the obtained results, there was a noticeable tendency: the higher the dose of the OCT, the higher the quantity of CXF released from the liposomes. Doubling the initial dose 0.13 OCT/LIP resulted in a doubling of acceleration of the leakage. The quickest leakage observed for the 0.31 OCT/LIP ratio occurred after ~180 s. In the case of the NegM, the results are more varied. As before, raising the dose resulted in a faster reaction, but here the original 0.13 OCT/LIP dose caused a small leakage of CXF. Doubling the dose allowed us to observe much stronger fluorescence and lipid damage within ~200 s from the start of the test to micellization. The highest leakage is observed at the highest OCT quantity. The presented results proved that the leakage on NLM was, quantitatively, greater. Because the incorporation of OCT in the membrane is a fast process, as shown with MD simulations, the initial process of CXF release should be related to the disruption of the membrane by OCT incorporation. Interestingly, the slopes were similar for both the NLM and NegM lipid vesicles, which agrees with results from simulations where the incorporation time was similar.

Statistical analysis of leakage data showed that the results are significantly different. The post hoc test showed that all are significantly different apart from both the NLM and NegM liposomes treated with 0.31 OCT/LIP and 0.25 OCT/LIP and NegM liposomes treated with either 0.25 OCT/LIP or 0.19 OCT/LIP. These results suggest that the disruptive effect is similar in both the NLM and NegM in higher concentrations of OCT. Surprisingly, the release of CXF, especially in lower concentrations of OCT, is quantitatively greater in neutral membranes. This strongly suggests that the disrupting effect of the OCT is not based on electrostatic interactions purely, hence undermining the possibility that the selectivity is based on electrical phenomena. The results are apparently contradictory to leakage experiments reported by Malanovic et al. (13), when PE/PG, PE/PG/CL, and *E. coli* lipid extracts were used as model membranes. For 0.13 OCT/LIP, both PE/PG and PC/PG systems are in agreement (around 10% leakage). Surprisingly, both *E. coli* total lipid extract and pure POPC systems showed 80 and 70% leakage, respectively. The difference occurs at higher (0.31) OCT/LIP, as in the PE/PG system, only 20% leakage is observed but almost 90% leakage in PC/PG systems. However, PE is significantly different lipid then PC when it comes to order parameter, resulting membrane curvature, and ability to assemble into vesicular structures. Moreover, it was reported that the mixing behavior of PC/PG and PE/PG differs. This could be partially caused by different molecular shapes of PE and PC as well as the hydrogen-bonding capacity of PE (62). Such a contrast could result in various lipid packing, different overall physicochemical properties, and different interactions with active molecules such as OCT. These changes could explain the observed differences in leakage induced by OCT between the PC/PG and PE/PG membrane model systems.

To this end, we decided to investigate whether the effect is based on mechanical disruption and selectivity. Firstly, we determined whether the OCT molecule has an effect on mechanical properties of membranes in general. We established bending rigidity changes of OCT incorporation in both the NLM and NegM. Bending rigidity in the NLM system increased after a small (up to 0.1 OCT/LIP) OCT addition. However, it decreased when OCT concentration was around 0.3 OCT/LIP. This was likely caused by membrane integrity loss. There was no statistical significance between 0.3 and 0.5 OCT/LIP. Such an effect was not observed in the case of NegM vesicles, for which the decrease of bending rigidity was observed even in the case of 0.1 OCT/LIP. However, there was no statistical difference between 0.1 and 0.3 OCT/LIP concentration in the NegM, which could correspond to the period of OCT incorporation when negative charges are neutralized by OCT. Only in higher concentrations (0.5 OCT/LIP) was the statistically significant decrease of bending rigidity observed, in much higher concentrations than in the NLM. Given results from leakage and ζ experi-

ments, this could suggest that loss of integrity was observed in higher concentrations in the NegM than in the NLM system. Substantial error bars for bending rigidity measurements could be due to inhomogeneous incorporation to individual GUVs, as well as aggregation in the membrane. The latter is confirmed by simulations. This is particularly visible in the case of 0.1 OCT/LIP. Such a situation would mean that bending rigidity value is a superposition between the vesicles with and without OCT. Bending rigidity change is presented in Fig. 2 *E*. It should be noted that OCT is inducing defects on GUV membranes. It was recently shown (63) that such defects may contribute to slight difference between determined and real membrane bending rigidity. As a result, we considered an alternative mechanism of action of OCT—specifically, that OCT initially influences membrane reorganization (an increase of bending), which is followed by mechanical disruption of the membrane if the OCT concentration is high enough (decrease of bending because of membrane leakage). The lesser leakage observed in the NegM corresponds well with the later decrease of bending compared with the NLM system. This phenomenon could be explained in two ways. Either more OCT concentration is required to neutralize the negative charge of the membrane before the OCT starts disruption or the NegM is much stiffer, hence such an effect. As was shown by Faizi et al., membranes with negatively charged lipids (such as PG) are stiffer (64). Dependence of the ζ potential on the negative surface charge was also investigated, which explains the somewhat paradoxical results obtained from ζ-potential measurements. The increased stiffness of the membrane makes it more resistant to external forces, as similarly seen in the case of stiffening by cholesterol (65). This supports our claim, as it would suggest that negatively charged membranes are much stiffer than neutral ones. Such results could also suggest that a negative charge on the membrane slows down the disruptive effect of OCT. Hence, our observation denies previous literature data explaining the origin of OCT interactions with lipids as a simple electrostatics phenomenon. Additionally, a nondirect premise can be presented, which strengthens this message. *E. coli* cells were reported to change their membrane phenotype to be stiffer to survive the effect of nanomechanical stress caused by ZnO nanorods (66). This suggests that increasing stiffness could be a cell's survival mechanism against mechanical membrane attack. A similar observation is, in a way, presented in our work, in which leakage of the stiffer NegM membrane is inferior to leakage observed in the NLM. To present it in order, the initial effect of OCT, when incorporated into a membrane, induces reorganization that changes its stiffness. For the NLM, if OCT concentration reaches high enough threshold, OCT particles or aggregates start to interact with each, causing a progressive decrease of stiffness, which results in much greater disruption of the membrane and resulted in CXF leakage in our experiment. This is slightly different in the NegM membrane because its native stiffness is higher.

OCT incorporation decreases the stiffness initially, which is followed by a longer period of stability before the disruption of membranes occurs. As shown by the ζ results, aggregation of OCT on the NegM surface is greater; the change is not strong enough to cause the magnitude of the membrane disruption that is observed in the NLM. As a result, quantitatively more OCT particles are required to disrupt the membrane, as additional decrease of the stiffness up to the point of neutral membrane needs to occur and/or negative charge on the membrane requires being balanced. This was observed in the case of 0.25 OCT/LIP and 0.31 OCT/LIP, when the stiffening effect of OCT was similar in both membrane systems (as observed by the fluorescent ratio). On the other hand, a leakage was observed in the OCT concentration region that corresponds to membrane neutralization. Although this can be partially explained by inhomogeneous incorporation of OCT, it also suggests that membrane's mechanical property change is more prevalent than the ζ-potential change.

Summary

In the Introduction, we postulated that the OCT mechanism of action may be based on strong adhesion to charged bacterial components of cell membranes and may be a basis for their selectivity over epithelial cells. Such a mode of action would result in cytoplasm leakage and ultimately cell death. The presented research clearly demonstrates that OCT selectivity nor mechanism is not based on the presence of charged component. Both, leakage was weaker, and incorporation occurred later in the case of charged but stiffer (NegM) membranes. Our results showed that the mechanism of action and likely selectivity of OCT is based on the mechanical property of the membrane, a high-level emerging property appearing after membrane formation and not existing for a single lipid. Even if cell biomechanics in bacteria is poorly investigated, strong differences between mammalian and cells were shown (67). Recently, it was reported that contrary to common conviction, the outer membrane can be stiffer than the cell wall and that mechanical loads are often balanced between these structures (68), which shows that bacteria may be in greater mechanical balance than initially thought. These results are also in agreement with Malanovic et al., who observed that leakage in *E. coli* polar extract was greater than in PE/PG/CL model membrane vesicles (13). It should be noted that those two models differ mostly by acyl-chain length and double bond presence, which strongly modify membrane mechanical properties. Furthermore, mammalian cells are usually stiffer than their lipid membrane models because of the presence of extracellular matrix, which is considered an important mechanical effector (69). The leakage experiment showed that the negatively charged membranes, which are stiffer, are less disruptive in the vicinity of OCT. MD studies showed that depending on membrane composition (and hence mechanics), different aggregate conformations are induced and changes in membrane packing are observed. Combining results from MD and experiments, it could be postulated that the OCT mechanism of action is based on membrane disruption of the membrane.

CHX

Location and behavior

The same procedures as in the case of OCT section were followed in the case of the CHX molecule. Three MD systems were created with a low and high concentrations of CHX for studying the antiseptic agent and lipid membrane interactions and behavior. Snapshots of the initial configuration of systems are presented in Fig. S2.

In the control NLM system, the CHX particle (see Fig. 3 *A*) reached the surface and anchored after 300 ns. In the BacM, the CHX particle reached the surface and anchored much faster, after 167 ns. In the NegM, the CHX particle reached the surface and anchored after 175 ns. In all types of membrane, after incorporation CHX took the shape of a staple, penetrating the monolayer with two acyl chain ends (as shown in Fig. 3 *B*), which is in strong agreement with results presented by Komljenović et al. and van Oosten et al. (70,71). Clearly, the CHX interaction with the membrane was stronger with the BacM, as both reaching the surface and anchoring were faster. However, on the NLM the chlorine atoms from the agent's acyl chain penetrated significantly deepest, reaching the level of 9.1 ± 2.5 Å from the bilayer center. In the case of the BacM and NegM, the CHX reached the levels of 10.3 ± 2.7 and 9.4 ± 3.3 Å, respectively, from the bilayer center. The detailed location of system components such as lipid fragments or agent molecules is presented in the partial density chart in Figs. S5 and S6. There was no significant difference in CHX behavior in 0 mM NaCl BacM and NegM systems besides much faster incorporation to membrane: 35 and 80 ns in the BacM and NegM, respectively. CHX anchored to the membrane and settled down on the edge region of the interphase close to the acyl chains. Interestingly, in the NLM we observed reduced membrane-agent interactions (see Fig. S9). CHX particles diffused above the membrane; the incorporation did not occur. This phenomenon was induced by decreased ion concentration. This suggests that mild ion shielding is required for CHX incorporation to occur when the membrane system is neutral.

In the case of aggregation studies, CHX molecules did not form solid aggregates that would preferentially interact with each other. Particles spread on both leaflets, penetrating them individually and directing their charged chains toward both membranes, leaving the spacer above as presented in Fig. 3 *C*. The entire CHX molecule anchors below the phosphorus hydrophilic groups, on the edge of membrane interphase and a hydrophobic region. Furthermore, CHX behavior was observed approximately for 1 μs, and
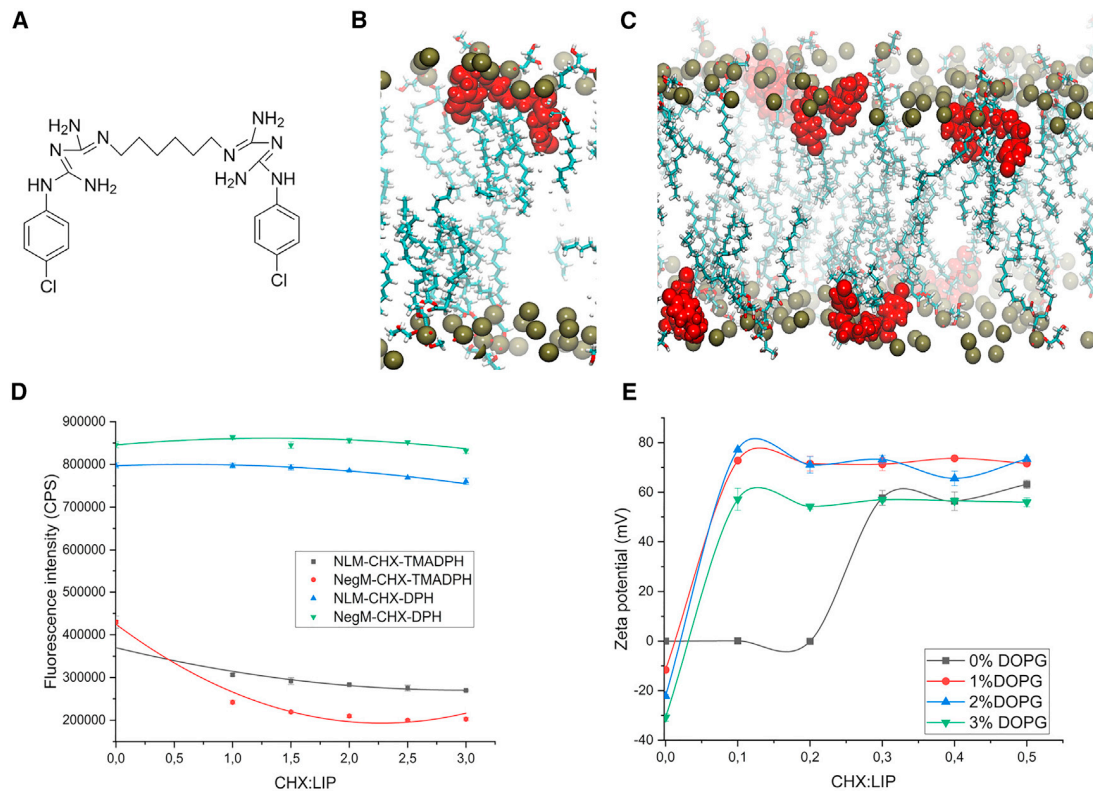
FIGURE 3 (A) Chemical structure of CHX and (B) single CHX molecule incorporated into BacM (several lipids have been hidden for clarity). OCT molecules, phosphorus atoms from lipid headgroups, and water surface have been colored in red, olive, and blue, respectively. (C) Visualization of CHX high concentration system, with agent molecules anchored to NLM, same colors as previously; (D) fluorograms from DPH and TMA-DPH probes indicating OCT localization in carbonyl-glycerol region; and (E) ζ-potential changes due to CHX titration for the POPC membranes with various DOPG composition. To see this figure in color, go online.

molecules incorporated firmly into the membranes, gently moving around without significantly modifying their positions. We did not see any significant changes in the membrane composition or a destructive effect after CHX action according to MD simulations, which is supported by previous studies (71,72). Furthermore, we did not observe substantial differences in CHX behavior in the 0 mM NaCl BacM and NegM systems. Similarly, CHX did not form aggregates but incorporated separately in a staple form. In the NLM, despite almost 1 μs simulation time, only partial limited CHX-membrane interaction was observed. From seven particles that were present in the system, only six incorporated into the membrane (see Fig. S10). Concerning the lower concentration of CHX in ion membranes, the thickness parameter is greater only in the BacM compared with the pure one, but all types of membranes exposed to CHX showed increased APL (see Table S1), which is in line with van Oosten et al.'s reports, accompanied by little to no change in thickness (71). When analyzing particular lipids, only slight fluctuations of APM are noticed. In no-salt systems, similar behavior is observed. Changes in lateral diffusion were observed after CHX incorporation. Incorporation of a single CHX molecule in general de-

creases lateral diffusion. Surprisingly, the incorporation of several CHX molecules resulted in an increased lateral diffusion (even when compared to pure systems). More detailed results are presented in Table S3. We cannot conclude with any specific behavior toward either charged and uncharged membranes or specific lipid type. Based on the APL obtained from MD simulation with higher concentrations, it can be directly noted that the parameter increased after CHX incorporation in almost all cases. The APM change reached even 5.3 Å^2 in the case of the BacM. Marginal fluctuations are followed in systems with counterions. The evolution of both parameters is included in Tables S1 and S2.

Additionally, DPH and TMA-DPH fluorescence probes were used to assess independently the location of CHX molecules in the membrane. Detailed fluorograms for both probes are presented in Fig. S14. The fluorescence intensity for both probes as a function of CHX concentration is presented in Fig. 3 D. Changes in the local environment of the TMA-DPH probe were observed, whereas no major changes were observed in the case of the DPH probe. These results suggest an accumulation of CHX within the outer membrane (interphase area) and no disturbances in the

alkyl-chain area. These results were in agreement with performed MD simulations. CHX did not localize at the level of the hydrophobic layer of the membrane; its preferential accumulation occurred in the edge region of interphase close to the acyl-chain region. This is in line with the previous studies in which, using neutron diffraction, the study CHX hexamethylene was detected near the hydrophobic-hydrophilic interface (70). The changes are not significantly different for NegM liposomes. In both cases, saturation occurs, which may suggest that there is a maximal available space on the surface of the nanocarrier available for CHX. These data are in agreement with the results obtained from the ζ-potential charge measurements.

ζ-potential measurements and partition coefficient

In a similar manner as before, we decided to study membrane structure and stability in the function of CHX concentration by determination of the ζ potential and dynamic light scattering and to evaluate the influence of membrane charge on interaction strength as well. The results presented in Fig. 3 E indicate a rapid nature of the interaction between CHX and the NegM compared to the NLM. Specifically, the slope of the ζ-potential change was highest for 1 and 2% DOPG and slightly decreased with 3% DOPG in the membrane. The NegM liposomes were characterized

by rapid saturation after the addition of CHX and the determination of the equilibrium state at a level of approximately +60 to +70 mV, which results directly from the partition coefficient of these substances. LogP of CHX was estimated as 5.48 using the SCIGRESS calculation tool. This indicates a high tendency of this substance to be located in the outer part of the membrane. Because the CHX net charge equals zero, experimental determination of water or membrane logP from ζ-potential measurements was not performed. Electrostatic interactions between the CHX molecule and the lipid phosphate groups lead to accumulation of the latter on the surface. The less rapid ζ-potential changes we observe in the NLM, as a peak value of 60 mV was obtained in 0.3 CHX/LIP concentration. The average size of vesicles determined using dynamic light scattering was slightly reduced in increasing CHX concentration (see Fig. S16). We also determined that the ζ-potential changes are not correlated with pH, which remains steady in various agent concentrations (see Fig. S17).

Destructive effect of agent and selectivity

To strengthen our message, we performed membrane self-assembly studies in the presence of CHX (see Fig. 4 A). In the case of randomly distributed PC lipids, formation of
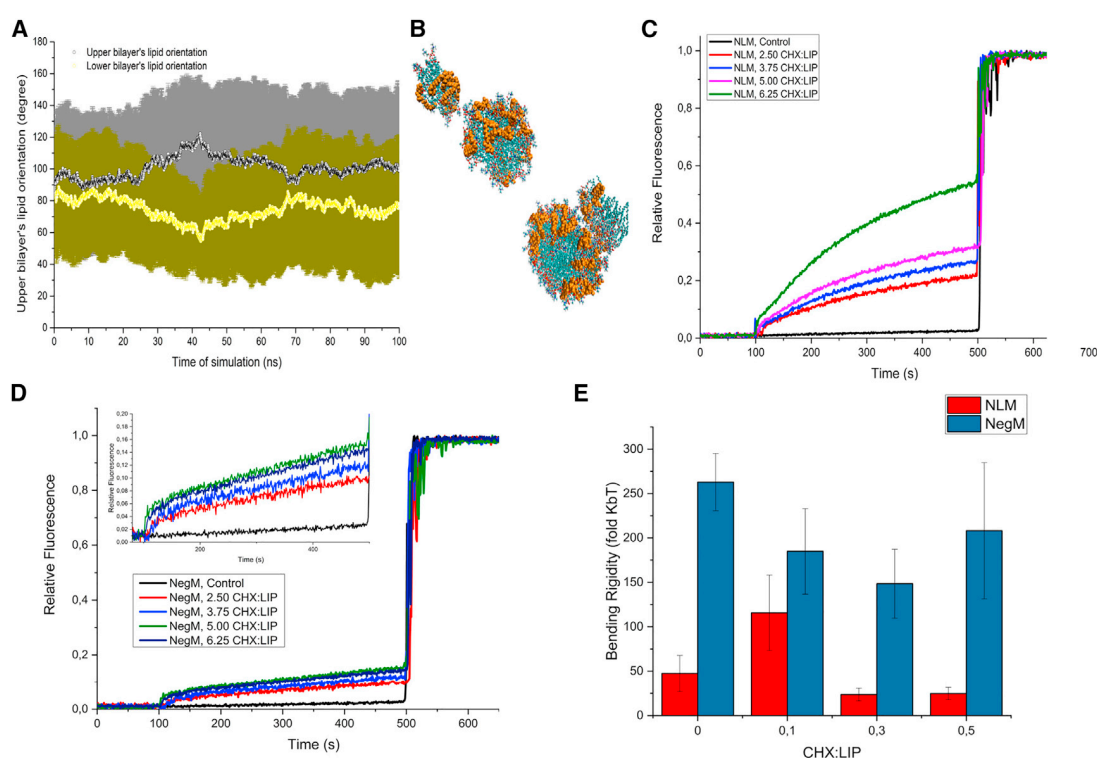

FIGURE 4 (*A*) Self-assembly MD simulation presenting interrupted membrane formation by OCT particles and (*B*) visualization of spherical membrane after self-assembly accompanied by CHX particles. (*C*) CXF leakage from NLM after CHX addition at 100 s, (*D*) CXF leakage from NegM after CHX addition at 100 s, and (*E*) bending rigidity analysis introduced by statistical approach; results obtained from vesicle fluctuation spectroscopy. To see this figure in color, go online.

the bilayer was observed after 60 ns with a 580 kcal/mol increase in VdW energy. However, in the case of randomly distributed lipids with CHX molecules (3:7 CHX/LIP), formation of the bilayer did not occur. Spherical lipid structures covered with CHX were formed instead, which are presented in Fig. 4 *B*. The VdW energy increase equaled 230 kcal/mol. This suggests that CHX influenced the self-assembly process of the membrane. This also indicates that CHX has an impact on membrane structure and/or properties.

To this end, the leakage of CXF loaded inside the liposomes induced by CHX was investigated. With the increasing ratio of CHX/lipid particles, the release of CXF was quantitively greater. However, the doses of CHX used during the experiment were significantly higher than in commercial products or physiological conditions. Interestingly, in the case of the NLM, the leakage of CXF was gradually increasing with time. In the case of the NegM, the leakage was almost linear and hardly noticeable at all. Despite significant doses, in both cases leakage was barely observed. The kinetics for both membranes is presented in Fig. 4, *C* and *D*. Because incorporation of CHX in membrane is a fast process, as we proved in MD simulations, the initial process of CXF release should be rapid, as it would be related to the disruption of the membrane by CHX incorporation. However, because of the quantities used, it is unlikely that the CHX antimicrobial mechanism of action is related to disruption of the membrane fluidity and/or structure. Nevertheless, we assessed the effect of CHX incorporation in the NLM and NegM on bending rigidity value. CHX induced in lower concentrations (0.1 CHX/LIP) an increase in bending rigidity in POPC systems. This was followed by a strong decrease for 0.3 CHX/LIP, making the membrane much more elastic. Successive addition of CHX did not significantly influence membrane mechanical properties. In the case of NegM vesicles, the only significant results were between 0/0.1 CHX/LIP and 0/0.3 CHX/LIP. Both 0.1/0.3 CHX/LIP and 0/0.5 CHX/LIP results were not significant. Such results suggest that after the initial addition of CHX to the NegM system, the additional doses of CHX did not change the mechanical behavior of the membrane. The lack of significance between 0/0.5 CHX/LIP can be easily explained by the presence of membrane defects such as buds that were observed in higher CHX concentrations. Such effects could contribute to measuring higher values of bending rigidity (63). The bending rigidity change is presented in Fig. 4 *E*. Moreover, we employed an average-based approach for bending rigidity determination presented in Fig. S19. It should be noted that CHX induces an ellipsoidal shape on GUV membranes. It was recently shown (63) that this could contribute to a slight difference between determined and real membrane bending rigidity. Interestingly, although the decrease of bending rigidity was substantial in the case of the NLM, mechanical disruption of the membrane did not occur, as

clearly seen in leakage experiments. The change of bending rigidity was much lower in the case of the NegM system, which corresponds well with the results from leakage experiments, in which stronger leakage was observed in the NLM system. Nevertheless, the observed leakage and changes in bending rigidity are not magnitude enough to assume that CHX is inducing the integrity loss based on mechanical properties. Neither the results of any experiments nor those of simulations indicated that there is any kind of electrostatic selectivity.

Summary

It was suggested by Epand et al. (43) that the possible antimicrobial mechanism of membrane-targeting agents is related to the disruption of membrane ability to spontaneously form microdomains. For instance, in *E. coli*, cardiolipin domains were observed under the microscope (73). With a significant change of mechanical properties, lack of vesicle leakage, and nonspecific changes in APL and lateral diffusion, we assume that the antimicrobial effect of CHX is related to changes in stiffness of the membrane, which can result in disruption of microdomain formation and/or loss of proteostasis for transmembrane proteins, which are crucial for microbe survival (74). All investigated systems were homogeneous (no domains); hence, possible effects due to heterogeneity could not be observed.

CONCLUSIONS

In this study, we have made an attempt to unravel the mechanism and selectivity of antimicrobial candidates, octenidine and chlorhexidine, in various lipid membrane systems. In molecular dynamics studies, we selected three types of lipid composition to represent neutral, negatively charged, and bacterial membranes. Our results indicate that a single molecule of both OCT and CHX is incorporated into all membranes in the same staple shape. A difference was observed with increasing concentration of compounds. In reference to OCT, an aggregate was formed first, and interaction with membrane was noted afterward. We also observed several shapes of aggregates depending on the lipid composition. The opposite tendency occurred in CHX behavior. It penetrated the bilayers singly and did not form aggregates, which is caused by the noticeably smaller partition coefficient, logP. Moreover, we assume that OCT forms aggregates preferentially to minimize the entropy of the system. Observed results of APL, membrane thickness, and lateral diffusion values indicated that both compounds firmly interact with all types of membranes. We determined by TMA-DPH and DPH fluorescent probes that accumulation of the OCT and CHX molecules is located in the carbonyl-glycerol region, which is in agreement with our simulations. To observe preferential accumulation and the particles' influence on membrane surface charge, we performed ζ-potential measurements. Interestingly,

interactions with the NLM were more rapid compared with the NegM one based on ζ-potential kinetics. We suppose that mutual repulsion of these compounds and their partition coefficients saturate the surface charge and neutralize the negative membrane charges; hence, the ζ-potential kinetics for NegM are slower for OCT and CHX. The ζ potential emphasized the differences in interaction between CHX and OCT with the NegM, despite the comparable localization in membrane. To detect the destructive properties of both molecules, we investigated self-assembly ability in MD of lipids in the presence of antimicrobial agents and CXF leakage from liposomes as an effect of agent presence. In both cases, membrane self-assembly was affected. Spherical structures were formed instead of a pure bilayer. The damaging properties of molecules are also noticeable during CXF leakage. However, they were less distinctive in the case of CHX. The NLM's exposure to OCT and CHX caused more intensive leakage compared with the NegM. We also investigated the effect of the investigated substances on membrane mechanical properties. The bending coefficient decreased significantly in both cases, making the membrane much more elastic. The presented research indicates that OCT shows a selective effect over membrane mechanical properties. Bending and stiffness of membrane occurs as an emerging property that could possibly serve as a means of selectivity. By further inducing mechanical changes, OCT would induce mechanical defects and loss of membrane integrity. Such a mode of action would result in cytoplasm leakage and ultimately cell death. Taking into account the change in mechanical properties, the effect of membrane self-aggregation, and nonspecific changes in both APL and lateral diffusion, we assume that the antimicrobial effect of CHX is related to decreased stiffness of the membrane, which can result in the disruption of microdomain formation and/or loss of proteostasis. In the case of CHX, mechanical changes did not induce considerable leakage of CXF from the liposomes. As a result, we believe that the possible CHX antimicrobial mechanism of membrane-targeting agents is based on the impediment of the membrane's ability to spontaneously form microdomains.

SUPPORTING MATERIAL

Supporting material can be found online at https://doi.org/10.1016/j.bpj.2021.06.027.

AUTHOR CONTRIBUTIONS

S.K., D.D., and K.S.-P. designed the research. D.D., M.R., K.S.-P., and B.H.-L. performed the experiments. M.R. and D.D. performed the MD simulations. M.R., D.D., and K.S.-P. analyzed data. S.K. provided funding and materials. M.R. and D.D. wrote the manuscript, which was revised by all authors.

REFERENCES

1. Russell, A. D. 2002. Antibiotic and biocide resistance in bacteria: introduction. *J. Appl. Microbiol.* 92 (*Suppl*):1S–3S.

2. World Health Organization. 2014. Antimicrobial resistance: global report on surveillance. WHO Press, Switzerland https://apps.who.int/iris/handle/10665/112642.

3. Ventola, C. L. 2015. The antibiotic resistance crisis: part 1: causes and threats. *P T.* 40:277–283.

4. Kong, K. F., L. Schneper, and K. Mathee. 2010. Beta-lactam antibiotics: from antibiosis to resistance and bacteriology. *APMIS.* 118:1–36.

5. Kramer, A. 2000. Hand disinfection and antiseptic of skin, mucous membranes, and wounds. *In* Dermatopharmacology of Topical Preparations. B. Gabard, C. Surber, P. Elsner, and P. Treffel, eds. Springer, pp. 121–134.

6. Gilbert, P., and L. E. Moore. 2005. Cationic antiseptics: diversity of action under a common epithet. *J. Appl. Microbiol.* 99:703–715.

7. Assadian, O. 2016. Octenidine dihydrochloride: chemical characteristics and antimicrobial properties. *J. Wound Care.* 25 (*Suppl 3*):S3–S6.

8. Sedlock, D. M., and D. M. Bailey. 1985. Microbicidal activity of octenidine hydrochloride, a new alkanediylbis[pyridine] germicidal agent. *Antimicrob. Agents Chemother.* 28:786–790.

9. Freeman, D. E., and J. A. Auer. 2012. Instrument preparation, sterilization, and antiseptics. *In* Equine Surgery. J. A. Auer and J. A. Stick, eds. Elsevier Inc., pp. 98–111.

10. Schneider, L. A., A. Körber, …, J. Dissemond. 2007. Influence of pH on wound-healing: a new perspective for wound-therapy? *Arch. Dermatol. Res.* 298:413–420, Published online November 8, 2006.

11. Al-Doori, Z., P. Goroncy-Bermes, …, D. Morrison. 2007. Low-level exposure of MRSA to octenidine dihydrochloride does not select for resistance. *J. Antimicrob. Chemother.* 59:1280–1281.

12. Kodedová, M., K. Sigler, …, D. Gášková. 2011. Fluorescence method for determining the mechanism and speed of action of surface-active drugs on yeast cells. *Biotechniques.* 50:58–63.

13. Malanovic, N., A. Ön, …, K. Lohner. 2020. Octenidine: novel insights into the detailed killing mechanism of Gram-negative bacteria at a cellular and molecular level. *Int. J. Antimicrob. Agents.* 56:106146.

14. Hübner, N.-O., J. Siebert, and A. Kramer. 2010. Octenidine dihydrochloride, a modern antiseptic for skin, mucous membranes and wounds. *Skin Pharmacol. Physiol.* 23:244–258.

15. Brill, F., P. Goroncy-Bermes, and W. Sand. 2006. Influence of growth media on the sensitivity of *Staphylococcus aureus* and *Pseudomonas aeruginosa* to cationic biocides. *Int. J. Hyg. Environ. Health.* 209:89–95.

16. Szostak, K., A. Czogalla, …, M. Langner. 2018. New lipid formulation of octenidine dihydrochloride. *J. Liposome Res.* 28:106–111.

17. Nicolae Dopcea, G., I. Dopcea, …, F. Matei. 2020. Resistance and cross-resistance in *Staphylococcus spp.* strains following prolonged exposure to different antiseptics. *J. Glob. Antimicrob. Resist.* 21:399–404.

18. Shepherd, M. J., G. Moore, …, L. J. Bock. 2018. *Pseudomonas aeruginosa* adapts to octenidine in the laboratory and a simulated clinical setting, leading to increased tolerance to chlorhexidine and other biocides. *J. Hosp. Infect.* 100:e23–e29.

19. Horner, C., D. Mawer, and M. Wilcox. 2012. Reduced susceptibility to chlorhexidine in staphylococci: is it increasing and does it matter? *J. Antimicrob. Chemother.* 67:2547–2559.

20. Kanisavaran, Z. M. 2008. Chlorhexidine gluconate in endodontics: an update review. *Int. Dent. J.* 58:247–257.

21. Eggers, M., T. Koburger-Janssen, …, S. Müller. 2018. Bactericidal and virucidal activity of povidone-iodine and chlorhexidine gluconate cleansers in an in vivo hand hygiene clinical simulation study. *Infect. Dis. Ther.* 7:235–247.

22. do Amorim, C. V. G., C. E. Aun, and M. P. A. Mayer. 2004. Susceptibility of some oral microorganisms to chlorhexidine and paramono-chlorophenol. *Braz. Oral Res.* 18:242–246.

23. Kropinski, A. M., J. Kuzio, …, R. E. W. Hancock. 1982. Chemical and chromatographic analysis of lipopolysaccharide from an antibiotic-supersusceptible mutant of *Pseudomonas aeruginosa. Antimicrob. Agents Chemother.* 21:310–319.

24. Thomas, B., and D. J. Stickler. 1979. Chlorhexidine resistance and the lipids of Providencia stuartii. *Microbios.* 24:141–150.

25. Wright, N. E., and P. Gilbert. 1987. Influence of specific growth rate and nutrient limitation upon the sensitivity of *Escherichia coli* towards chlorhexidine diacetate. *J. Appl. Bacteriol.* 62:309–314.

26. Copin, R., W. E. Sause, …, B. Shopsin. 2019. Sequential evolution of virulence and resistance during clonal spread of community-acquired methicillin-resistant *Staphylococcus aureus. Proc. Natl. Acad. Sci. USA.* 116:1745–1754.

27. Cieplik, F., N. S. Jakubovics, …, A. Al-Ahmad. 2019. Resistance toward chlorhexidine in oral bacteria-is there cause for concern? *Front. Microbiol.* 10:587.

28. Cheung, H. Y., M. M. K. Wong, …, S. K. Chiu. 2012. Differential actions of chlorhexidine on the cell wall of *Bacillus subtilis* and *Escherichia coli. PLoS One.* 7:e36659.

29. Chawner, J. A., and P. Gilbert. 1989. Interaction of the bisbiguanides chlorhexidine and alexidine with phospholipid vesicles: evidence for separate modes of action. *J. Appl. Bacteriol.* 66:253–258.

30. Chawner, J. A., and P. Gilbert. 1989. Adsorption of alexidine and chlorhexidine to *Escherichia coli* and membrane components. *Int. J. Pharm.* 55:209–215.

31. Davies, A. 1973. The mode of action of chlorhexidine. *J. Periodontal Res. Suppl.* 12:68–75.

32. Hugo, W. B., and A. R. Longworth. 1965. Cytological aspects of the mode of action of chlorhexidine diacetate. *J. Pharm. Pharmacol.* 17:28–32.

33. Elferink, J. G. R., and H. L. Booij. 1974. Interaction of chlorhexidine with yeast cells. *Biochem. Pharmacol.* 23:1413–1419.

34. Hugo, W. B., and A. R. Longworth. 1964. Some aspects of the mode of action of chlorhexidine. *J. Pharm. Pharmacol.* 16:655–662.

35. Rye, R. M., and D. Wiseman. 1968. Some observations on the use of absorbance measurements in bacteriology. *J. Pharm. Pharmacol.* 20:23S–25S.

36. Chawner, J. A., and P. Gilbert. 1989. A comparative study of the bactericidal and growth inhibitory activities of the bisbiguanides alexidine and chlorhexidine. *J. Appl. Bacteriol.* 66:243–252.

37. Longworth, A. R. 1971. Inhibition and Destruction of the Microbial Cell. Academic Press, New York.

38. Banerjee, D., U. Sarkar, and D. Roy. 2013. Multicomponent adsorption of chlorhexidine gluconate in presence of a cationic surfactant: role of electrostatic interactions and surface complexation. *J. Environ. Chem. Eng.* 1:241–251.

39. Freitas, L. B., N. Vassilakos, and T. Arnebrant. 1993. Interactions of chlorhexidine with salivary films adsorbed at solid/liquid and air/liquid interfaces. *J. Periodontal Res.* 28:92–97.

40. Costalonga, B. L. P., R. C. da Silva, …, C. Molina. 2012. Interaction of chlorhexidine with biomembrane models on glass ionomer by using the Langmuir-Blodgett technique. *Colloids Surf. B Biointerfaces.* 97:57–61.

41. Gottenbos, B., D. W. Grijpma, …, H. J. Busscher. 2001. Antimicrobial effects of positively charged surfaces on adhering Gram-positive and Gram-negative bacteria. *J. Antimicrob. Chemother.* 48:7–13.

42. Sohlenkamp, C., and O. Geiger. 2016. Bacterial membrane lipids: diversity in structures and pathways. *FEMS Microbiol. Rev.* 40:133–159.

43. Epand, R. M., and R. F. Epand. 2009. Lipid domains in bacterial membranes and the action of antimicrobial agents. *Biochim. Biophys. Acta.* 1788:289–294.

44. Drabik, D., J. Doskocz, and M. Przybyło. 2018. Effects of electroformation protocol parameters on quality of homogeneous GUV populations. *Chem. Phys. Lipids.* 212:88–95.

45. Drabik, D., M. Przybyło, …, M. Langner. 2016. The modified fluorescence based vesicle fluctuation spectroscopy technique for determination of lipid bilayer bending properties. *Biochim. Biophys. Acta.* 1858:244–252.

46. Freire, J. M., M. M. Domingues, …, M. A. R. B. Castanho. 2011. Using zeta-potential measurements to quantify peptide partition to lipid membranes. *Eur. Biophys. J.* 40:481–487.

47. Frisch, M. J., G. W. Trucks, X. Li…, 2016. Gaussian 16, Revision. Gaussian Inc., Wallingford CT https://gaussian.com/gaussian16/.

48. Jo, S., T. Kim, …, W. Im. 2008. CHARMM-GUI: a web-based graphical user interface for CHARMM. *J. Comput. Chem.* 29:1859–1865.

49. Humphrey, W., A. Dalke, and K. Schulten. 1996. VMD: visual molecular dynamics. *J. Mol. Graph.* 14:33–38, 27–28..

50. Giorgino, T. 2019. Computing diffusion coefficients in macromolecular simulations: the diffusion coefficient tool for VMD. *J. Open Source Software.* 4:1698.

51. Kholina, E. G., I. B. Kovalenko, …, P. S. Orekhov. 2020. Cationic antiseptics facilitate pore formation in model bacterial membranes. *J. Phys. Chem. B.* 124:8593–8600.

52. Lentz, B. R. 1989. Membrane "fluidity" as detected by diphenylhexatriene probes. *Chem. Phys. Lipids.* 50:171–190.

53. Demchenko, A. P., Y. Mély, …, A. S. Klymchenko. 2009. Monitoring biophysical properties of lipid membranes by environment-sensitive fluorescent probes. *Biophys. J.* 96:3461–3470.

54. do Canto, A. M. T. M., J. R. Robalo, …, L. M. S. Loura. 2016. Diphenylhexatriene membrane probes DPH and TMA-DPH: a comparative molecular dynamics simulation study. *Biochim. Biophys. Acta.* 1858:2647–2661.

55. Cundall, R. B., I. Johnson, …, I. H. Munro. 1979. Photophysical properties of DPH derivatives. *Chem. Phys. Lett.* 64:39–42.

56. Prendergast, F. G., R. P. Haugland, and P. J. Callahan. 1981. 1-[4-(Trimethylamino)phenyl]-6-phenylhexa-1,3,5-triene: synthesis, fluorescence properties, and use as a fluorescence probe of lipid bilayers. *Biochemistry.* 20:7333–7338.

57. Poojari, C., N. Wilkosz, …, T. Róg. 2019. Behavior of the DPH fluorescence probe in membranes perturbed by drugs. *Chem. Phys. Lipids.* 223:104784.

58. Nazari, M., M. Kurdi, and H. Heerklotz. 2012. Classifying surfactants with respect to their effect on lipid membrane order. *Biophys. J.* 102:498–506.

59. Stewart, C. A., Y. Finer, and B. D. Hatton. 2018. Drug self-assembly for synthesis of highly-loaded antimicrobial drug-silica particles. *Sci. Rep.* 8:895.

60. Pan, H., J. N. Marsh, …, S. A. Wickline. 2012. Postformulation peptide drug loading of nanostructures. Methods in Enzymology. Academic Press Inc, pp. 17–39.

61. Chen, R. F., and J. R. Knutson. 1988. Mechanism of fluorescence concentration quenching of carboxyfluorescein in liposomes: energy transfer to nonfluorescent dimers. *Anal. Biochem.* 172:61–77.

62. Sevcsik, E., G. Pabst, …, K. Lohner. 2008. Interaction of LL-37 with model membrane systems of different complexity: influence of the lipid matrix. *Biophys. J.* 94:4688–4699.

63. Faizi, H. A., C. J. Reeves, …, R. Dimova. 2020. Fluctuation spectroscopy of giant unilamellar vesicles using confocal and phase contrast microscopy. *Soft Matter.* 16:8996–9001.

64. Faizi, H. A., S. L. Frey, …, P. M. Vlahovska. 2019. Bending rigidity of charged lipid bilayer membranes. *Soft Matter.* 15:6006–6013.

65. Drabik, D., M. Gavutis, …, A. R. Ulčinas. 2020. Determination of the mechanical properties of model lipid bilayers using atomic force microscopy indentation. *Langmuir.* 36:13251–13262.

66. Matuła, K., Ł. Richter, …, R. Hołyst. 2019. Phenotypic plasticity of *Escherichia coli* upon exposure to physical stress induced by ZnO nanorods. *Sci. Rep.* 9:8575.

67. Harper, C. E., and C. J. Hernandez. 2020. Cell biomechanics and mechanobiology in bacteria: challenges and opportunities. *APL Bioeng.* 4:021501.

68. Rojas, E. R., G. Billings, …, K. C. Huang. 2018. The outer membrane is an essential load-bearing element in Gram-negative bacteria. *Nature.* 559:617–621.

69. Handorf, A. M., Y. Zhou, …, W. J. Li. 2015. Tissue stiffness dictates development, homeostasis, and disease progression. *Organogenesis.* 11:1–15.

70. Komljenović, I., D. Marquardt, …, E. Sternin. 2010. Location of chlorhexidine in DMPC model membranes: a neutron diffraction study. *Chem. Phys. Lipids.* 163:480–487.

71. Van Oosten, B., D. Marquardt, …, T. A. Harroun. 2014. Small molecule interaction with lipid bilayers: a molecular dynamics study of chlorhexidine. *J. Mol. Graph. Model.* 48:96–104.

72. Van Oosten, B., D. Marquardt, and T. A. Harroun. 2017. Testing high concentrations of membrane active antibiotic chlorhexidine via computational titration and calorimetry. *J. Phys. Chem. B.* 121:4657–4668.

73. Fishov, I., and C. L. Woldringh. 1999. Visualization of membrane domains in *Escherichia coli*. *Mol. Microbiol.* 32:1166–1172.

74. Barák, I., and K. Muchová. 2013. The role of lipid domains in bacterial cell processes. *Int. J. Mol. Sci.* 14:4050–4065.

Chapter 7

Paper 2

A Systematic Approach: Molecular Dynamics Study and Parametrisation of Gemini Type Cationic Surfactants

A Systematic Approach: Molecular Dynamics Study and Parametrisation of Gemini Type Cationic Surfactants

Mateusz Rzycki [1,2,*], Aleksandra Kaczorowska [2], Sebastian Kraszewski [2] and Dominik Drabik [2,3]

1 Department of Experimental Physics, Faculty of Fundamental Problems of Technology, Wroclaw University of Science and Technology, 50-370 Wroclaw, Poland
2 Department of Biomedical Engineering, Faculty of Fundamental Problems of Technology, Wroclaw University of Science and Technology, 50-370 Wroclaw, Poland; aleksandra.kaczorowska@pwr.edu.pl (A.K.); sebastian.kraszewski@pwr.edu.pl (S.K.); dominik.drabik@uwr.edu.pl (D.D.)
3 Laboratory of Cytobiochemistry, Faculty of Biotechnology, University of Wroclaw, 50-383 Wroclaw, Poland
* Correspondence: mateusz.rzycki@pwr.edu.pl

Abstract: The spreading of antibiotic-resistant bacteria strains is one of the most serious problem in medicine to struggle nowadays. This triggered the development of alternative antimicrobial agents in recent years. One of such group is Gemini surfactants which are massively synthesised in various structural configurations to obtain the most effective antibacterial properties. Unfortunately, the comparison of antimicrobial effectiveness among different types of Gemini agents is unfeasible since various protocols for the determination of Minimum Inhibitory Concentration are used. In this work, we proposed alternative, computational, approach for such comparison. We designed a comprehensive database of 250 Gemini surfactants. Description of structure parameters, for instance spacer type and length, are included in the database. We parametrised modelled molecules to obtain force fields for the entire Gemini database. This was used to conduct in silico studies using the molecular dynamics to investigate the incorporation of these agents into model E. coli inner membrane system. We evaluated the effect of Gemini surfactants on structural, stress and mechanical parameters of the membrane after the agent incorporation. This enabled us to select four most likely membrane properties that could correspond to Gemini's antimicrobial effect. Based on our results we selected several types of Gemini spacers which could demonstrate a particularly strong effect on the bacterial membranes.

Keywords: gemini; molecular dynamics; force field; parametrisation; antimicrobial; membranes

1. Introduction

Antimicrobial resistance against available antibiotics has been acknowledged as one of the most serious problems in medicine nowadays. This resulted in a surge of new research works related to the synthesis of novel compounds that could serve as a potential modern-generation groups of antimicrobial particles. One of these groups are Gemini surfactants (initially referred to as bis-surfactants), which are heavily reported for their antimicrobial effect [1]. In recent years, Gemini surfactants have been heavily addressed in the world of science. Over the past five years, more than 130 articles dealing with the subject of Gemini surfactants have been published, among which researchers determined the methods of synthesis of new compounds, their physicochemical properties and even their potential use or application.

Gemini surfactants have unique structural properties. They consist of two amphiphilic groups connected by a spacer at the head level, which can be both hydrophilic and hydrophobic [2,3]. They have at least two hydrophobic chains and two ionic or polar groups. There is a great variety in their structure e.g., short and long methylene groups can be used as a linker, stiff (stilbene), polar (polyether) and nonpolar (aliphatic) groups can be used as a linker [2,3]. The ionic group can be positive (ammonium) or negative (phosphorus,

sulfur, carboxylase), while the polar non-ionic groups can be polyether or sugar. Most Gemini surfactants have a symmetrical structure with two identical polar groups and two identical chains (but there are also Gemini that are asymmetrical or with three polar groups or chains) [4]. A universal scheme of Gemini is presented in Figure 1.
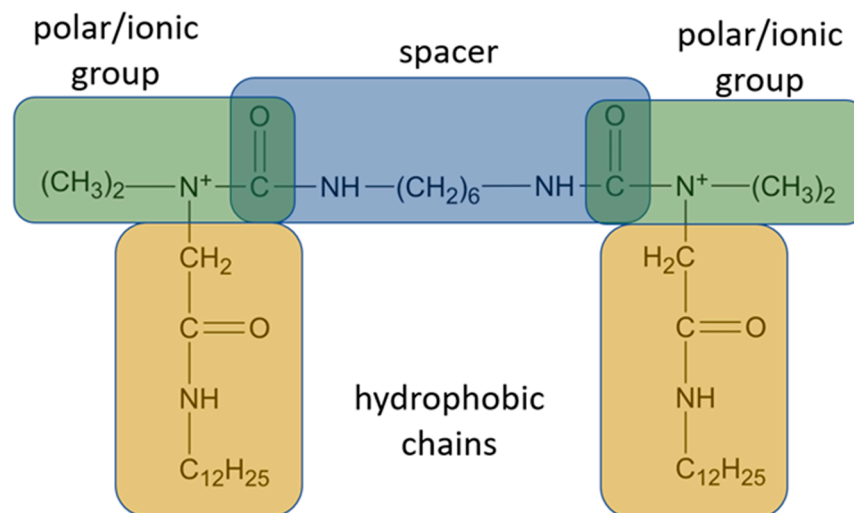

Figure 1. General scheme of Gemini structure classification presented on QAS-type spacer Gemini molecule.

A major part of synthesised Gemini surfactants has performed exquisite antibacterial properties against both Gram-positive and Gram-negative bacteria [5–7]. The most common antibacterial particles of this group are based on quaternary ammonium salts (QAS). Such salts prevent the development of bacteria and fungi; therefore, they are used on a large scale for cleaning, maintenance and disinfection. There were several attempts to evaluate the effectiveness of antibacterial activity of Gemini surfactants. However, these are usually limited to the compound structure—it is directly associated with the type and length of spacer in the molecule and/or the length of hydrophobic chains [8–10]. Numerous scientists proved that number of carbon atoms is correlated with the antimicrobial activity [11,12]. It has been established that a greater number of carbons in the molecule's structure increases its antibacterial activity, and the presence of 12 carbon atoms cause the greatest antibacterial response. It was proposed that the shorter chains might not interact with the hydrophobic region of the bilayer as smoothly and immediately as the longer ones [13]. However, very long tails might curve and twist disqualifying the interactions with negatively charged membrane surfaces by covering cationic head groups. Although it is believed that the major element in the surfactant antimicrobial properties is connected to the hydrophobic chain. It was confirmed that the head group type and structure are also essential factors of biological activity as in the case of QAS molecules [14]. Moreover, Moran et al. revealed that the structure of the hydrophilic core also plays an important role in antimicrobial effects [15,16].

Nevertheless, as mentioned earlier, all works focus only on the structural differences of Gemini surfactants. Furthermore, the conclusions are usually limited to one subgroup of Gemini compounds, hence when analysed more globally, are often mutually contradictory. The reported antimicrobial activity is based on minimum inhibitory concentration (MIC), which strongly depends on the protocol used [17]. The studies reporting the interactions and the effect of Gemini on membranes—with particular emphasis on their properties and potential rupture—are scarce in the literature. There are only available few studies on commercially available Gemini surfactants such as octenidine (OCT) [18–20]. This is quite surprising as membrane destruction was emphasised as one of the potential targets for antimicrobial effect [21,22]. To this end, in our work we have focused on systematic theoretical studies of Gemini agents. Specifically, we have reviewed available literature and

recreated the structure of the synthesised Gemini particle groups. This was followed by the classification of molecules into subgroups and the parametrisation of the compounds to create force fields for molecular dynamics studies. As a result, we obtained 250 valid force fields of Gemini class surfactants. Finally, we have selected valid representatives of the subgroups and investigated their interaction with lipid membranes. The selection of representatives was partially determined by the conclusions of structural studies. We ended with 25 selected particles used in molecular dynamics studies. The model membrane system was based on the inner membrane of *E. coli*. In this work we report the theoretical effect of Gemini class surfactants on properties and behaviour of the membrane. Additionally, the incorporation and behaviour of the molecules were also assessed. Based on our systematic characterisation of membrane system, we selected four parameters that were strongly affected by Gemini agents' incorporation. Those were: area compressibility, bending rigidity, lateral diffusion coefficient and surface tension. This selection of impactful parameters allowed us to make a preliminary selection of Gemini molecules groups that could show strong antimicrobial effect from those analysed. This work could provide a means for more detailed studies of Gemini class surfactants and their interaction with lipid membrane models. Such systematic computational analysis provides in silico method to select, from the group of molecules, the ones that are most likely candidates for antimicrobial compounds. It can result in decreasing the amount of expensive synthesis work, which can restrain this type of studies. In a further perspective, it could help in initial scanning of the molecules and facilitate comparison between different MIC studies to determine valid candidates for next-generation antimicrobial substances.

2. Results and Discussion

2.1. Parametrisation

Variety of different Gemini type molecules are synthesised and characterised every year in various literature reports. However, usually their antimicrobial effectiveness is described by a single MIC experiment using various protocols and bacteria families, after which they are left forgotten. Perhaps the new antimicrobial agents, more effective than currently available, have been already synthesised. Due to the shortcomings of the MIC experiments and the inability of systematic comparison it could be impossible to use them. Furthermore, these molecules have a specific biophysical effect on membranes, although are rarely used in molecular dynamic studies due to the missing of an appropriate parametrisation. To this end, we have collected the structures of synthesised Gemini molecules from a significant number of recent literature reports [1,3,7,10,23–49]. Using SCIGRESS software, these structures were designed and preliminarily optimised in the water solvent. It was followed by their equilibration and determination of the Hessian matrix was carried out using Gaussian software. Finally, data from both geometry and a Hessian matrix were used for parametrisation of modelled particles and the force fields creation. This approach was successfully used beforehand to create force fields for various particles [18,50,51]. In Supporting Materials (SM) we have delivered the detailed base of modelled 250 particles (see Microsoft Excel datasheet) with optimised force fields (see included zip file). Force fields are ready-to-use in NAMD software however, a detailed description on how to prepare them for GROMACS users was also included. Molecules were divided into groups based on the origin of the spacer. Each molecule is characterised by the molecular scheme, segment name, spacer formula, length of the spacer, length and formula of chain components and the presence of organic salt. Additionally, based on the modelled molecule structure, partition coefficient (logP) and critical micelle concentration (CMC) were determined. Several molecules were presented as a preview in Table 1 while the total selection is included in Table S1. The theoretical value of logP could be useful for molecule selection as it can indicate whether the molecule incorporates into the membrane in the first place. On the other hand, CMC value may suggest the aggregation behaviour of investigated agents. However, it should be noted that the algorithm is based on phenomenological values hence CMC should be only considered as an approximation.

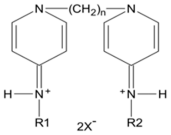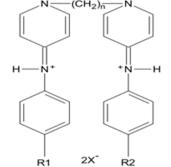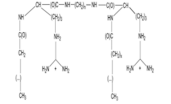**Table 1.** Representation of selected modelled molecules from detailed base included in Supporting Materials.
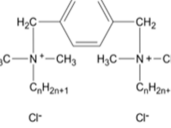
Group	Scheme	ID	Seg Name	Linker	Linker Length (n)	Chain Compound (R1 or R2)	Number of Carbons in R1/R2 (m)	Number of Carbons from N+	Chemical Formula	Organic Salt	log10 (CMC)	Ref.
Alkyl Bisp		Alk_6_12	A6G	$(CH_2)_6$	6	$C_{12}H_{25}$	12	12	$C_{40}H_{72}N_4$	Br	−4.09	[1]
Aryl Bisp		Ary_8_00b	AC2	$(CH_2)_8$	8	F	0	6	$C_{30}H_{34}F_2N_4$	Cl	−3.49	[1]
fQAS		fQS12_12	F0A	$C_{12}H_{16}F_8$	12	$C_{12}H_{25}$	12	12	$C_{40}H_{78}F_8N_2$	Br-	−6.65	[45]
Ring		Rin_01_12b	RI1	C_6H_4	1	$C_{12}H_{25}$	12	12	$C_{36}H_{70}N_2$	Cl	−3.63	[46]

Table 1. *Cont.*

Group	Scheme	ID	Seg Name	Linker	Linker Length (n)	Chain Compound (R1 or R2)	Number of Carbons in R1/R2 (m)	Number of Carbons from N+	Chemical Formula	Organic Salt	log10 (CMC)	Ref.
Ester		Est_2_12	E2D	C_2H_4	2	$C_{12}H_{25}$	12	15	$C_{36}H_{74}N_2O_4$	Br	−4.21	[35]
Ionic		Ion_4_12	I4C	$CH_2CH_2OCH_2CH_2$4	4	$C_{12}H_{25}$	12	12	$C_{38}H_{82}N_2O_5$	Br	−4.8	[10]
QAS		QAS_4_12	Q4A	C_4H_6	4	$C_{12}H_{25}$	12	12	$C_{32}H_{70}N_2$	Br/Cl	−2.61	[27,36]
tQAS		tQS_4_1002	T4F	$(CH_2)_4$	4	R1: $C_{10}H_{21}$ R2: C_2H_5	10 & 2	18	$C_{40}H_{86}N_2O_{10}$	I	−5,82	[49]

2.2. Membrane Characterisation

As previously stated, Gemini molecules are well-known for their antimicrobial activity. It was considered by Epand et al. [21] as well as shown in the OCT studies, that this effect is related to membrane disruption [18]. The effect of those Gemini molecules on the membrane properties was assessed to determine the properties that most likely correspond to the antimicrobial effect. A number of molecules were selected to investigate the effect of Gemini particles on membrane's behaviour. Specifically, at least one molecule from each group was selected. Since in several works [52–56] it was reported that strongest antimicrobial effect was observed for Gemini agents with chain length equal to 12 carbon atoms, such condition was adapted during molecule selection from the group. All of the investigated molecules, except diGalactose (dGl), were incorporated into the membrane during the simulation time. The dGl molecule fluctuated over the bilayer surface, maintaining a 30 ± 4 Å distance from phosphorous atoms in lipid heads. The explanation of a lack of incorporation for dGl most likely lies in the negative logP of the molecule. A detailed location of system components such as lipid fragments or Gemini molecules has been presented in the partial density chart in Figure S1–S5 in SM. Selected screenshots of the systems with anchored molecules are presented in Figure 2. The membrane composition was selected in such a way to most accurately reflect the inner membrane of *E. coli* [21,57].
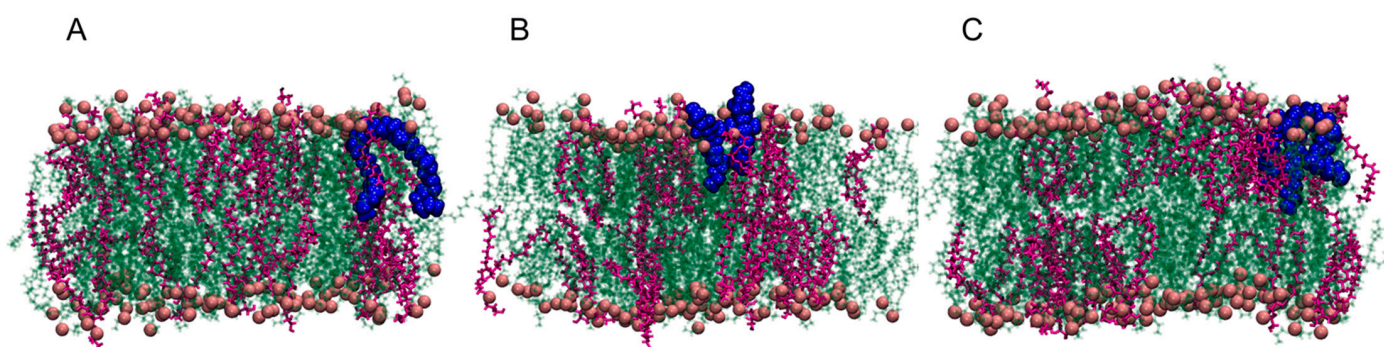

Figure 2. Selected screenshots of the systems with incorporated molecules, (**A**) Ole, (**B**) tQS, (**C**) hQS.

Membrane with incorporated Gemini molecules was thoroughly analysed to determine its properties such as area per lipid, membrane thickness, interdigitation, penetration depth, lateral diffusion, bending and tilt rigidities, area compressibility and surface tension. From such set of parameters four most likely candidates were chosen that could correspond to the antimicrobial effect. Those are membrane compressibility, bending rigidity, lateral diffusion and surface tension. The detailed characterisation of Gemini effect on the membrane, including all of the investigated parameters, is presented in SM Table S2. In this work, we additionally simulated the OCT molecule and we used it as a positive control. We assume that the effect on the membrane of these commercially available molecules could serve as a guidepost regarding desirable changes in selected properties. Since other molecules might indicate a much different mode of action therefore in our selection, we took into account the possible different mechanisms. Such a mechanism could induce a different magnitude of parameter change. As a result, we were also considering, in our selections, the extremum parameter changes, not only guided by the tendencies given by the effect of OCT. Concerning our analysis, we selected the four most changeable bilayer parameters reflecting membrane-agent interaction and potential antimicrobial activity. We deliver a total set of parameters in SM Table S2. The rest of the determined parameters were not selected due to insignificant differences between the analysed systems. Membrane thickness was, in general, determined to be between 39 and 41 Å. The difference of 2 Å between extreme particles with uncertainty equal to 1 Å was enough to exclude this parameter as an influential one. Similarly, tilt bending ranged from 9.9 up to 10.9 fold $K_b T$ with an uncertainty of 0.3 fold $K_b T$. For APL, when the leaflet in which the Gemini

agent incorporated is analysed, the values range between 58 and 62 Å^2. Only two cases are extreme, which are 67.0 ± 3.3 Å^2 for aryl bispiridine (Ary) and 64.8 ± 2.7 Å^2 for glucose (Glu). Interestingly, both of those spacers were highlighted as possible antimicrobial based on analysis of other significant parameters.

The area compressibility is one of the most robust parameters in our dataset, hence we predict that it may be an adequate property reflecting antimicrobial effect on the membrane. This mechanical parameter quantifies the energetic cost associated with the membrane's area stretching and/or compressing. For high values of area compressibility, the membrane is resistant to external pressure. For low values the membrane loses its resistivity. Both cases can result in inability of proper cell function. The determined values of area compressibility of bilayers with incorporated Gemini molecules are presented in Figure 3. The area compressibility of positive control—membrane with incorporated OCT—is almost seven times higher than in the case of the model membrane. Interestingly, membrane area compressibility with incorporated Adamantane (Adm) is higher than in the case of positive control. Four other molecules from the ester (Est), higher quaternary ammonium salt (hQAS), oligomeric QAS (o-QAS) and pyridine (Pyr) group also induced significant growth in the area compressibility. Furthermore, two Gemini molecules had a decreasing effect on the area compressibility of the membrane. Specifically, those from Saccharide (Sch) and Alkyl Bispyridinamine (Alk) group.
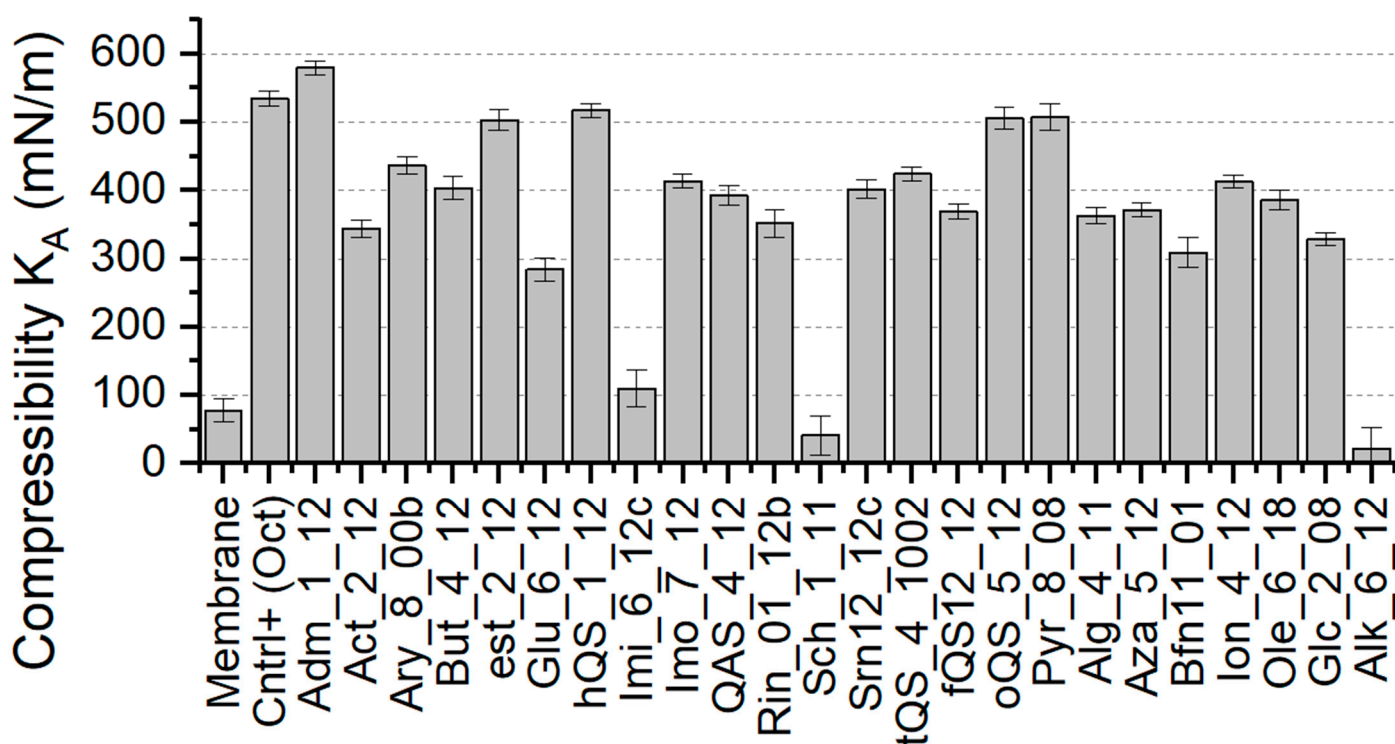

Figure 3. Determined values of compressibility (K_A) for membrane system with incorporated Gemini molecules.

In our previous work we highlighted that mechanical parameter such as bending rigidity play an important role in OCT mode of action [18]. To this end we selected this parameter as a likely and promising candidate that correspond to antimicrobial activity. Briefly, bending rigidity quantifies the energetic cost associated with the membrane bending. The determined values of bending rigidity of membranes with incorporated Gemini agents are presented in Figure 4. First, the difference between pure membrane and the positive control is not statistically significant. To our knowledge, the OCT effect on bending rigidity is closely related to the aggregation properties rather than the effect of a single molecule action [18]. Nevertheless, several Gemini molecules significantly affected the bending behaviour of membranes. Considering OCT as a positive control we found the activity of

several agents such as ionic (Ion), alginine (Alg), Pyr, butene (But) and glucose (Glu) as not statistically significant, hence similar to OCT. If, however, the strongest difference between pure membrane is considered, aryl bispiridine (Ary), imino (Imo), oQAS, gluconamid (Glc) were the most active candidates.
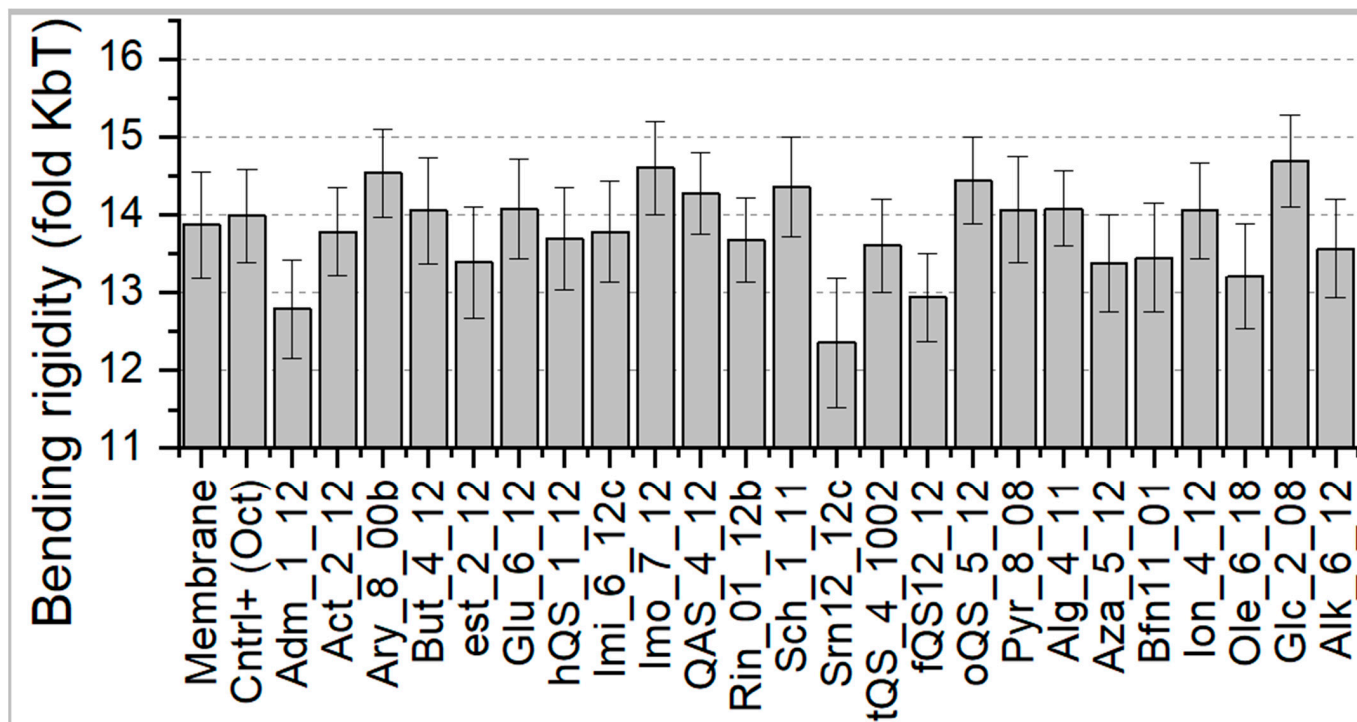

Figure 4. Calculated values of bending rigidity for membrane systems with incorporated Gemini molecules.

Lateral diffusion is a property that defines the mobility of lipid molecules in the membrane plane. Changes in lateral diffusion of the lipids could result in changes of movement of proteins, which can affect the activity of transporters and channel proteins [58]. Such an effect on proteins could significantly impede the functioning of microbe cells and correspond to antimicrobial effect of Gemini molecules. Although this dependency is not strictly related to the Gemini's destructive effect on the membrane, it also should be considered as a factor. The values of lateral diffusion of lipid molecules are presented in Figure 5. Our positive control indicates that decreasing effect on lateral diffusion should be desirable however, the antimicrobial effect of OCT is based on membrane disruption and cannot be considered as a factor in this case. Results obtained for model membrane are in strong agreement with the GUVs *E. coli* mimicking studies, i.e., experimental diffusion coefficient equals D = 6.09 $\mu m^2/s$ [59]. Interestingly, different antimicrobial agent-thymol induced growth in lipids mobility, supporting the agent translocation [59]. To this end we selected three lowest and three highest values of lateral diffusion for selected agents that influence this membrane property. Gemini molecules that strongly increased the lateral diffusion of lipids on membranes were But, imidazolium (Imi) and Pyr. On the other hand, Gemini molecules that strongly decreased the lateral diffusion were o-QAS, Imo and Glu.

Finally, the surface tension was determined for membranes with incorporated Gemini agents. Briefly, surface tension is defined as a cohesive force that keeps the cell membrane intact. Hence, its fluctuations may be very informative and extremely important for the determination of the antimicrobial mode of action based on the membrane disruption. Values of the membrane surface tension influenced by Gemini detergents are presented in Figure 6. The surface tension of membrane treated with OCT was twice as high than in the model membrane's case. Interestingly, a significant number of investigated molecules had much stronger effect on membrane surface tension compared to the positive control. Three

groups with the highest surface tension fluctuations were Ary, Aza and Alk. Additionally, the activity of several molecules such as hQS, Imo and Pyr led to decreased membrane tension. This should also be considered as change that could result in antimicrobial effect. Pure membrane exhibited natively certain surface tension hence, any strong deviation from this value could result in disruption of biological processes on the membrane.
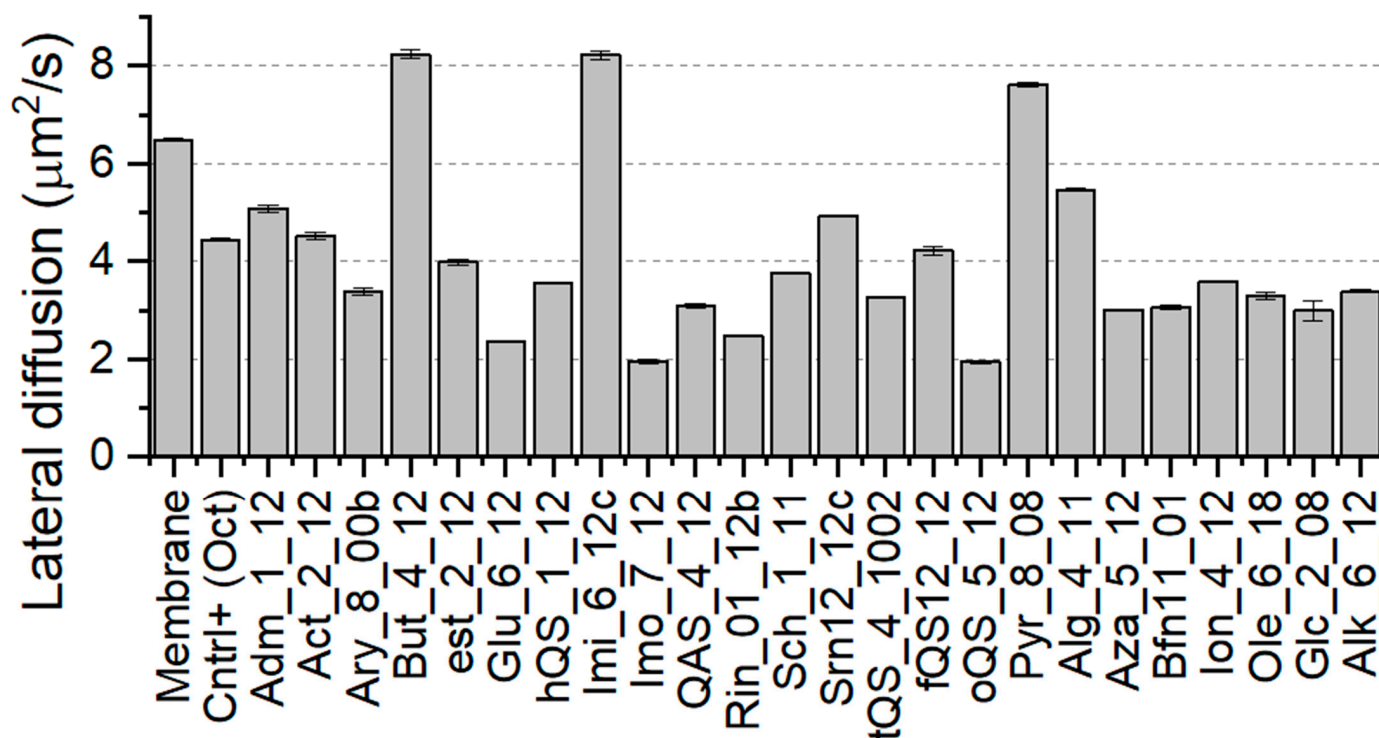

Figure 5. Determined values of lateral diffusion (2D) for membrane systems with incorporated Gemini molecules.

Taking into account our results oQAS, Pyr, Imo groups from the Gemini family may exhibit strong antimicrobial effects. These molecules act as prominent candidates since three from four selected membrane parameters were significantly affected. Wang et al. in their experimental work [60] reported that presence of oxygen atom in oQAS spacer chain introduces higher flexibility and reduction of coulombic repulsion allows long side alkyl chain to tighter aggregation. This stays in line with our results since the oQAS molecules deeply penetrate the bilayer affecting membrane diffusion and mechanical properties. Moreover, Wettig et al. [61] highlighted unique transfection properties of Imo compared to other synthesised molecules since additional flexibility from extra methylene unit between nitrogen centres and readily protonated imino group is present. In our opinion, given molecule properties may influence the membrane resulting in limited tension and diffusion. Interestingly, both oQAS and Imo agents have similarities in structures (latter has additional nitrogen and methylene units in the spacer region) and induce comparable change in the membrane's properties. Similarly, Quagliotto et al. [31] in the experimental work reported that increased Pyr concentration reduced the surface tension. This is in accordance with our theoretical approach where we observed significant limitations in membrane surface tension. Other vital candidates, that were selected based on two from four parameters, are Ary, Glu, hQAS and Alk. In the experimental work, Bailey et al. [1] concluded that Ary and Alk agents showed antimicrobial effectiveness, according to MIC. However, the latter showed weaker activity when compared to Ary. The authors emphasised that in the case of alkyl series the most effective agents are those with 22 up to 30 carbon atoms in the molecule. These could influence the character of membrane–molecule interactions and thus result in the fluctuation of membrane parameters. Our results also highlighted hQAS, which may be associated with molecule rigid spacer and three-charged headgroup

indicating affinity to negative membranes [24]. Finally, Kumar et al. [38] reported that Glu shows excellent surface-active properties and low cytotoxicity, which stay in agreement with our findings based on membrane parameters variation. This selection was presented in Table 2. Despite suggested membrane thinning in reported experimental works we did not observe significant occurrence nor changes in acyl chain interdigitation in our studies (see Table S2) [62,63]. Moreover, in a significant part of analysed molecules, we observed their preferential localisation in the carbonyl-glycerol region. This was influenced by neither how long the alkyl chain nor the spacer were (see Figure S1–S5). Nevertheless, experimental comparison studies using uniformed protocol are required to confirm whether selected parameters directly correspond to the discussed antimicrobial effect.
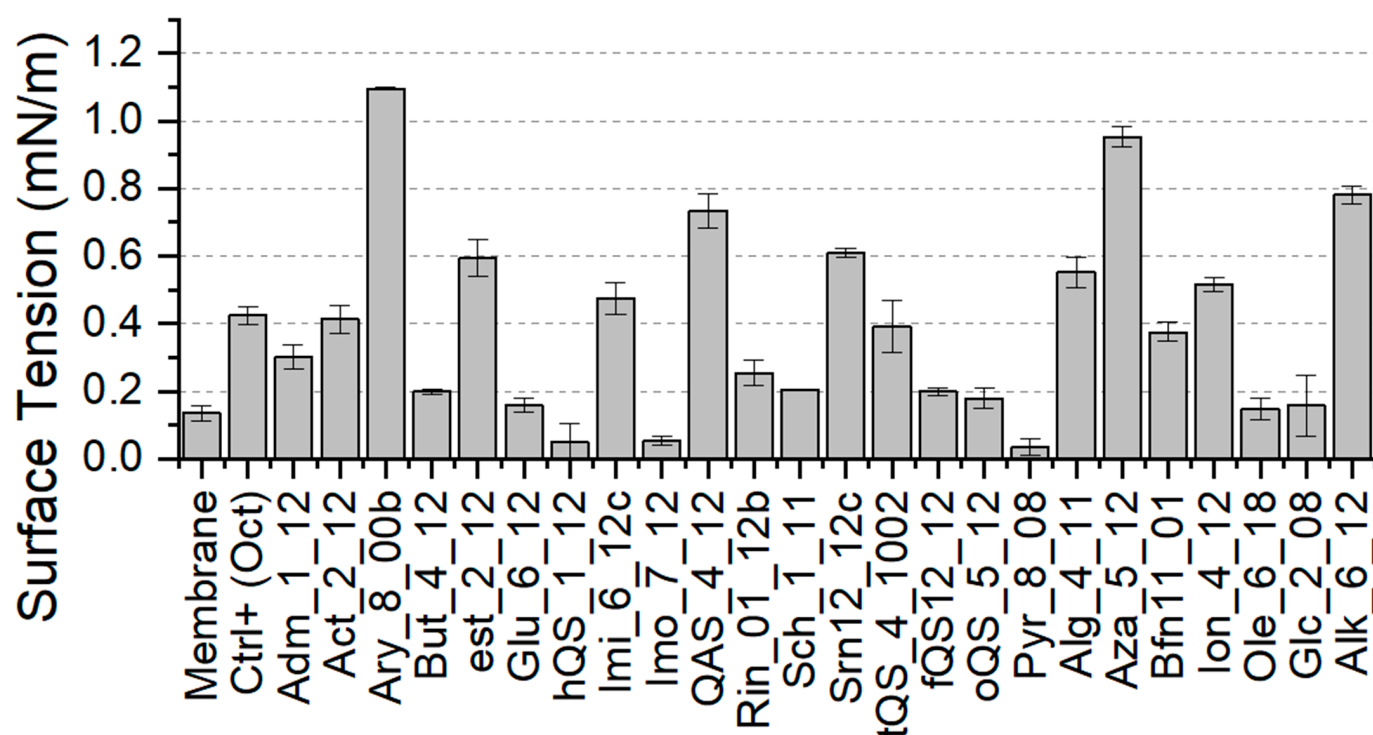

Figure 6. Surface tension, which was determined for membrane systems after the incorporation of investigated Gemini molecules.

Table 2. Selected potential antimicrobial candidates from each parameter group. It is suggested to compare those in experimental studies. Frequently appearing molecules were bolded to emphasise their repetition between different parameters consideration.

Compressibility K_A [mN/m]	Bending Rigidity [fold $K_B T$]	Lateral Diffusion [μm^2/s]	Surface Tension [mN/m]
o-QAS	**o-QAS**	**o-QAS**	Aza
Pyr	Ion	**Pyr**	**Pyr**
Adm	**Imo**	**Imo**	**Imo**
Est	**But**	**But**	
Sch	**Ary**	Imi	**Ary**
	Glu	**Glu**	
hQAS	Alg		**hQAS**
Alk	Glc		**Alk**

3. Materials and Methods

3.1. Molecule Parametrisation

Quantum level calculations were performed using the Gaussian 2016 software package [64]. The equilibrium geometry of investigated Gemini molecules was calculated using density functional theory (DFT) (B3LYP)/6-31++G (d) level of theory; first with Loose Self Consistent Field (SCF) procedure, then with Tight. The solvent effect was taken into consideration using the integral equation formalism of the polarisable continuum model IEFPCM. Temperature was set to 300 K. Supplementary analysis based on the construction of the Hessian matrix (the matrix of second derivatives of the energy with respect to geometry) was also performed for further use in the force field parameterisation. The specific geometric and electronic data, such as bond lengths, angles, dihedrals and charge distribution were extracted from a Hessian matrix. The charge distribution was determined from the RESP charge calculations as being the most adapted to reproduce the molecular behaviour with the subsequently used CHARMM force field. For logP determination, the octanol/water partitioning coefficient was calculated using SCIGRESS software (SCIGRESS, Molecular modeling software, FQS Poland, ver. FJ-3.3.3). For CMC determination, the algorithm proposed by Mozrzymas was used [65]. It is based on phenomenological values and second-order connectivity index, that was determined using SCIGRESS software. Molecule schemes were prepared using MoleculeSketch (v. 2.2.3).

3.2. Molecular Dynamics Simulations

The all-atom models of the membranes were generated using CHARMM-GUI membrane builder [66]. The bacterial membrane model consisted of 80% PYPE, 15% PYPG, 5% PVCL2 [21,57]. The lipid bilayer was solvated with TIP3P water molecules (100 water molecules per lipid) and 240 mM NaCl were added based on literature data [67].

MD simulations were performed using the GROMACS (version 2020.4) package with the CHARMM36 force field [68,69]. Membrane systems were first minimised with the steepest descent algorithm for energy minimisation. Further calculations were carried out in the NPT ensemble (constant Number of particles, Pressure and Temperature) with Berendsen thermostat and barostat using semi-isotropic coupling at T = 303.15 K with time constant τ = 1 ps and p = 1 bar with τ = 5 ps. The primary part of the NPT calculations was performed using the leap-frog integrator with a 1 fs timestep. Afterwards, for the further NPT ensemble at T = 303.15 K, τ = 1 ps and p = 1 bar, τ = 5 ps, a Nose-Hoover thermostat [70] and Parrinello-Rahman barostat [71] were used. The second part of long-run production was carried out for 500 ns using the leap-frog integrator. Chemical bonds between hydrogen and heavy atoms were constrained to their equilibrium values with the LINCS algorithm, while long-range electrostatic forces were evaluated using the particle mesh Ewald (PME) method [72] with the integration timestep of 2 fs. Based on simulated pure membranes, the behaviour of Gemini surfactants was investigated. Molecules were placed on average 2.5 nm above the membrane leaflet and the same MD procedure was employed. For visualisation purpose, Visual Molecular Dynamics (VMD) was used [73].

3.3. Membrane System Characteristics

Membrane Thickness and Area per Lipid. Both area per lipid and membrane thickness were determined using self-made MATLAB scripts (Matlab R2019a). Briefly, for each leaflet Z-position on all phosphorus atoms were averaged, and distance between average Z-positions between each of leaflets was calculated for each frame. The final membrane thickness value is an average over analysed trajectory. Similarly, for each frame position of phosphorus atoms (or Gemini atom on the Z-level corresponding to phosphorus atoms) each leaflet was subjected to Voronoi tessellation. The average area for all lipid molecules was calculated for each leaflet and frame and was averaged over the analysed trajectory.

Bending rigidity and Tilt rigidity. Both bending rigidity and tilt rigidities were determined using self-made MATLAB scripts that were based on the works of Doktorova et al. [74]. Briefly, a probability distribution for both tilt and splay are determined for all

lipids over all analysed time steps. Tilt is defined as an angle between the lipid director (vector between lipid head–midpoint between C2 and P atoms–and lipid tail–midpoint between 16th carbon atoms) and bilayer normal. Lipid splay Sr is defined as divergence of an angle formed by the directors of neighbouring lipids providing that they are weakly correlated.

Compressibility. Compressibility was determined using self-made MATLAB scripts based on the work of Doktorova et al. [75]. Briefly, a real-space analysis of local thickness fluctuations is sampled from the simulations for carbon atoms. This is followed by determination of reference surface and calculation of potential mean force from fluctuations from whole analysed trajectory to determine compressibility for given leaflet.

Lateral Diffusion Coefficient. The diffusion coefficient from the 2D mean square displacement (MSD) equation was calculated Diffusion Coefficient Tool [76] from the slope of the MSD curve through Einstein's relation. This relation is presented in Equation (1), where M (t) is the MSD at a range of lag time tau and E represents the dimensionality (XY). For the computation accuracy, only phosphorous atoms (in the range of 20 Å from surfactant) of all lipids were considered.

$$D(\tau) = \frac{M(\tau)}{2E\tau} \tag{1}$$

Interdigitation. For all provided systems the fluctuation of lipid interdigitation was determined using MEMBPLUGIN available in VMD software [77]. It is given in length units and reflects the interdigitation between opposite leaflets in the system—unless no interdigitation occurs it is equal to zero.

Penetration Depth. The depth of surfactant penetration was measured with respect to the membrane centre. From the last 50 ns of the trajectory the positions of the deepest placed carbon atoms on each alkyl chain were taken and evaluated with respect to the distance between phosphorous atoms divided by two, which represent the membrane centre.

Surface tension. The surface tension of membranes with anchored Gemini surfactants was computed using gmx energy function build-in GROMACS software using pressure tensor (Pxx, Pyy, Pzz values according to the Irving-Kirkwood method [78–80] and Equation (2), where L is the length of the simulation box in z dimension and represents an ensemble average given from gmx energy.

$$\gamma = \frac{L}{2} \langle P_{zz} - \frac{P_{xx} + P_{yy}}{2} \rangle \tag{2}$$

Significance test. Significance tests were performed using OriginLab OriginPro 9.0 software. Specifically, one-way ANOVA was performed and was supplemented with post-hoc Tukey test to determine significance between individual populations.

4. Conclusions

In this work, we optimised and parametrised 250 Gemini molecules. We described each of those molecules with theoretical values of logP and log (CMC) as well as provided a detailed description of those molecules in the attached spreadsheet. Additionally, we included those parametrised force fields in SM for future simulation studies. This may be remarkably helpful in further antimicrobial action studies, as a significant number of Gemini cationic molecules with various spacers were modelled and parametrised. Such systematic summarisation may be extensively used not only for theoretical studies but also for experimental ones with the aim to deliver comprehensive knowledge and molecular mechanism of surfactant effectiveness. Furthermore, we selected 25 molecules from various groups and simulated their behaviour in systems with membrane mimicking the inner membrane of *E. coli*. This detailed characterisation of parameters allowed us to extract four types of parameters—area compressibility, bending rigidity, lateral diffusion coefficient and membrane surface tension—that could correspond to the antimicrobial

effect of those molecules. Based on our preliminary screening we concluded that the type of Gemini molecules that could exhibit strong antimicrobial effects are oQAS, Pyr, Imo. Additionally, other possible candidates are Ary, Glu, hQAS and Alk. In this work we proposed and deliver a uniform theoretical approach to compare Gemini surfactant effectiveness. Nevertheless, this systematic approach should be confirmed experimentally to provide solid biological relevance.

Supplementary Materials: The following are available online at https://www.mdpi.com/article/10.3390/ijms222010939/s1: (1) Gemini molecules database (.xls). (2) Complete force-fields for Gemini molecules from the database (.zip). (3) Supporting materials (.docx) including system density profiles of investigated agents, table with membrane system characterisation and instruction for NAMD FF to GROMACS FF conversion.

Author Contributions: Conceptualisation, M.R. and D.D.; methodology, M.R., A.K. and D.D.; validation, M.R. and D.D.; formal analysis, M.R. and D.D.; investigation, M.R., A.K. and D.D.; resources, S.K.; data curation, M.R., A.K. and D.D.; writing—original draft preparation, M.R. and D.D.; writing—review and editing, M.R., A.K. and D.D.; visualisation, M.R. and D.D.; supervision, D.D.; project administration, S.K.; funding acquisition, S.K. All authors have read and agreed to the published version of the manuscript.

Data Availability Statement: Most of the data are available in the manuscript supplementary information, including force fields. The simulation data presented in this study are available on request from the corresponding author due to GBs files sizes.

Conflicts of Interest: The authors declare no conflict of interest.

References

1. Bailey, D.M.; DeGrazia, C.G.; Hoff, S.J.; Schulenberg, P.L.; O'Connor, J.R.; Paris, D.A.; Slee, A.M. Bispyridinamines: A new class of topical antimicrobial agents as inhibitors of dental plaque. *J. Med. Chem.* **2002**, *27*, 1457–1464. [CrossRef]
2. Brycki, B.E.; Kowalczyk, I.H.; Szulc, A.; Kaczerewska, O.; Pakiet, M. Multifunctional gemini surfactants: Structure, synthesis, properties and applications. *Appl. Charact. Surfactants, Reza Najjar* **2017**, 97–155. [CrossRef]
3. Hait, S.; Moulik, S. Gemini surfactants: A distinct class of self-assembling molecules. *Curr. Sci.* **2002**, *82*, 1101–1111.
4. Zana, R. Dimeric and oligomeric surfactants. Behavior at interfaces and in aqueous solution: A review. *Adv. Colloid Interface Sci.* **2002**, *97*, 205–253. [CrossRef]
5. Koziróg, A.; Brycki, B.; Pielech-Przybylska, K. Impact of cationic and neutral gemini surfactants on conidia and hyphal forms of Aspergillus brasiliensis. *Int. J. Mol. Sci.* **2018**, *19*, 873. [CrossRef]
6. Kuperkar, K.; Modi, J.; Patel, K. Surface-active properties and antimicrobial study of conventional cationic and synthesized symmetrical gemini surfactants. *J. Surfactants Deterg.* **2012**, *15*, 107–115. [CrossRef]
7. Menger, F.M.; Mbadugha, B.N.A. Gemini surfactants with a Disaccharide Spacer. *J. Am. Chem. Soc.* **2001**, *123*, 875–885. [CrossRef]
8. Zhong, X.; Guo, J.; Fu, S.; Zhu, D.; Peng, J. Synthesis, surface property and antimicrobial activity of cationic gemini surfactants containing adamantane and amide groups. *J. Surfactants Deterg.* **2014**, *17*, 943–950. [CrossRef]
9. Pernak, J.; Branicka, M. The properties of 1-alkoxymethyl-3-hydroxypyridinium and 1-alkoxymethyl-3-dimethylaminopyridinium chlorides. *J. Surfactants Deterg.* **2003**, *6*, 119–123. [CrossRef]
10. Li, H.; Yu, C.; Chen, R.; Li, J.; Li, J. Novel ionic liquid-type Gemini surfactants: Synthesis, surface property and antimicrobial activity. *Colloids Surf. A Physicochem. Eng. Asp.* **2012**, *395*, 116–124. [CrossRef]
11. Wang, L.; Qin, H.; Ding, L.; Huo, S.; Deng, Q.; Zhao, B.; Meng, L.; Yan, T. Preparation of a novel class of cationic gemini imidazolium surfactants containing amide groups as the spacer: Their surface properties and antimicrobial activity. *J. Surfactants Deterg.* **2014**, *17*, 1099–1106. [CrossRef]
12. Tawfik, S.M.; Abd-Elaal, A.A.; Shaban, S.M.; Roshdy, A.A. Surface, thermodynamic and biological activities of some synthesized Gemini quaternary ammonium salts based on polyethylene glycol. *J. Ind. Eng. Chem.* **2015**, *30*, 112–119. [CrossRef]
13. Bao, Y.; Guo, J.; Ma, J.; Li, M.; Li, X. Physicochemical and antimicrobial activities of cationic gemini surfactants with polyether siloxane linked group. *J. Mol. Liq.* **2017**, *242*, 8–15. [CrossRef]

14. Gilbert, P.; Moore, L.E. Cationic antiseptics: Diversity of action under a common epithet. *J. Appl. Microbiol.* **2005**, *99*, 703–715. [CrossRef] [PubMed]

15. Koch, A.L. Bacterial wall as target for attack past, present, and future research. *Clin. Microbiol. Rev.* **2003**, *16*, 673–687. [CrossRef] [PubMed]

16. Morán, C.; Clapés, P.; Comelles, F.; García, T.; Pérez, L.; Vinardell, P.; Mitjans, M.; Infante, M.R. Chemical structure/property relationship in single-chain arginine surfactants. *Langmuir* **2001**, *17*, 5071–5075. [CrossRef]

17. Schuurmans, J.; Nuri Hayali, A.; Koenders, B.; ter Kuile, B. Variations in MIC value caused by differences in experimental protocol. *J. Microbiol. Methods* **2009**, *79*, 44–47. [CrossRef] [PubMed]

18. Rzycki, M.; Drabik, D.; Szostak-Paluch, K.; Hanus-Lorenz, B.; Kraszewski, S. Unraveling the mechanism of octenidine and chlorhexidine on membranes: Does electrostatics matter? *Biophys. J.* **2021**, *120*, 3392–3408. [CrossRef]

19. Malanovic, N.; Ön, A.; Pabst, G.; Zellner, A.; Lohner, K. Octenidine: Novel insights into the detailed killing mechanism of Gram-negative bacteria at a cellular and molecular level. *Int. J. Antimicrob. Agents* **2020**, *56*. [CrossRef]

20. Hübner, N.-O.; Siebert, J.; Kramer, A. Octenidine dihydrochloride, a modern antiseptic for skin, mucous membranes and wounds. *Skin Pharmacol. Physiol.* **2010**, *23*, 244–258. [CrossRef]

21. Epand, R.M.; Epand, R.F. Bacterial membrane lipids in the action of antimicrobial agents. *J. Pept. Sci.* **2011**, *17*, 298–305. [CrossRef]

22. Epand, R.M.; Epand, R.F. Lipid domains in bacterial membranes and the action of antimicrobial agents. *Biochim. Biophys. Acta* **2009**, *1788*, 289–294. [CrossRef] [PubMed]

23. Silva, S.G.; Oliveira, I.S.; do Vale, M.L.C.; Marques, E.F. Serine-based gemini surfactants with different spacer linkages: From self-assembly to DNA compaction. *Soft Matter* **2014**, *10*, 9352–9361. [CrossRef] [PubMed]

24. Han, Y.; Wang, Y. Aggregation behavior of gemini surfactants and their interaction with macromolecules in aqueous solution. *Phys. Chem. Chem. Phys.* **2011**, *13*, 1939–1956. [CrossRef] [PubMed]

25. Ding, Z.; Hao, A. Synthesis and surface properties of novel cationic gemini surfactants. *J. Dispers. Sci. Technol.* **2010**, *31*, 338–342. [CrossRef]

26. Di Meglio, C.; Rananavare, S.B.; Sönke Svenson, A.; Thompson, D.H. Bolaamphiphilic phosphocholines: Structure and phase behavior in aqueous media. *Langmuir* **1999**, *16*, 128–133. [CrossRef]

27. Datta, S.; Biswas, J.; Bhattacharya, S. How does spacer length of imidazolium gemini surfactants control the fabrication of 2D-Langmuir films of silver-nanoparticles at the air–water interface? *J. Colloid Interface Sci.* **2014**, *430*, 85–92. [CrossRef] [PubMed]

28. Brycki, B.; Szulc, A. Gemini alkyldeoxy-D-glucitolammonium salts as modern surfactants and microbiocides: Synthesis, antimicrobial and surface activity, biodegradation. *PLoS ONE* **2014**, *9*, e84936. [CrossRef]

29. Sheikh, M.S.; Khanam, A.J.; Matto, R.U.H.; Kabir-Ud-Din. Comparative study of the micellar and antimicrobial activity of gemini-conventional surfactants in pure and mixed micelles. *J. Surfactants Deterg.* **2013**, *16*, 503–508. [CrossRef]

30. Obłąk, E.; Piecuch, A.; Guz-Regner, K.; Dworniczek, E. Antibacterial activity of gemini quaternary ammonium salts. *FEMS Microbiol. Lett.* **2014**, *350*, 190–198. [CrossRef]

31. Quagliotto, P.; Barolo, C.; Barbero, N.; Barni, E.; Compari, C.; Fisicaro, E.; Viscardi, G. Synthesis and characterization of highly fluorinated gemini pyridinium surfactants. *European, J. Org. Chem.* **2009**, *2009*, 3167–3177. [CrossRef]

32. Marín-Menéndez, A.; Montis, C.; Díaz-Calvo, T.; Carta, D.; Hatzixanthis, K.; Morris, C.J.; McArthur, M.; Berti, D. Antimicrobial nanoplexes meet model bacterial membranes: The key role of cardiolipin. *Sci. Rep.* **2017**, *7*, 1–13. [CrossRef]

33. Brycki, B.; Kowalczyk, I.; Kozirog, A. Synthesis, molecular structure, spectral properties and antifungal activity of polymethylene-α,ω-bis(n,n- dimethyl-n-dodecyloammonium bromides). *Molecules* **2011**, *16*, 319–335. [CrossRef] [PubMed]

34. Gospodarczyk, W.; Kozak, M. Interaction of two imidazolium gemini surfactants with two model proteins BSA and HEWL. *Colloid Polym. Sci.* **2015**, *293*, 2855–2866. [CrossRef]

35. Pietralik, Z.; Kołodziejska, Ż.; Weiss, M.; Kozak, M. Gemini surfactants based on bis-imidazolium alkoxy derivatives as effective agents for delivery of nucleic acids: A structural and spectroscopic study. *PLoS ONE* **2015**, *10*, e0144373. [CrossRef]

36. Pietralik, Z.; Krzysztoń, R.; Kida, W.; Andrzejewska, W.; Kozak, M. Structure and conformational dynamics of DMPC/dicationic surfactant and DMPC/dicationic surfactant/DNA systems. *Int. J. Mol. Sci.* **2013**, *14*, 7642–7659. [CrossRef] [PubMed]

37. Kamboj, R.; Singh, S.; Bhadani, A.; Kataria, H.; Kaur, G. Gemini imidazolium surfactants: Synthesis and their biophysiochemical study. *Langmuir* **2012**, *28*, 11969–11978. [CrossRef] [PubMed]

38. Kumar, V.; Chatterjee, A.; Kumar, N.; Ganguly, A.; Chakraborty, I.; Banerjee, M. d-Glucose derived novel gemini surfactants: Synthesis and study of their surface properties, interaction with DNA, and cytotoxicity. *Carbohydr. Res.* **2014**, *397*, 37–45. [CrossRef] [PubMed]

39. Sakai, K.; Umezawa, S.; Tamura, M.; Takamatsu, Y.; Tsuchiya, K.; Torigoe, K.; Ohkubo, T.; Yoshimura, T.; Esumi, K.; Sakai, H.; et al. Adsorption and micellization behavior of novel gluconamide-type gemini surfactants. *J. Colloid Interface Sci.* **2008**, *318*, 440–448. [CrossRef]

40. Massi, L.; Guittard, F.; Levy, R.; Duccini, Y.; Géribaldi, S. Preparation and antimicrobial behaviour of gemini fluorosurfactants. *Eur. J. Med. Chem.* **2003**, *38*, 519–523. [CrossRef]

41. Łuczyński, J.; Frąckowiak, R.; Włoch, A.; Kleszczyńska, H.; Witek, S. Gemini ester quat surfactants and their biological activity. *Cell. Mol. Biol. Lett.* **2013**, *18*, 89–101. [CrossRef]

42. Tatsumi, T.; Zhang, W.; Nakatsuji, Y.; Miyake, K.; Matsushima, K.; Tanaka, M.; Furuta, T.; Ikeda, I. Preparation, surface-active properties, and antimicrobial activities of bis(alkylammonium) dichlorides having a butenylene or a butynylene spacer. *J. Surfactants Deterg.* **2001**, *4*, 271–277. [CrossRef]

43. Tatsumi, T.; Imai, Y.; Kawaguchi, K.; Miyano, N.; Ikeda, I. Antimicrobial activity of cationic gemini surfactant containing an oxycarbonyl group in the lipophilic portion against gram-positive and gram-negative microorganisms. *J. Oleo Sci.* **2014**, *63*, 137–140. [CrossRef]

44. Ronsin, G.; Kirby, A.J.; Rittenhouse, S.; Woodnutt, G.; Camilleri, P. Structure and antimicrobial activity of new bile acid-based gemini surfactants. *J. Chem. Soc. Perkin Trans. 2* **2002**, *7*, 1302–1306. [CrossRef]

45. Piętka-Ottlik, M.; Lewińska, A.; Jaromin, A.; Krasowska, A.; Wilk, K.A. Antifungal organoselenium compound loaded nanoemulsions stabilized by bifunctional cationic surfactants. *Colloids Surf. A Physicochem. Eng. Asp.* **2016**, *510*, 53–62. [CrossRef]

46. Pérez, L.; Torres, J.L.; Manresa, A.; Solans, C.; Infante, M.R. Synthesis, aggregation, and biological properties of a new class of gemini cationic amphiphilic compounds from arginine, bis (Args). *Langmuir* **1996**, *12*, 5296–5301. [CrossRef]

47. Zhong, X.; Guo, J.; Feng, L.; Xu, X.; Zhu, D. Cationic Gemini surfactants based on adamantane: Synthesis, surface activity and aggregation properties. *Colloids Surf. A Physicochem. Eng. Asp.* **2014**, *441*, 572–580. [CrossRef]

48. Machuca, L.M.; Reno, U.; Plem, S.C.; Gagneten, A.M.; Murguía, M.C.; Machuca, L.M.; Reno, U.; Plem, S.C.; Gagneten, A.M.; Murguía, M.C. N-acetylated gemini surfactants: Synthesis, surface-active properties, antifungal activity, and ecotoxicity bioassays. *Adv. Chem. Eng. Sci.* **2015**, *5*, 215–224. [CrossRef]

49. Silva, S.G.; Alves, C.; Cardoso, A.M.S.; Jurado, A.S.; de Lima, M.C.P.; Vale, M.L.C.; Marques, E.F. Synthesis of gemini surfactants and evaluation of their interfacial and cytotoxic properties: Exploring the multifunctionality of serine as headgroup. *Eur. J. Org. Chem.* **2013**, *2013*, 1758–1769. [CrossRef]

50. Barucha-Kraszewska, J.; Kraszewski, S.; Ramseyer, C. Will C-Laurdan dethrone Laurdan in fluorescent solvent relaxation techniques for lipid membrane studies? *Langmuir* **2013**, *29*, 1174–1182. [CrossRef] [PubMed]

51. Drabik, D.; Chodaczek, G.; Kraszewski, S. Effect of amyloid-β monomers on lipid membrane mechanical parameters–potential implications for mechanically driven neurodegeneration in Alzheimer's disease. *Int. J. Mol. Sci.* **2021**, *22*, 18. [CrossRef]

52. Shaban, S.M.; Aiad, I.; Moustafa, H.Y.; Hamed, A. Amidoamine Gemini surfactants based dimethylamino propyl amine: Preparation, characterization and evaluation as biocide. *J. Mol. Liq.* **2015**, *212*, 907–914. [CrossRef]

53. Pérez, L.; Garcia, M.T.; Ribosa, I.; Vinardell, M.P.; Manresa, A.; Infante, M.R. Biological properties of arginine-based gemini cationic surfactants. *Environ. Toxicol. Chem.* **2002**, *21*, 1279–1285. [CrossRef] [PubMed]

54. Pringle, M.J.; Brown, K.B.; Miller, K.W. Can the Lipid Theories of Anesthesia Account for the Cutoff in Anesthetic Potency in Homologous Series of Alcohols? *Mol. Pharmacol.* **1981**, *19*, 49–55. [PubMed]

55. Chernomordik, L.; Kozlov, M.M.; Zimmerberg, J. Lipids in biological membrane fusion. *J. Membr. Biol.* **1995**, *146*, 1–14. [CrossRef] [PubMed]

56. Piecuch, A.; Obłąk, E.; Guz-Regner, K. Antibacterial activity of alanine-derived gemini quaternary ammonium compounds. *J. Surfactants Deterg.* **2016**, *19*, 275–282. [CrossRef] [PubMed]

57. Rzycki, M.; Kraszewski, S.; Drabik, D. Towards mimetic membrane system. In *International Conference on Computational Science*; Springer: Cham, Switzerland, 2021; pp. 551–563. [CrossRef]

58. Ramadurai, S.; Duurkens, R.; Krasnikov, V.V.; Poolman, B. Lateral diffusion of membrane proteins: Consequences of hydrophobic mismatch and lipid composition. *Biophys. J.* **2010**, *99*, 1482–1489. [CrossRef]

59. Sharma, P.; Parthasarathi, S.; Patil, N.; Waskar, M.; Raut, J.S.; Puranik, M.; Ayappa, K.G.; Basu, J.K. Assessing barriers for antimicrobial penetration in complex asymmetric bacterial membranes: A case study with thymol. *Langmuir* **2020**, *36*, 8800–8814. [CrossRef]

60. Wang, X.; Wang, J.; Wang, Y.; Yan, H.; Li, P.; Thomas, R. Effect of the nature of the spacer on the aggregation properties of gemini surfactants in an aqueous solution. *Langmuir* **2003**, *20*, 53–56. [CrossRef] [PubMed]

61. Wettig, S.D.; Wang, C.; Verrall, R.E.; Foldvari, M. Thermodynamic and aggregation properties of aza- and imino-substituted gemini surfactants designed for gene delivery. *Phys. Chem. Chem. Phys.* **2007**, *9*, 871–877. [CrossRef] [PubMed]

62. Neubauer, D.; Jaśkiewicz, M.; Bauer, M.; Olejniczak-Kęder, A.; Sikorska, E.; Sikora, K.; Kamysz, W. Biological and physico-chemical characteristics of arginine-rich peptide gemini surfactants with lysine and cystine spacers. *Int. J. Mol. Sci.* **2021**, *22*, 3299. [CrossRef]

63. Ruiz, A.; Pinazo, A.; Pérez, L.; Manresa, A.; Marqués, A.M. Green catanionic gemini surfactant–lichenysin mixture: Improved surface, antimicrobial, and physiological properties. *ACS Appl. Mater. Interfaces* **2017**, *9*, 22121–22131. [CrossRef] [PubMed]

64. Frisch, M.J.; Trucks, G.W.; Schlegel, H.B.; Scuseria, G.E.; Robb, M.A.; Cheeseman, J.R.; Scalmani, G.; Barone, V.; Petersson, G.A.; Nakatsuji, H. *Gaussian 16, Revision 2016*; Gaussian Inc.: Wallingford, UK, 2016. Available online: https://gaussian.com/citation/ (accessed on 23 July 2019).

65. Mozrzymas, A. Modelling of the critical micelle concentration of cationic gemini surfactants using molecular connectivity indices. *J. Solution Chem.* **2013**, *42*, 2187–2199. [CrossRef] [PubMed]

66. Wu, E.L.; Cheng, X.; Jo, S.; Rui, H.; Song, K.C.; Dávila-Contreras, E.M.; Qi, Y.; Lee, J.; Monje-Galvan, V.; Venable, R.M.; et al. CHARMM-GUI membrane builder toward realistic biological membrane simulations. *J. Comput. Chem.* **2014**, *35*, 1997–2004. [CrossRef] [PubMed]

67. Szatmári, D.; Sárkány, P.; Kocsis, B.; Nagy, T.; Miseta, A.; Barkó, S.; Longauer, B.; Robinson, R.C.; Nyitrai, M. Intracellular ion concentrations and cation-dependent remodelling of bacterial MreB assemblies. *Sci. Rep.* **2020**, *10*, 1–13. [CrossRef]

68. Klauda, J.B.; Venable, R.M.; Freites, J.A.; O'Connor, J.W.; Tobias, D.J.; Mondragon-Ramirez, C.; Vorobyov, I.; MacKerell, A.D.; Pastor, R.W. Update of the CHARMM all-atom additive force field for lipids: Validation on six lipid types. *J. Phys. Chem. B* **2010**, *114*, 7830–7843. [CrossRef] [PubMed]

69. Abraham, M.J.; Murtola, T.; Schulz, R.; Páll, S.; Smith, J.C.; Hess, B.; Lindah, E. Gromacs: High performance molecular simulations through multi-level parallelism from laptops to supercomputers. *SoftwareX* **2015**, *1–2*, 19–25. [CrossRef]

70. Evans, D.J.; Holian, B.L. The Nose–Hoover thermostat. *J. Chem. Phys.* **1998**, *83*, 4069. [CrossRef]

71. Parrinello, M.; Rahman, A. Polymorphic transitions in single crystals: A new molecular dynamics method. *J. Appl. Phys.* **1998**, *52*, 7182. [CrossRef]

72. Darden, T.; York, D.; Pedersen, L. Particle mesh Ewald: An N·log(N) method for Ewald sums in large systems. *J. Chem. Phys.* **1998**, *98*, 10089. [CrossRef]

73. Humphrey, W.; Dalke, A.; Schulten, K. VMD: Visual molecular dynamics. *J. Mol. Graph.* **1996**, *14*, 33–38. [CrossRef]

74. Doktorova, M.; Harries, D.; Khelashvili, G. Determination of bending rigidity and tilt modulus of lipid membranes from real-space fluctuation analysis of molecular dynamics simulations. *Phys. Chem. Chem. Phys.* **2017**, *19*, 16806–16818. [CrossRef] [PubMed]

75. Doktorova, M.; LeVine, M.V.; Khelashvili, G.; Weinstein, H. A new computational method for membrane compressibility: Bilayer mechanical thickness revisited. *Biophys. J.* **2019**, *116*, 487–502. [CrossRef] [PubMed]

76. Giorgino, T. Computing diffusion coefficients in macromolecular simulations: The diffusion coefficient tool for VMD. *J. Open Source Softw.* **2019**, *4*, 1698. [CrossRef]

77. Guixà-González, R.; Rodriguez-Espigares, I.; Ramírez-Anguita, J.M.; Carrió-Gaspar, P.; Martinez-Seara, H.; Giorgino, T.; Selent, J. MEMBPLUGIN: Studying membrane complexity in VMD. *Bioinformatics* **2014**, *30*, 1478–1480. [CrossRef]

78. Irving, J.H.; Kirkwood, J.G. The statistical mechanical theory of transport processes. IV. The equations of hydrodynamics. *J. Chem. Phys.* **2004**, *18*, 817. [CrossRef]

79. Bacle, A.; Gautier, R.; Jackson, C.L.; Fuchs, P.F.J.; Vanni, S. Interdigitation between triglycerides and lipids modulates surface properties of lipid droplets. *Biophys. J.* **2017**, *112*, 1417–1430. [CrossRef]

80. Bourasseau, E.; Homman, A.-A.; Durand, O.; Ghoufi, A.; Malfreyt, P. Calculation of the surface tension of liquid copper from atomistic Monte Carlo simulations. *Eur. Phys. J. B* **2013**, *86*, 251. [CrossRef]

Chapter 8

Paper 3

Towards Mimetic Membrane Systems in Molecular Dynamics:
Characteristics of *E. Coli* Membrane System

Towards Mimetic Membrane Systems in Molecular Dynamics: Characteristics of *E. Coli* Membrane System

Mateusz Rzycki[1,2]([✉]) [iD], Sebastian Kraszewski[2] [iD], and Dominik Drabik[2,3] [iD]

[1] Department of Experimental Physics, Faculty of Fundamental Problems of Technology, Wroclaw University of Science and Technology, Wroclaw, Poland
mateusz.rzycki@pwr.edu.pl
[2] Department of Biomedical Engineering, Faculty of Fundamental Problems of Technology, Wroclaw University of Science and Technology, Wroclaw, Poland
[3] Laboratory of Cytobiochemistry, Faculty of Biotechnology, University of Wroclaw, Wroclaw, Poland

Abstract. Plenty of research is focused on the analysis of the interactions between bacteria membrane and antimicrobial compounds or proteins. The hypothesis of the research is formed according to the results from the numerical models such as molecular docking or molecular dynamics. However, simulated membrane models often vary significantly from the real ones. This may lead to inaccurate conclusions. In this paper, we employed molecular dynamic simulations to create a mimetic *Escherichia coli* full membrane model and to evaluate how the membrane complexity may influence the structural, mechanical and dynamical mainstream parameters. The impact of the O-antigen region presence in the outer membrane was also assessed. In the analysis, we calculated membrane thickness, area per lipid, order parameter, lateral diffusion coefficient, interdigitation of acyl chains, mechanical parameters such as bending rigidity and area compressibility, and also lateral pressure profiles. We demonstrated that outer membrane characteristics strongly depend on the structure of lipopolysaccharides, changing their properties dramatically in each of the investigated parameters. Furthermore, we showed that the presence of the inner membrane during simulations, as it exists in a full shell of *E. coli*, significantly changed the measured properties of the outer membrane.

Keywords: Molecular dynamics · Mimetic systems · Lipid membrane model

1 Introduction

Escherichia coli is one of the most frequently investigated bacteria being responsible for common infections among humans and animals [1, 2]. This strain is widely used for antimicrobial studies [3–5]. It belongs to the Gram-negative ones which membranes consist of the outer (OM) and the inner membrane (IM) separated by the periplasm. OM is an asymmetric bilayer primarily composed of lipopolysaccharides (LPS) in the top leaflet and phospholipids (PL) in the bottom one [6]. It serves as a protective shield

preventing the entry of toxic compounds e.g. antibiotics [7, 8]. The LPS is composed of three segments: lipidA-the hydrophobic fatty surface forming the base of the top OM leaflet, a phosphorylated, highly anionic core and an O-antigen unit composed of sugar chains performing a hydrophilic surface [7, 9]. IM has a dynamic structure mostly formed by phosphatidylethanolamine (PE), phosphatidylglycerol (PG) and cardiolipin (CL) [10, 11].

In computational studies on bacteria membranes, methods such as molecular dynamics are often employed [12]. This allows observation of the behavior of studied molecules up to the atomic level. However, many modelled systems are simplified and limited to one particular membrane even for Gram-negative bacteria [13–16]. Piggot *et al.* performed the analysis on the base model of OM *E. coli* with embedded FecA protein, presenting the LPS structure on the upper leaflet, while the lower one was composed of PE and PG [15]. A similar model was proposed by Wu *et al.* a few years earlier where a couple of LPS structures were studied [13]. One of the most comprehensive approaches was delivered by Hwang *et al.* where the two – inner and outer membranes were separately modelled and analyzed [14]. While those models are quite close to reality, they may significantly differ from the real OM/IM bacterial membrane or even experimental models. This may result in influencing the outcome results.

In this work, we investigate the changes in membrane properties with the increasing complexity of the systems to better reflect bacterial membrane and to draw attention that both OM and IM should not be studied separately for better biological context. For this purpose, we created five bacterial membrane models based on the composition of *E. coli*. We started from simple pure IM and pure OM (with and without O-antigen units used). To better reflect the natural conditions we created whole OM/IM bacteria membrane system (first without O-antigen units and latter with O-antigen units). Each of the systems was analyzed in detail to characterize the topological and mechanical properties of the membranes in investigated systems and to present the influence on how structural complexity can affect membrane behavior.

2   Methods

The all-atom models of the membranes were generated using CHARMM-GUI membrane builder [17]. The IM model consisted of 80% PYPE, 15% PYPG, 5% PVCL2 [10, 11, 18]. The lipid bilayer was solvated with TIP3P water molecules (100 water molecules per lipid) and 240 mM NaCl were added based on literature data [19]. Final IM configuration included: 256 PYPE, 48 PYPG, 16 PVCL2, 276 Na$^+$, 196 Cl$^-$ and 32000 TIP3P molecules.

The OM models were composed of 75% PYPE and 25% PYPG in the upper leaflet and 100% LPS in the lower one [13, 20]. The type1 of lipidA, R1 core and repeating units of O6-antigen were included in the LPS sequence. The length of the O6-antigens was adapted based on results published by Wu *et al.* [13, 21]. The number of LPS molecules and phospholipids was equally adjusted to the total lipid area occupied on each leaflet. The same procedure of solvation and ion addition was employed as before, except for Ca^{2+} ions, which were automatically added based on LPS length to neutralize the system. Afterward, molecular dynamics (MD) simulations of two asymmetric LPS based bilayers were performed. The upper leaflet contained: lipidA, R1 core and 2

repeating units of O6-antigen (OMA) and lipidA, R1 core (OM0). Final OMA and OM configuration included: 52 LPS, 120 PYPE, 40 PYPG, 260 Ca^{2+}, 232 Na^+, 112 Cl^-, 28964 TIP3, and 60 LPS, 144 PYPE, 48 PYPG, 300 Ca^{2+}, 168 Na^+, 120 Cl^- and 27856 TIP3P molecules respectively. Three-dimensional periodic boundary conditions were applied to deal with potential energy disruption due to the origin of cell discontinuity.

MD simulations of pure membranes were performed using the GROMACS (version 2020.4) package with the CHARMM36 force field [22, 23]. Each system was first minimized using the steepest descent algorithm for energy minimization. Calculations were carried out in the NPT ensemble (constant Number of particles, Pressure and Temperature) using a Nose-Hoover thermostat at T = 303.15 K and semi-isotropic coupling with Parrinello-Rahman barostat at p = 1bar. The long-run production was conducted for at least 300 ns using the leap-frog integrator. Chemical bonds between hydrogen and heavy atoms were constrained to their equilibrium values by the LINCS algorithm, while long-range electrostatic forces were evaluated using the particle mesh Ewald (PME) method, which allowed us to employ the integration timestep of 2 fs.

The complete bacterial membrane models: LIPA (IM + OMA) and LIP0 (IM + OM0) have been constructed by assembling IM and OM separated by a small water slab (2.4 nm, 4140 water molecules) imitating the periplasm. The minimization procedure and NPT ensemble were carried out according to the same protocol as described above. We analyzed the last 10 ns of all simulations using a combination of GROMACS tools, self-made MATLAB (The MathWorks, Natick, MA) scripts, VMD and VMD's dedicated plugins such as MEMBPLUGIN 1.1 [24] for interdigitation calculation.

The order parameter of the acyl chains was obtained using:

$$S_{CH} = \frac{3}{2}\left\langle cos^2\,\theta \right\rangle - \frac{1}{2} \tag{1}$$

where θ for a particular carbon atom is the angle between the bilayer normal and carbon-hydrogen bond.

The diffusion was calculated in the Diffusion Coefficient Tool [25] from the slope of the mean-squared displacement (MSD) curve through Einstein's relation. For the computation accuracy, only phosphorous atoms of all lipids were taken into account.

$$D(\tau) = \frac{M(\tau)}{2E\tau} \tag{2}$$

where $M(\tau)$ – is the MSD at a range of lag time τ and E represents the dimensionality (two in our case - XY).

Lateral Pressure profiles (LPPs) were computed using a custom version of GROMACS-LS [26]. The obtained beforehand trajectories were adapted to comply with the software requirements, thus the calculations of the PME electrostatic forces were settled to cutoff. We also adjusted the cutoff to 2.2nm according to Vanegas *et al.* [26, 27]. The lateral component of pressure tensor ($P_L(z) = 0.5 \times (P_{xx}(z) + P_{yy}(z))$) and the normal component ($P_N = P_{zz}$) are computed from the GROMACS-LS output. Finally, LPPs $\pi(z)$ was determined from:

$$\pi(z) = P_L(z) - P_N. \tag{3}$$

Bending rigidity was determined using the real space fluctuation method [28]. Briefly, a probability distribution for both tilt and splay is determined for all lipids over the last

10 ns of simulation. Tilt is defined as an angle between the lipid director (vector between lipid head – the midpoint between C2 and P atoms – and lipid tail – the midpoint between last carbon atoms) and bilayer normal. Lipid splay is defined as divergence of an angle formed by the directors of neighboring lipids providing that they are weakly correlated. Area compressibility was determined using a method developed by Doktorova *et al.* [29]. Briefly, a real-space analysis of local thickness fluctuations is sampled from the simulations.

Determined parameters' statistical significance was performed using one-way ANOVA significance test with Tukey post hoc test in Origin 2018 (OriginLabs) software.

3   Results

Each of the investigated systems was characterized thoroughly. In the Fig. 1 and Fig. 2 we present LIPA and LIP0 systems in detail, including their density profiles and graphical representation. Structural, stress and mechanical parameters of lipid membranes were determined. We studied whether simplification of biological membranes, which is common for numerical simulations, is feasible. We assume that significant differences between the systems may result in the different occurrence of biological phenomena.
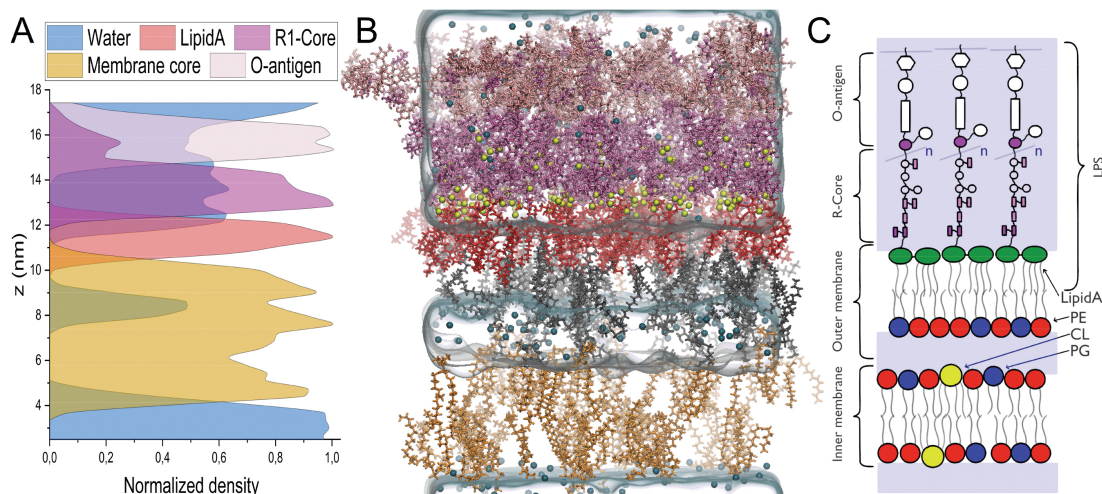

Fig. 1. A) Density profile of LIPA regions. B) LIPA system visualization (several lipids are hidden for clarity). The Inner membrane, outer membrane, lipidA, R-Core, O-antigen region, water, calcium ions, sodium together with chlorine ions have been colored orange, gray, red, magenta, pink, azure, yellow and dark blue, respectively. C) Graphical representation of created LIPA system. (Color figure online)

For the structural aspect of the membrane, we decided to perform a standard analysis with a couple more comprehensive parameters afterward. To understand and characterize the molecular effect of LPS on the membrane and/or additional membrane in complex systems, we determined different bilayer properties such as membrane thickness (MT), area per lipid (APL), order parameter, interdigitation and lateral diffusion. Membrane thickness was determined between phosphorus atoms, while the area per lipid was determined using Voronoi tessellation. The results of structural characteristics are presented in Table 1. All of the parameters were statistically distinct.
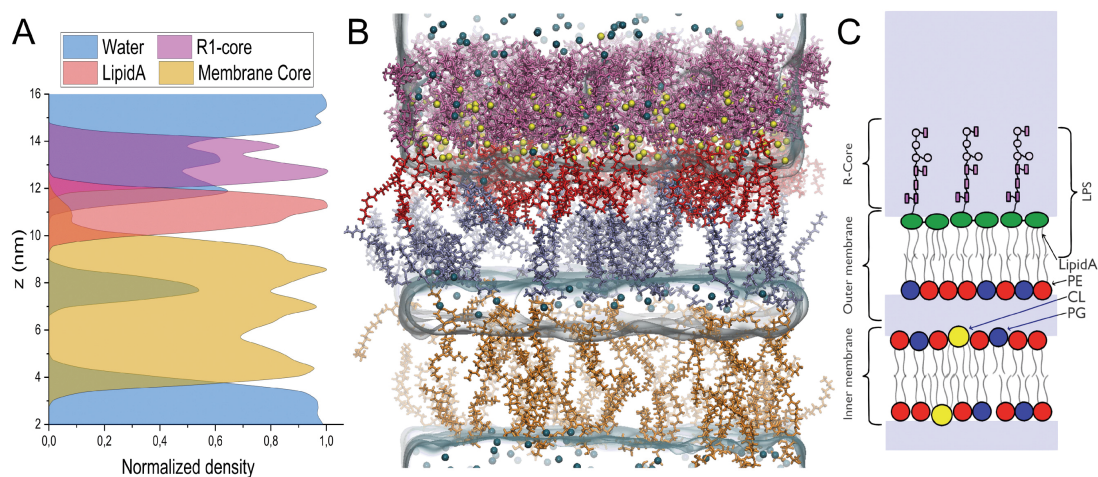
Fig. 2. A) Density profile of LIP0 regions. B) LIP0 system visualization (several lipids are hidden for clarity). The inner membrane, outer membrane, lipidA, R-Core, water, calcium ions, sodium together with chlorine ions have been colored in orange, ice blue, red, magenta, azure, yellow and dark blue, respectively. C) Graphical representation of created LIP0 system. (Color figure online)
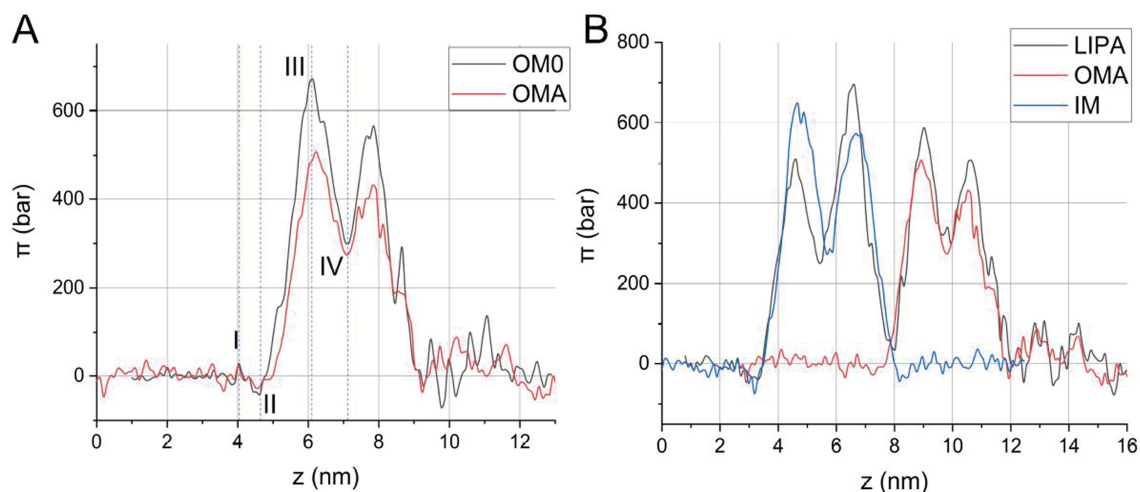

Fig. 3. Lateral pressure profile of A) OM0 and OMA, B) LIPA system with corresponding pure bilayer components OMA and IM.

Further structural characterization was enhanced with a description of lipid behavior in the systems. For this purpose, lateral mobility, which is usually described by the lateral diffusion coefficient, was investigated. The diffusion coefficient from the 2D mean square displacement equation was calculated. Obtained values were statistically significantly different between the investigated systems. Finally, the determination of acyl chain interdigitation to assess interactions between the leaflets itself was performed. The parameter allows estimating whether O-antigens presence may influence the interactions between the leaflets. As before the differences in values of interdigitation were statistically significant between the investigated systems.

Additionally, to provide a wider insight into the flexibility of the acyl chains, the order parameter was calculated. Presented values were averaged over the whole trajectories for clarity and collected in Table 2. We report values for the sn-2 unsaturated chain in

the following manner: initial atoms in the acyl chain (Start), atoms before double bond (Midpoint), and the final (End). Standard deviations are not included, since in all cases are below 0.02.

Table 1. Comparison of structural and dynamic parameters between pure and complex membranes[a].

Membrane	Lipid type	MT_{P-P}	APL_1	APL_2	Interdigitation	Diffusion
		Å	Å^2	Å^2	Å	μm^2/s
IM	Total	39.9 ± 0.4	56.6 ± 1.8	58 ± 2	4.9 ± 0.4	–
	PYPE		58 ± 1	59.1 ± 0.6		12.0 ± 0.1
	PYPG		63 ± 2	61.7 ± 2.3		15.8 ± 0.1
	PVCL2		88 ± 4	78 ± 4		12.8 ± 0.1
OMA	Total	35.5 ± 0.2	194.2 ± 3.3	60.3 ± 1.9	5.0 ± 0.3	–
	PYPE		–	60.8 ± 0.7		6.4 ± 0.1
	PYPG		–	66.5 ± 2.0		6.1 ± 0.1
	LipidA		194.2 ± 3.3	–		0.6 ± 0.1
OM0	Total	37.2 ± 0.2	183 ± 2	55.6 ± 1.5	4.3 ± 0.2	–
	PYPE		–	56.4 ± 0.4		10.0 ± 0.1
	PYPG		–	59.7 ± 1.3		7.7 ± 0.2
	LipidA		183 ± 2	–		0.9 ± 0.1
LIPA	Outer	33.3 ± 0.6	183 ± 3	59 ± 1	4.9 ± 0.4	–
	PYPE		–	64.7 ± 0.6		2.8 ± 0.0
	PYPG		–	66.5 ± 1.1		3.2 ± 0.2
	LipidA		183 ± 3	–		0.3 ± 0.1
	Inner	35.0 ± 0.7	55 ± 2	62.8 ± 2.4	5.0 ± 0.3	–
	PYPE		59 ± 1	61 ± 1		8.4 ± 0.1
	PYPG		63 ± 3	65 ± 2		11.3 ± 0.2
	PVCL2		65 ± 2	75 ± 3		10.2 ± 0.3
LIP0	Outer	35.3 ± 0.4	182.7 ± 4.4	59.6 ± 1.1	7.1 ± 0.5	–
	PYPE		–	63.9 ± 0.5		3.4 ± 0.1
	PYPG		–	67 ± 1		4.2 ± 0.1
	LipidA		182.7 ± 4.4	–		0.2 ± 0.1
	Inner	38.8 ± 0.4	61.3 ± 2.2	65 ± 2	5.9 ± 0.2	–
	PYPE		62.4 ± 0.6	63.3 ± 0.7		7.0 ± 0.1
	PYPG		60.1 ± 1.5	70 ± 2		9.0 ± 0.1
	PVCL2		75 ± 3	82 ± 3		12.7 ± 0.1

[a]MT_{P-P} - membrane thickness measure between phosphorous atoms from opposite leaflets; APL_1, APL_2 - the area per lipid on the upper and lower leaflet, respectively; IM – inner membrane; OM0 – outer membrane without antigens; OMA – outer membrane with antigens; LIP0 – mimetic *E. coli* system without antigens; LIPA – mimetic *E. coli* system with O-antigens

Stress characterization was done by evaluation of the stress profile along bilayer normal and determination of the lateral pressure profile (LPP) π(z). As a reference, we

Table 2. Acyl chain order parameter from pure and complex systems.

Membrane	Lipid type	Order parameter		
		Start	Midpoint	End
IM	PYPE	0.24	0.13	0.12
	PYPG	0.23	0.13	0.12
	PVCL	0.20	0.11	0.09
OM0	PYPE	0.24	0.13	0.12
	PYPG	0.25	0.13	0.12
	LipidA	0.20	0.15	0.10
OMA	PYPE	0.20	0.10	0.08
	PYPG	0.21	0.10	0.10
	LipidA	0.17	0.14	0.07
LIP0	PYPE	0.20	0.09	0.08
	PYPG	0.19	0.11	0.09
	PVCL	0.22	0.09	0.07
	PYPE	0.20	0.09	0.08
	PYPG	0.19	0.11	0.09
	LipidA	0.20	0.23	0.13
LIPA	PYPE	0.22	0.12	0.10
	PYPG	0.21	0.11	0.09
	PVCL	0.23	0.09	0.08
	PYPE	0.22	0.12	0.10
	PYPG	0.22	0.11	0.09
	LipidA	0.18	0.17	0.08

present Fig. 3 where the lateral pressure profile of OM's and LIPA combined with pure IM and OMA was calculated. For other systems, we collected the peak values (see Table 3).

The introduced LPPs indicate a similar tendency between basic and complex membrane. Starting from the bulk solvent, the first minor positive peak may be distinguished as a water-headgroup interface (I), indicating the repulsive forces from lipids. Further, the negative peak (II) is visible presenting glycerol region, including attractive hydrophobic forces [30], while subsequent major peak denotes the acyl chain region (III) and finish at the bilayer center nearby 6 nm (IV).

Finally, mechanical characterization of membranes is performed. Such characterization allows assessing very subtle changes induced by sugar-coating of LPS or additional membrane complexity. Both area compressibility (K_A) and bending rigidity (κ) are determined (see Table 3). All reported values are statistically significantly different.

Table 3. Mechanical and pressure properties of pure and complex systems[b].

Membrane	κ	κ_{tilt}	K_{A1}	K_{A2}	K_A	Lateral pressure
	kbT	kbT	mN/m	mN/m	mN/m	bar
IM	22.1 ± 0.6	10.6 ± 0.3	133 ± 20	133 ± 17	133 ± 15	647 ± 21
OMA	22.7 ± 0.4	13.3 ± 0.4	18 ± 12	84 ± 27	29 ± 10	508 ± 11
OM0	29.2 ± 0.4	17.1 ± 0.2	57 ± 6	141 ± 34	81 ± 18	670 ± 30
LIPA						
outer	25.0 ± 0.5	15.8 ± 0.6	41.7 ± 5.3	126.3 ± 5.4	62.7 ± 5.2	588 ± 16
inner	16 ± 1	4.8 ± 0.3	165 ± 24	31 ± 23	51 ± 20	695 ± 14
LIP0						
outer	26.4 ± 0.9	15.0 ± 0.7	58.8 ± 4.6	86.2 ± 7.1	70.0 ± 5.4	690 ± 26
inner	16.8 ± 0.4	7.3 ± 0.8	34 ± 9	42 ± 27	37 ± 17	533 ± 21

[b]κ – bending rigidity; κ_{tilt} – tilt; K_{A1}, K_{A2}, K_A – compressibility of the upper leaflet, lower leaflet, and total membrane, respectively; IM – inner membrane; OM0 – outer membrane without antigens; OMA – outer membrane with antigens; LIP0 – mimetic *E. coli* system without antigens; LIPA – mimetic *E. coli* system with antigens

4   Discussion

For a comprehensive analysis, we decided to divide the discussion section into two subsections. First, we focus on the impact of the O-antigen segment on the asymmetric outer membrane. Next, we draw attention to the discrepancies in the complete bacterial membrane systems compared to single membrane model systems.

4.1   The Effect of the O-antigen Region Presence on the Outer Membrane Parameters

In the outer membrane systems, we observe significant differences between OM0 and OMA, as the latter one is equipped with an extra O-antigen region. The presence of that structure induces membrane thickness reduction and APL extension in the upper leaflet (see Table 1). Interestingly, this directly influences the lower leaflet, where the total APL is lower than in the corresponding leaflet in OM0 system. The change of membrane thickness is proportional to the interdigitation of the acyl chains in the outer bilayer. We may conclude that the reduction in bilayer thickness is accompanied by the growth of the interdigitation [31]. The presence of O-antigens increases the interdigitation between the lipidA and PE:PG leaflets, which is followed by thickness reduction. However, analysis of the interdigitation in asymmetric membranes with the LPS layer is not straightforward. Shearer *et al.* suggested that the properties of OM systems are much more dependent on the dynamics and structure of the LPS segment [32].

   The diffusion coefficient analysis showed a significant difference between OMA and OM0 systems as well. The occurrence of additional sugar coating substantially limits the

mobility of the whole membrane. It remains consistent with the previous works [33–35]. The O-antigen essentially impacts the lower leaflet of the outer membrane, since PE and PG fluidity is restricted by 36% and 21%, respectively.

The calculated order parameter indicated that in both cases ordering trend is decreasing toward the bilayer center (see Table 2), our results are consistent with the ones presented by Wu *et al.* [13]. Interestingly the presence of the O-antigen segment affects membranes as values on both leaflets are lower.

Both OMA and OM0 exhibit a similar pressure trend along the bilayer normal (see Fig. 3). Noteworthy, much higher lateral stress was denoted at the lower leaflet at the OM0 system, reaching the top value of 670 ± 30 bar, while on OMA only 508 ± 11 bar was observed. Since the presented membranes are not symmetric, the lateral pressure on the upper and lower leaflets varies, however, both in a similar manner. A slightly noticeable shift at the bilayer center represents the interdigitation parameter of both membranes and remains consistent with values in Table 1. Since the interdigitation in OMA acyl chains is more intense, the plot downhill is deeper. Since the presence of the antigens in the membrane decreases the lateral pressure and lateral diffusion, this change could have a significant influence on the behavior of the system. Changes in both parameters could influence for instance membrane transport [36].

The presence of antigens in the LPS leaflet induced significant mechanical changes (see Table 3). All of the parameters - bending rigidity, tilt, and compressibility - were lower when O-antigens were present compared to the membrane without antigens. Such a difference is not surprising, as additional O-antigens are in the water part of the system, hence exposing the leaflet to additional repulsive forces, making the structure less resistant and exhibiting more fluctuations. Since lateral diffusion and lateral pressure are lower when antigens are present it can be concluded that membrane is, at least in the interphase region, more ordered. Such a conclusion cannot be made for the acyl chain region, as interdigitation increases when O-antigens are present.

4.2 The Comparison of *E. Coli* Membrane Models

The models presented in this study require a detailed analysis of their topological and mechanical characteristics. To this end, we decided to compare those properties for both inner and outer membranes from the *E. coli* models to pure ones. Taking into account the entire set of membranes, LIPA and LIP0 exhibit reduced bilayer thickness in both inner and outer membrane cases. Major differences we observe between pure IM and LIPA where the thickness reduction was supported with cardiolipin (CL) APL decrement of 12.3% (4.9 Å) and 26.1% (23 Å^2), respectively (see Table 1). In LIP0 structure modifications occurred in the inner membrane and the lower leaflet of the outer one when comparing APL and thickness parameters. Interestingly, significant reduction may be observed in the upper leaflet of the LIPA outer membrane, since lipidA reduced APL by 10 Å^2. Analysis of the interdigitation parameter between acyl chains from opposite leaflets seems to be slightly different than before. Obtained values from the LIPA system did not vary enough and were not significant compared to IM and OMA models with extra O-antigens. Thus, this parameter is not sensitive to the complexity of the membranes. However, the opposite pathway has been presented in LIP0 system. The interdigitation pitched up by 20.4% (to 5.9 ± 0.2 Å) on IM and by 65.1% (to 7.1 ± 0.5 Å)

on OM, respectively. Similarly, as before this phenomenon is inversely correlated to the bilayer thickness, where the decrease is accompanied by the interdigitation increase. We confirmed that the presence of O-antigens escalates the interdigitation between acyl chains from the opposite leaflet, followed by thickness reduction.

Furthermore, investigation of the diffusion coefficient revealed that in comprehensive models LIPA and LIP0 the mobility of the lipid particles is substantially limited. In LIP0, PE and lipidA fluidity was almost three and four times reduced, compared to OM0. A similar situation appears when analyzing LIPA and OMA, PE and lipidA mobility is limited more than twice in both cases. In pure OMA long sugar chains O-antigen reduce the fluidity of the whole membrane, which is accompanied by a corresponding interdigitation parameter. Further, the difference in fluidity of OMA and OM0 outer membranes was reduced in the whole bacteria systems.

Noteworthy the ordering of acyl chains is not as clear as, on pure outer membranes, observed fluctuations in several cases are not statistically significant (see Table 2). However, we indicate that the sn-2 ordering in the inner membrane of both LIPA and LIP0 compared to pure IM significantly decreased.

Afterward, we compared the LPPs of the LIPA and LIP0 to indicate the stress tensor contrasts resulted from O-antigen presence (see Fig. 3). Pure IM exhibits higher lateral stress at the lower leaflet since extreme values are reached compared to the LIPA membrane. Marginal shifts at the bilayer center represent the interdigitation of both membranes and remain consistent with values in Table 1. Finally, LIPA reaches the top stress value of 695 ± 14 bar at the upper leaflet of the inner membrane. Pressure on the outer membrane was lower than in the case of the inner. In LIPA the total lateral pressure in the inner and outer membrane is higher compared to pure ones (IM and OMA) and it was interestingly distributed mostly on adjacent leaflets. In our opinion growth of pressure on the upper leaflet from the inner membrane and the lower leaflet from the outer membrane supports the complex system formation, while the highest lateral stress occurs there.

Moving forward to the mechanical characterization the differences in mechanical properties are also statistically significant when the additional membrane is present in the system (see Table 3). Obtained κ values from pure systems are consistent with those delivered by Hsu *et al.* [33]. In the case of IM bending rigidity was lower in IM of both LIPA and LIP0 when compared to the model IM system. The opposite tendency was observed in the case of area compressibility where IM of LIPA and LIP0 had, in general, lower values than in the model system. Similar to Jefferies *et al.* we notice that various LPS composition differ in the matter of mechanical strength or mobility [37]. Differences can be observed in the case of OM, however, due to the presence of antigens, the tendency is less straightforward. Bending rigidity values of OM in LIPA and LIP0 systems are in between the values of the model OM system with and without O-antigens. This suggests that additional bilayer in the system stabilizes the system with antigens but also increases the whole dynamics of the membrane without antigens. This is also valid for the area compressibility parameter of whole membranes, however, became more complicated to evaluate when individual leaflet compressibilities were taken into account. Nevertheless, it should be noted that the presence of the second membrane in the simulated system strongly affected the mechanical behavior of both membranes when

compared to single membrane model systems, and should be considered in numerical studies for better biological context.

5   Conclusions

In this paper, we performed a detailed study of structural, mechanical and stress parameters of lipid membranes mimicking the *E. coli* dual membrane system. We showed the changes of numerically determined parameters with progressive complexity of the membrane systems. We presented that LPS-rich outer membrane properties strongly depend on the structure of LPS itself, changing dramatically each of the investigated parameters. Furthermore, we showed that the presence of the second (inner) membrane, mimicking the OM/IM relation in *E. coli*, significantly influenced primary membrane properties as well. Such changes may be crucial for interaction origins between particles and the membrane. As a result, common biological phenomena could not be observed numerically - or will behave differently from reality - if the simplified membrane model is used in the simulation. In future perspectives, the interactions of membrane-active particles and membranes in various membrane mimetic systems should be investigated.

References

1. Crémet, L., et al.: Comparison of three methods to study biofilm formation by clinical strains of Escherichia coli. Diagn. Microbiol. Infect. Dis. **75**, 252–255 (2013). https://doi.org/10.1016/j.diagmicrobio.2012.11.019
2. Tenaillon, O., Skurnik, D., Picard, B., Denamur, E.: The population genetics of commensal Escherichia coli. Nat. Rev. Microbiol. **8**, 207–217 (2010). https://doi.org/10.1038/nrmicro2298
3. Malanovic, N., Ön, A., Pabst, G., Zellner, A., Lohner, K.: Octenidine: novel insights into the detailed killing mechanism of Gram-negative bacteria at a cellular and molecular level. Int. J. Antimicrob. Agents **56**, 106146 (2020). https://doi.org/10.1016/j.ijantimicag.2020.106146
4. Alvarez-Marin, R., Aires-de-Sousa, M., Nordmann, P., Kieffer, N., Poirel, L.: Antimicrobial activity of octenidine against multidrug-resistant Gram-negative pathogens. Eur. J. Clin. Microbiol. Infect. Dis. **36**(12), 2379–2383 (2017). https://doi.org/10.1007/s10096-017-3070-0
5. Koburger, T., Hubner, N.-O., Braun, M., Siebert, J., Kramer, A.: Standardized comparison of antiseptic efficacy of triclosan, PVP-iodine, octenidine dihydrochloride, polyhexanide and chlorhexidine digluconate. J. Antimicrob. Chemother. **65**, 1712–1719 (2010). https://doi.org/10.1093/jac/dkq212
6. Wang, X., Quinn, P.J.: Endotoxins: lipopolysaccharides of gram-negative bacteria. Subcell. Biochem. **53**, 3–25 (2010). https://doi.org/10.1007/978-90-481-9078-2_1
7. Raetz, C.R.H., Whitfield, C.: Lipopolysaccharide endotoxins (2002). https://doi.org/10.1146/annurev.biochem.71.110601.135414

8. Ebbensgaard, A., Mordhorst, H., Aarestrup, F.M., Hansen, E.B.: The role of outer membrane proteins and lipopolysaccharides for the sensitivity of Escherichia coli to antimicrobial peptides. Front. Microbiol. **9**, 2153 (2018). https://doi.org/10.3389/fmicb.2018.02153

9. Erridge, C., Bennett-Guerrero, E., Poxton, I.R.: Structure and function of lipopolysaccharides (2002). https://doi.org/10.1016/S1286-4579(02)01604-0

10. Sohlenkamp, C., Geiger, O.: Bacterial membrane lipids: diversity in structures and pathways (2015). https://doi.org/10.1093/femsre/fuv008

11. Epand, R.M., Epand, R.F.: Lipid domains in bacterial membranes and the action of antimicrobial agents (2009). https://doi.org/10.1016/j.bbamem.2008.08.023

12. De Vivo, M., Masetti, M., Bottegoni, G., Cavalli, A.: Role of molecular dynamics and related methods in drug discovery (2016). https://doi.org/10.1021/acs.jmedchem.5b01684

13. Wu, E.L., et al: Molecular dynamics and NMR spectroscopy studies of E. coli lipopolysaccharide structure and dynamics. Biophys. J. **105**, 1444–1455 (2013). https://doi.org/10.1016/j.bpj.2013.08.002

14. Hwang, H., Paracini, N., Parks, J.M., Lakey, J.H., Gumbart, J.C.: Distribution of mechanical stress in the Escherichia coli cell envelope. Biochim. Biophys. Acta - Biomembr. **1860**, 2566–2575 (2018). https://doi.org/10.1016/j.bbamem.2018.09.020

15. Piggot, T.J., Holdbrook, D.A., Khalid, S.: Conformational dynamics and membrane interactions of the E. coli outer membrane protein FecA: a molecular dynamics simulation study. Biochim. Biophys. Acta (BBA) – Biomem. **1828**(2), 284–293 (2013). https://doi.org/10.1016/j.bbamem.2012.08.021

16. Chen, J., Zhou, G., Chen, L., Wang, Y., Wang, X., Zeng, S.: Interaction of graphene and its oxide with lipid membrane: a molecular dynamics simulation study. J. Phys. Chem. C. **120**, 6225–6231 (2016). https://doi.org/10.1021/acs.jpcc.5b10635

17. Wu, E.L., et al.: CHARMM-GUI membrane builder toward realistic biological membrane simulations (2014). https://doi.org/10.1002/jcc.23702

18. Kanonenberg, K., et al.: Shaping the lipid composition of bacterial membranes for membrane protein production. Microb. Cell Fact. **18**, 131 (2019). https://doi.org/10.1186/s12934-019-1182-1

19. Szatmári, D., et al.: Intracellular ion concentrations and cation-dependent remodelling of bacterial MreB assemblies. Sci. Rep. **10**, 12002 (2020). https://doi.org/10.1038/s41598-020-68960-w

20. Strauss, J., Burnham, N.A., Camesano, T.A.: Atomic force microscopy study of the role of LPS O-antigen on adhesion of E. coli. J. Mol. Recognit. **22**(5), 347–355 (2009). https://doi.org/10.1002/jmr.955

21. Wu, E.L., et al.: E. coli outer membrane and interactions with OmpLA. Biophys. J. **106**, 2493–2502 (2014). https://doi.org/10.1016/j.bpj.2014.04.024

22. Klauda, J.B., et al.: Update of the CHARMM all-atom additive force field for lipids: validation on six lipid types. J. Phys. Chem. B. **114**, 7830–7843 (2010). https://doi.org/10.1021/jp101759q

23. Abraham, M.J., et al.: Gromacs: high performance molecular simulations through multi-level parallelism from laptops to supercomputers. SoftwareX. **1–2**, 19–25 (2015). https://doi.org/10.1016/j.softx.2015.06.001

24. Guixà-González, R., et al.: MEMBPLUGIN: studying membrane complexity in VMD. Bioinformatics **30**, 1478–1480 (2014). https://doi.org/10.1093/bioinformatics/btu037

25. Giorgino, T.: Computing diffusion coefficients in macromolecular simulations: the diffusion coefficient tool for VMD. J. Open Source Softw. **4**(41), 1698 (2019). https://doi.org/10.21105/joss.01698

26. Vanegas, J.M., Torres-Sánchez, A., Arroyo, M.: Importance of force decomposition for local stress calculations in biomembrane molecular simulations. J. Chem. Theory Comput. **10**, 691–702 (2014). https://doi.org/10.1021/ct4008926

27. Bacle, A., Gautier, R., Jackson, C.L., Fuchs, P.F.J., Vanni, S.: Interdigitation between triglycerides and lipids modulates surface properties of lipid droplets. Biophys. J. **112**, 1417–1430 (2017). https://doi.org/10.1016/j.bpj.2017.02.032

28. Drabik, D., Chodaczek, G., Kraszewski, S., Langner, M.: Mechanical properties determination of DMPC, DPPC, DSPC, and HSPC solid-ordered bilayers. Langmuir **36**, 3826–3835 (2020). https://doi.org/10.1021/acs.langmuir.0c00475

29. Doktorova, M., LeVine, M.V., Khelashvili, G., Weinstein, H.: A new computational method for membrane compressibility: bilayer mechanical thickness revisited. Biophys. J. **116**, 487–502 (2019). https://doi.org/10.1016/j.bpj.2018.12.016

30. Marsh, D.: Lateral pressure profile, spontaneous curvature frustration, and the incorporation and conformation of proteins in membranes. Biophys. J. **93**, 3884–3899 (2007). https://doi.org/10.1529/biophysj.107.107938

31. Devanand, T., Krishnaswamy, S., Vemparala, S.: Interdigitation of lipids induced by membrane–active proteins. J. Membr. Biol. **252**(4–5), 331–342 (2019). https://doi.org/10.1007/s00232-019-00072-7

32. Shearer, J., Khalid, S.: Communication between the leaflets of asymmetric membranes revealed from coarse-grain molecular dynamics simulations. Sci. Rep. **8**, 1805 (2018). https://doi.org/10.1038/s41598-018-20227-1

33. Hsu, P.C., Samsudin, F., Shearer, J., Khalid, S.: It is complicated: curvature, diffusion, and lipid sorting within the two membranes of escherichia coli. J. Phys. Chem. Lett. **8**, 5513–5518 (2017). https://doi.org/10.1021/acs.jpclett.7b02432

34. Domínguez-Medina, C.C., et al.: Outer membrane protein size and LPS O-antigen define protective antibody targeting to the Salmonella surface. Nat. Commun. **11**, 1–11 (2020). https://doi.org/10.1038/s41467-020-14655-9

35. Piggot, T.J., Holdbrook, D.A., Khalid, S.: Electroporation of the E. coli and S. aureus membranes: molecular dynamics simulations of complex bacterial membranes. J. Phys. Chem. B. **115**, 13381–13388 (2011). https://doi.org/10.1021/jp207013v

36. Camley, B.A., Lerner, M.G., Pastor, R.W., Brown, F.L.H.: Strong influence of periodic boundary conditions on lateral diffusion in lipid bilayer membranes. J. Chem. Phys. **143**, 243113 (2015). https://doi.org/10.1063/1.4932980

37. Jefferies, D., Shearer, J., Khalid, S.: Role of o-antigen in response to mechanical stress of the E. coli outer membrane: insights from coarse-grained MD simulations. J. Phys. Chem. B. **123**(17), 3567–3575 (2019). https://doi.org/10.1021/acs.jpcb.8b12168

Chapter 9

Paper 4

Diptool—A Novel Numerical Tool for Membrane Interactions Analysis,
Applying to Antimicrobial Detergents and Drug Delivery Aids

Article

Diptool—A Novel Numerical Tool for Membrane Interactions Analysis, Applying to Antimicrobial Detergents and Drug Delivery Aids

Mateusz Rzycki [1,2,]*[iD], Sebastian Kraszewski [2][iD] and Marta Gładysiewicz-Kudrawiec [1][iD]

1   Department of Experimental Physics, Faculty of Fundamental Problems of Technology,
    Wroclaw University of Science and Technology, 50-370 Wroclaw, Poland;
    marta.gladysiewicz-kudrawiec@pwr.edu.pl
2   Department of Biomedical Engineering, Faculty of Fundamental Problems of Technology,
    Wroclaw University of Science and Technology, 50-370 Wroclaw, Poland; sebastian.kraszewski@pwr.edu.pl
*   Correspondence: mateusz.rzycki@pwr.edu.pl

Abstract: The widespread problem of resistance development in bacteria has become a critical issue for modern medicine. To limit that phenomenon, many compounds have been extensively studied. Among them were derivatives of available drugs, but also alternative novel detergents such as Gemini surfactants. Over the last decade, they have been massively synthesized and studied to obtain the most effective antimicrobial agents, as well as the most selective aids for nanoparticles drug delivery. Various protocols and distinct bacterial strains used in Minimal Inhibitory Concentration experimental studies prevented performance benchmarking of different surfactant classes over these last years. Motivated by this limitation, we designed a theoretical methodology implemented in custom fast screening software to assess the surfactant activity on model lipid membranes. Experimentally based QSAR (quantitative structure-activity relationship) prediction delivered a set of parameters underlying the Diptool software engine for high-throughput agent-membrane interactions analysis. We validated our software by comparing score energy profiles with Gibbs free energy from the Adaptive Biasing Force approach on octenidine and chlorhexidine, popular antimicrobials. Results from Diptool can reflect the molecule behavior in the lipid membrane and correctly predict free energy of translocation much faster than classic molecular dynamics. This opens a new venue for searching novel classes of detergents with sharp biologic activity.

Keywords: surfactants; numerical tool; drug delivery; free energy calculation; molecular dynamics; lipid membranes

1. Introduction

The increasing problem of antibiotic resistance was identified by The World Health Organization as one of the current major threats to global health [1]. Unless novel medicines can be developed, millions more people may die each year. One of the approaches to limit this phenomenon involves the application of antibacterial candidates with a broad spectrum of activity. The molecular target of those compounds is not well defined in microbial cells, but it is safe to guess that it could be the cell membranes or their components. The complex interaction with various cellular structures may significantly reduce the bacteria's resistance development [2,3]. Cationic Gemini surfactants belong to a class of compounds with broad-spectrum activity, effective against Gram-positives and Gram-negatives even in low concentrations, and are also used in drug nanoparticles delivery. Beyond biomedical applications, specific Gemini detergents are also used in the paint industry as corrosion inhibitors [4,5]. In the recent decade, only a few new classes of surface-active compounds have been discovered and have attracted the attention of researchers and industrial innovation units. Recently, several novel groups of bio-active detergents have been synthesized

and reported [6–9]. The latest classes of amphiphilic-structured compounds are formed by Gemini surfactants, which are made of two aliphatic hydrocarbon chains and two hydrophilic head groups bonded by a rigid or flexible spacer. The spacer can be a symmetrized bonding that uses two of the same molecules (e.g., a disulfide bridge), whereas the head groups can be composed of: phosphate, sulfone, carboxyl, sulfate ethylammonium, or pyrrolidine residues. Gemini surfactants were already proven experimentally to have a high antimicrobial capacity [10–12], and in the future may be applied in facilitating drug delivery across membranes [13,14]. Unfortunately, direct antibacterial effectiveness comparison between groups of agents is often unfeasible due to the various bacterial strains used, and multiple, not always coherent, approaches of minimum inhibitory concentration (MIC) measurements. Thus, a delivery of clear, specific structural parameters of agents that may enhance antimicrobial action remains elusive. Many attempts were proposed to explain key structure components or the membrane disruption mechanism itself [15–20], without clear success. Instead of incoherent experimental procedures among different laboratories, a theoretical approach would better address this issue, offering additional insights at the molecular level. Molecular dynamics (MD) simulation can be successfully applied to explore the behavior and activity of synthesized molecules, opening the middle-throughput analyses in silico [21]. In MD the interactions are explored by solving Newton's laws of motion for the system (i.e., bacterial lipid membrane and antimicrobial agent), fully taking into account the water environment. Those simulations may reflect the real biological environment and overcome the experiment shortcomings up to the atomic level. The antibacterial effect of surfactant activity has already been studied in this way many times, and the interactions of the model molecules, octenidine (OCT) and chlorhexidine (CHX) with mimetic membranes, have been repeatedly described [21,22]. The chemical structures of antimicrobial agents OCT and CHX are presented in Figure 1.
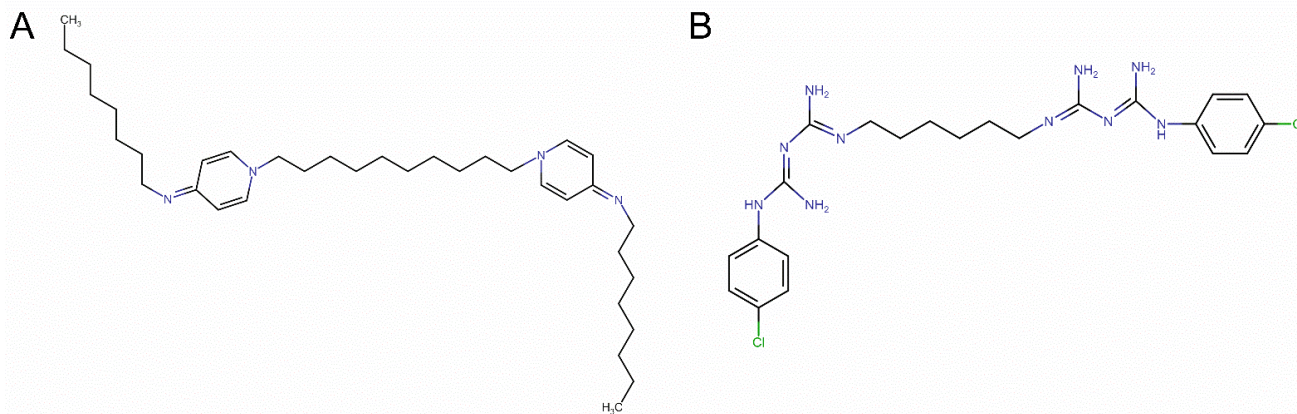

Figure 1. The chemical structures of antibacterial agents (**A**) OCT and (**B**) CHX.

In general, the molecular dynamics approach is a very versatile method but requires a lot of resources and time to effectively generate the results. Hence, molecular docking tools dedicated to protein-drug interactions have emerged in the field of pharmaceutical research. The molecular docking approach, based on quickly scored interactions without an explicit water environment presence, becomes an increasingly important tool for discovering new drugs by opening the high-throughput analyses in silico [23,24]. It offers an opportunity to model at the atomic level the interaction of small molecules with proteins, however, explaining the fundamental biochemical processes. Although docking is a much more lightweight and way faster method than MD, it has some serious limitations, such as the impossibility of docking molecules to the entire lipid membrane structure due to its essential dynamics, which molecular docking does not address [23].

As there is an increasing interest to rapidly assess the molecular interactions of selected molecules with lipid membranes, we decided to provide a numerical tool in response to these needs. Here we present a novel and unique tool that covers the gap between MD and

docking approaches, allowing the investigation of agent-lipid membrane interactions as fast as docking does but with MD precision enabling high-throughput analyses for interactions between detergents and lipids in antibacterial context. Due to the lack of unambiguous parameters determining the effectiveness of molecule-lipid membrane interactions, we used the quantitative structure-activity relationship (QSAR) method [25] to extract statistically significant properties for previously well-studied model Gemini detergents, OCT and CHX. In detail, employing data from experimentally verified various Gemini molecules delivered by Minbiole group [15,26–30], we selected 138 agents and derived a quantum QSAR, where only macroscopic descriptors such as dipole moment, partition coefficient (logP), and some structural parameters occurred as most significant for effective interactions with lipids. Descriptors were chosen to provide antimicrobial performance, comparable to standardized MIC form literature study, to ensure reproducibility of macroscopic biological phenomenon of membrane dissolution.

In this work, we introduce the methodology and the screening tool for a rapid determination of the Gemini agent affinity to various types of homogenous lipid membranes providing particle trajectory visualization and free energy analysis. We validated our tool on two commercially available and frequently studied antibacterial molecules: OCT and CHX. Additionally, we compare the results from our tool with the free energy calculations obtained directly from MD with the adaptive biasing force (ABF) approach for different lipid membranes.

2. Materials and Methods

2.1. Background

The QSAR method allows correlating the biological activity of the compound with valued physiochemical properties. Hydrophobic, electronic, or steric properties (descriptors) allow the analyzing of large databases of many agents that evoke a biological response in various molecular pathways. Some descriptors are difficult to clarify, taking into consideration the indirect representation of chemical structures. To counteract this, QSAR methods are powerfully supported by many mathematical approaches starting from multiple linear regression (MLR) [31–33] through an artificial neural network (ANN) [34–37] to machine learning (ML) [38,39]. These studies have a significant impact on recognition and understanding of the molecular mechanism of drug action, allowing the design of new and more specific candidates. Hence, since the last decade, chemoinformatics [40] has been booming and plays a significant role in discovering new drugs [41]. Moreover, the European Commission in the New Chemical Policy REACH (Registration, Evaluation and Authorization of Chemicals, European Union) recognized the method as relevant, whereas the information from alternative sources may assist in determining the presence of insecure properties of the substance, and may, in some cases, substitute for the results of animal tests [42]. In this study, our purpose was to create QSAR GA (genetic algorithm) on a set of 138 cationic Gemini surfactant molecules and to define parameters that significantly affect the potency of the antibacterial effect. In the QSAR regression model, the regression coefficient (r^2) indicates the relationship correlation, whereas the cross-validation regression coefficient (CVr^2) indicates the prediction accuracy of the model. Our major goal was to demonstrate that the phenomenon is not always straightforward, hence we focus on parameters to assess which are significant. We created several quantum QSAR linear regression models (quantum means with descriptors describing molecule at quantum level) based on delivered set of coherent MIC values for *Pseudomonas Aeruginosa*, *Escherichia Coli*, *Enterococcus Faecalis*, and *Staphylococcus Aureus* using SCIGRESS 3.3.3 (Fujitsu Ltd., Tokyo, Japan). Based on our dataset, 472 descriptors were found for every bacteria strain. We performed a 5-descriptor QSAR model for particular bacteria strains and subsequently, we decided to focus on the three most frequently occurring and most significant, but not bond-related parameters in the output– i.e., dipole moment, logP, and size, successively (see Table 1).

Table 1. Results from 5-Descriptor QSAR Calculations from *E. faecalis*, *E. coli*, *S. aureus*, and *P. aeruginosa* datasets with the Parameters' Relative Importance. Frequently Appearing Descriptors were Bolded.

E. faecalis		*E. coli*	
Descriptor	**Relative Importance**	**Descriptor**	**Relative Importance**
length/width	**0.1920**	*length/width*	**0.2316**
logP	**0.8700**	*logP*	**0.8331**
hydrophobic dipole moment	**0.3655**	*hydrophobic dipole moment*	**0.3816**
Hydrogen count	−0.1418	double bond count	−0.2713
$1.0/Csp^3$ bonded to 2 C	1.0000	$1.0/Csp^3$ bonded to 2 C	1.0000
S. aureus		*P. aeruginosa*	
Descriptor	**Relative Importance**	**Descriptor**	**Relative Importance**
length/width	**0.3422**	*length/width*	**0.3644**
logP	**0.8358**	*logP*	**0.8829**
hydrophobic dipole moment	**0.4667**	*hydrophobic dipole moment*	**0.4782**
atomic charge weighted positive area-atomic charge weighted negative area	0.1409	charge weighted nonpolar area	−0.2206
$1.0/Csp^3$ bonded to 2 C	1.0000	$1.0/Csp^3$ bonded to 2 C	1.0000

The $1.0/Csp^3$ bonded to 2C is an overlapping structural parameter associated with hybridized carbon atoms attached to exactly two carbon atoms; as it cannot be directly implemented into the calculation core as a force source, it was omitted. Based on these results, we employed dipole–dipole interaction as a calculation engine, thus implementing the first significant relationship from the obtained models. A more detailed description of motion is described in the Theory section. Partition coefficient (*logP*) and *length/width* (*size*) were included as subsequent parameters in our screening tool. The coefficient *logP* determines a measure of lipophilicity of a compound. i.e., drug and describes its ability to pass through the cell membrane barrier. It is identified as a drug distribution ratio between aqueous and organic layers at an equilibrium state [43]. To define the partition coefficient, arbitrary concentration units are often used (instead of potentials); however, the use of molarity is also useful, thus the logarithm of the partition coefficient can be determined from the chemical potentials [44].

$$log_{10}P = \frac{\mu^w - \mu^o}{RT \ln(10)} = \frac{\Delta H_{\text{transfer}}}{RT \ln(10)} \tag{1}$$

where μ^w and μ^o are excess chemical potentials of the Gemini agent in water and octanol respectively, R is the gas constant, T is the temperature, and 2.303 equals $\approx \ln(10)$. In this approach, we decided to introduce the structural parameter (*size*) which defines the *length/width* of the molecule. For general use, the molecular structure is considered as a sphere, described by radius R, thus the degrees of freedom are reduced.

The particular lipid and Gemini agent dipole moments were extracted from molecular dynamics trajectories using MOPAC 2016 (Molecular Orbital PACkage, Stewart Computational Chemistry, Colorado Springs, CO, USA) software with PM7 method [45,46]. Briefly, the specific approximation for intermolecular interactions used in PM7 was parameterized using experimental and high-level ab initio reference data, augmented by a new type of reference data intended to better define the structure of parameter space [46]. Dipole moments were derived for each lipid and agent in the system from 200 ns trajectories, and the mean values and standard deviations are used as inputs to our screening tool.

2.2. Theory and Calculation

In our approach, we accumulate particle motion by reducing this motion to that of an agent particle in a conservative field. The agents in this case are the OCT and CHX particles. The cell membrane was treated as a system of dipoles μ placed in a medium described as a

dielectric permittivity ε_r. The molecule enters the membrane from the aqueous environment described by the parameters ε_r and viscosity η. The particle is treated as a dipole attached to the sphere and moving in conservative field derived from dipoles constituting the cell membrane. Membrane dipoles are generated from the normal distribution of range of values defined by the mean lipid dipole value $+/-$ standard deviation, which were formerly calculated for each lipid type from the 200 ns of molecular dynamics trajectory (see Table 2). As a result, a unique membrane is generated automatically by our Diptool engine and takes part in the further computation procedure. In this conservative field we can describe force F corresponding to the potential energy E_p:

$$\vec{F} = -\frac{dE_p}{d\vec{r}} \tag{2}$$

Table 2. Derived Dipole Moments of Lipids and Agents from MD Simulations.

Dipole Moment in Particular Axis		X (D)	Y (D)	Z (D)	TOTAL (D)
	PC	0.34 ± 11.29	-0.37 ± 11.39	1.65 ± 8.44	18.27 ± 2.32
Particle type	PG	0.14 ± 10.17	0.29 ± 10.09	-35.08 ± 8.29	39.19 ± 4.69
	OCT	0.69 ± 7.08	2.12 ± 8.14	-0.51 ± 12.78	16.12 ± 4.55
	CHX	2.74 ± 15.46	2.21 ± 10.37	-0.55 ± 10.25	24.73 ± 8.72

Energy E_p comes from each lipid constituting membrane at distance r, and generates dipole-dipole interaction, which can be calculated considering the electrostatic interaction between the membrane-forming charges and the dipole of the studied molecule:

$$E_p = \sum \frac{\mu_i \cdot \mu}{4\pi\varepsilon_0\varepsilon_r r_i^3} \tag{3}$$

where μ_i is dipole element of membrane and ε_r is relative dielectric permittivity that equals 88.0 for water and 4.0 [47,48] for the membrane, and r_i is the distance between two dipoles. The summation proceeds over all dipoles in the considered membrane. Hence, only the electrostatic interaction between two dipoles is considered, omitting the rotation of dipoles relative to each other. However, it is a good enough approximation in a situation when one treats the particle as a point mass. Such a procedure can be used if the size of the molecule is much smaller than the size of the membrane, which is the case. Velocity and acceleration vectors can be described by:

$$\vec{v} = \vec{a} \cdot \Delta t \tag{4}$$

$$\vec{a} = \frac{d\vec{v}}{dt} = -\frac{1}{m}\frac{dE_p}{d\vec{r}} \tag{5}$$

where m is the particle masses and in our case equal 623.84 g/moL and 505.452 g/moL for OCT and CHX, respectively. Position vectors of particles are described by coordinates $r = (x, y, z)$. Numerical formulas give the equations corresponding to Verlet algorithm [49]:

$$\vec{r^n} = \vec{r^{n-2}} + 2\Delta t\vec{v^n} \tag{6}$$

$$\vec{v^{n+1}} = \vec{v^{n-1}} - 2\Delta t\frac{1}{m}\frac{d}{d\vec{r}}E_p(r^n, t^n) \tag{7}$$

where $v = (v_x, v_y, v_z)$ is a velocity vector, and n numerate step of calculation. The potential energy E_p of the dipole–dipole interaction is a function of the particle position and time t. The iteration producing the velocity is carried forward to the iterated position. Such a procedure affects the stability of the algorithm, thus we added the term of resistance force F_R corresponding to the environment viscosity η:

$$\vec{F_R} = -b\vec{v} = -6\pi\eta R\vec{v} \tag{8}$$

where R is a sphere radius of an agent particle. In our calculation we put $R = 10^{-14}$ m and $\eta = 0.89 \times 10^{-3}$ Pa·s for water and 934×10^{-3} Pa·s for the membrane. We assume the particle is an ideal sphere with a radius of R, which is related to *size* parameter. In this way, the number of degrees of freedom was limited. The radius is so small that the sphere can be treated as a point mass. Integrating resistance force to the propagation equations we get for position and velocity:

$$\vec{r^n} = \vec{r^{n-2}} + 2\Delta t \vec{v^{n-1}}$$
$$\vec{v^{n+1}} = \vec{v^{n-1}} - 2\Delta t \frac{1}{m} \frac{d}{d\vec{r}} E_p(r^n, t^n) - \frac{b}{m} \vec{v^{n-1}} 2\Delta t \tag{9}$$

Gibbs free energy can be determined deriving acceptance rules for NPT ensemble (where N is number of particles, P is pressure, and T is temperature), as it is also in MD. To define the probability density, and knowing the conjugate variables ($N \to \mu$, $V \to P$, $T \to E$) in the NPT ensemble μ, V, and E will vary, thus in given probability distribution, moves are accepted to satisfy a detailed balance. Assuming that in the thermodynamic limit, all ensembles are equivalent, the change of free energy can be calculated as the work between the states A and B [50,51]:

$$\Delta G = W_{A \to B} \tag{10}$$

The system can be described using Hamiltonian $H(v_x, v_y, v_z, x, y, z)$. If the temperature and volume of the system is maintained to calculate the change in Gibbs free energy, it is sufficient to determine this quantity. This Hamiltonian consists of the potential energy E_p and the kinetic part considering the velocity:

$$H(v_x, v_y, y_z, x, y, z) = E_p + \frac{mv^2}{2} \tag{11}$$

The kinetic energy of our molecule is limited to $k_b T$ (where k_b is the Boltzmann constant), avoiding excessive velocity. Such a procedure allows eliminating the unrealistic results. Once the Hamiltonian in each point has been determined, one can calculate the change in Gibbs free energy between the initial state A and the final state B:

$$\Delta G_{A \to B} = H_B - H_A \tag{12}$$

If non-conservative forces are acting in the simulated system, we must also consider the kinetic energy component. Above the $k_b T$ constraint, the kinetic energy is only affected by the energy resulting from the dipole–dipole interaction, so the Hamiltonian then simplifies. In addition, we have considered the situation that during the agent's transfer the environment changes from aqueous to membrane (*logP* parameter). Then, when a particle approaches the membrane, it must overcome additional potential (Equation (1)), and the Hamiltonian takes form:

$$\Delta H_{\text{transfer}} = \ln(10) RT log_{10} P \tag{13}$$

By consequence, if in the next step of iteration there is a change in ε_r then the Gibbs energy is calculated according to:

$$\Delta G_{A \to B} = H_B - H_A + \Delta H_{\text{transfer}} \tag{14}$$

This approach also works when the particle is pushed out of the membrane.

The presented numerical algorithm allows us to determine the trajectory and Gibbs free energy for any particle represented as a dipole in a conservative field produced by other dipoles. This algorithm is very simplified and assumes only interactions between dipoles, with minor corrections (η and *logP*), and omits other interactions. However, qualitatively it allows us to estimate the macroscopic response of the membrane system with fair accuracy.

2.3. Molecular Dynamics Validation

The proposed methodology was verified using free energy profiles in molecular dynamics simulations. The all-atom models of the membranes were generated using CHARMM-GUI membrane builder [52]. In this work PC (1-palmitoyl-2-oleoyl-glycero-3-phosphocholine) and PG (1-palmitoyl-2-oleoyl-sn-glycero-3-phospho-(1′-rac-glycerol)) lipids were selected for the comparison of the agents' behavior in neutral (100% POPC) and negatively charged (100% POPG) environments, reflecting mammalian and bacterial inner membranes, respectively. The TIP3P water model was employed and counterions were included in PG. Finally, both membranes were composed of 200 lipids (100 per monolayer).

MD simulations were performed using the NAMD (version 2.14, University of Illinois, Urbana, IL, USA) package [53] with the CHARMM36 force field [54]. Calculations were carried out in the NPT ensemble (constant number of particles, pressure, and temperature) at constant pressure (1 atm) and temperature (300 K) using the Langevin piston method and Langevin dynamics [55]. Short and long-range interactions were computed every 1 and 2 time-steps, respectively. Long-range electrostatic forces were evaluated using the particle mesh Ewald (PME) method [56], which allowed us to employ the integration timestep of 2 fs. Finally, 200 ns of pure membrane trajectories were produced and taken as an input to the free energy method.
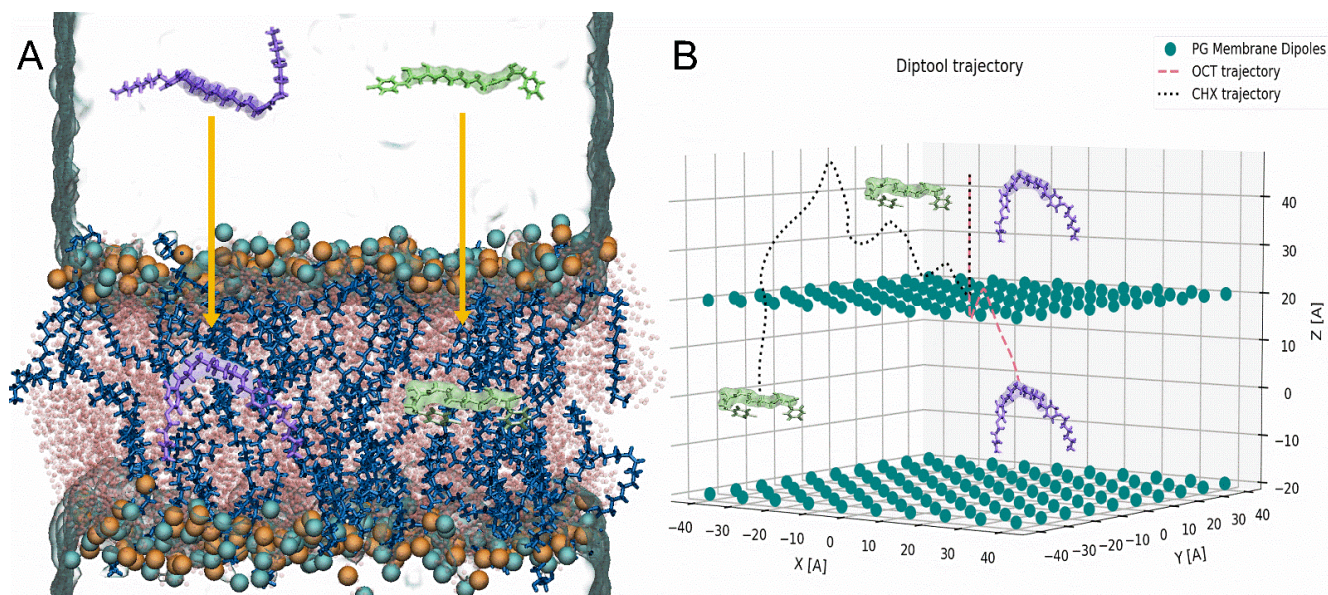

Figure 2. Initial and final trajectories obtained from (**A**) ABF−method, (**B**) Diptool software on PG membranes. CHX: green sticks and surface, OCT: violet sticks and surface, POPG: blue and pink sticks, phosphorous atoms: cyan beads, nitrogen atoms: orange beads and PG membrane dipoles: teal beads.

From a bunch of available protocols, the ABF method was selected because it is an established and precise approach [57,58]. The free energy profiles were obtained using the ABF extension implemented in NAMD software. The integrated collective variables module [59] was applied to the delivered MD simulation protocol. The agent molecules were placed 45 Å over the bilayer center, and the reaction coordinate is consistent with the membrane normal vector between the center of mass of the membrane and the center of mass of the agent spacer. The number of atoms in antimicrobial particles was intentionally reduced to limit the degrees of freedom and molecules' fluctuation. Therefore, the most rigid region (spacer) of OCT and CHX was selected using C14–C23 atoms and C7–C16, respectively (highlighted in Figure 2). The minimal sampling of 50,000 samples along for each step was applied, employing 0.2 Å width step along the reaction coordinate. Finally, at least 0.7 µs was produced to obtain each free-energy profile. For visualization and analysis purposes, Visual Molecular Dynamics was used (VMD) [60]. Here OCT and CHX

molecules were employed from our previous work where the description of molecular parametrization was presented in detail [21].

2.4. Data Visualization and Analysis

Diptool is provided with a dedicated engine written in C++ and visualization package implemented in Python (Python Software Foundation, Wilmington, DA, USA.) and requires version 3.7 or higher. Three-dimensional trajectories and energy profile plots are generated based on delivered input from the Diptool engine and MD ABF. It uses the following libraries: matplotlib, math, pyplot, numpy, seaborn. The Diptool engine is compiled C++ code (*Diptool_engine.exe*) where initial parameters such as dipole moments and errors, membrane size, area per lipid (APL), Gemini agent mass, and its dipoles need to be delivered in a parameter text file (*param.txt*). Diptool should be executed from an included python script (Diptool_run.py), in which the tool engine is embedded and automatically launched, and after finished calculations a trajectory and energy plots are generated. In the meantime, three files with plotted membrane position, agent trajectory, and energy profiles are produced, respectively. In *membrane.txt* file the dipoles arrangement in X, Y, Z direction are stored, *data.txt* include the agent trajectory in the X, Y, Z axes, and finally *energy.txt* contain the energy profile with respect to the bilayer normal—Z direction. The python visualization code was commented including several hints to simplify the usage. Apart from Diptool engine calculations, the MD free energy profiles may be visualized for quick comparison. In the Supplementary materials, complete Diptool software with exemplary files for initial runs is delivered.

Significance tests and plots were performed using OriginLab Origin 2018 software (OriginLab, Northampton, MA, USA). Specifically, one-way ANOVA was applied with post-hoc Tukey test to determining significance between individual populations with the significance level at 0.05.

3. Results and Discussion

The membranes have been described in Diptool as a set of dipoles that interact with each other and with surfactant dipoles as well. To obtain dipole moments of particular lipids and agents, corresponding trajectories from MD were employed. From the 200 ns of simulations we extracted dipole moments for every molecule in the bilayer, resulting in set of 400,000 dipoles in the X Y Z direction. The average and the standard deviation of the Diptool input is presented in Table 2. The lipid positions and mobility affect the wide range of obtained data, which results in the high fluctuations of standard deviation. In this approach, we decided to avoid averaging the error to derive a wider range for random membrane components generator and deliver a complex expertise of membrane-agent interactions. Such a procedure allows employing many types of lipids reflecting many membrane species supposing that dipole moments are known. Additionally, at this stage a membrane size may be adjusted in all axes, whereas a number of lipids is automatically calculated based on the given volume and APL. In this work we decided to compare the Gemini agents behavior in neutral and negatively charged environments using PC and PG lipids [61,62]. These are commonly used in both experimental and theoretical work, because the latter is one of the major components in bacterial bilayer structures, whereas PC is mimicking eukaryotic cell membranes. That system configuration often allows demonstrating distinct and selective behavior of active compounds such as OCT and CHX in various membrane systems [21,63,64]. A different behavior may also be visible due to those particular lipids yielding various dipole moments, especially in the Z-axis and in the total value as well.

Similarly, as in MD, Diptool allows to register, i.e., trajectories and energies and analyze them afterward. However, employing the average and standard deviation of system components in the tool may deliver slightly different results whenever used. That combination allows for a more comprehensive case study about selected surfactants accompanied by given lipids. In Figure 2 the snapshots from MD trajectories (Figure 2A) and Diptool

(Figure 2B) are presented where OCT and CHX behavior were investigated in membrane systems. In all cases, an agent particle was placed 45 Å above the membrane center, and their trajectories seem to present similar features. The surfactant molecule approaches the membrane surface, penetrating it and facing the bilayer center afterward. Although Diptool uses a different core of motion, the modeled trajectories correspond to those from both steered and classical MD. The Diptool trajectories may vary significantly in the subsequent runs because dipole location and value are different. However, the starting and ending point reached by tested molecules remain consistent. Based on given trajectories, significant differences in behavior between CHX and OCT may be noticed. In the case of OCT, a small molecule fluctuation at the membrane interface may be observed, whereas CHX particles indicated higher resistance and took a little longer to reach the membrane center (see Figure 2B).

The second main feature derived from Diptool is the system energy calculation, which corresponds to the free energy calculation provided by the MD−ABF method. The results from both methods for OCT and CHX molecules are presented in Figure 3. An essential part of the free energy determination is the difference associated with the molecule translocation toward the membrane from bulk water to bilayer center—ΔG_{trans} [57]. The free energy calculations illustrated that in a neutral membrane, OCT spontaneously crosses the bilayer interface, exhibiting the deepest well of ~9 kcal/mol; hence, it is the most thermodynamically favorable location (see Figure 3A). This corresponds to our previous studies, where we indicated theoretically and experimentally that OCT locate in the carbonyl−glycerol region preferentially [21]. Subsequently, an expected high energy barrier towards the membrane center occurs as also reported in other work focused on the transport of charged particles from water to the hydrophobic core [57,65]. Although surfactant can easily access the membrane, the translocation to another leaflet is energetically demanding. As stated, the ΔG_{trans} is the difference between ΔG_{bulk} and ΔG_{core} [57] and yields ~0.5 kcal/mol. The core motion of Diptool is unique, therefore, the final energy plot also indicates individual regions. First, a small energy barrier of ~1 kcal/mol may be noticed at the membrane interface, which is related to dipole−dipole interactions between particle and the zwitterionic lipids. Because the agent trajectory is correlated with membrane normal, and a corresponding vector dipole moment does not yield extreme values, only a small peak representing the barrier is visible. Similarly, as in the ABF−method, the local minimum in the membrane is reached near the carbonyl−glycerol area. Moving forward, facing the bilayer center, the energy barrier occurs again from the hydrophobic core. The total OCT's $\Delta G_{D.trans}$ using Diptool reached ~1.7 kcal/mol, which successfully screened the agent behavior compared to the extensive ABF calculations. In the case of charged PG membranes (see Figure 3B), the free energy associated with OCT indicates slight fluctuations near the membrane surface of ~0.5 kcal/mol, while subsequently a ~6 kcal/mol well is reached. The largest barrier to overcome was faced in the direction of the membrane center yielding total a ΔG_{trans} of ~4.5 kcal/mol. In the results from Diptool, the system differences may be clearly visible, due to large peak of ~3 kcal/mol at the membrane entry caused by negatively charged lipids. Further, local membrane minimum is reached (~1.3 kcal/mol) and the final hydrophobic barrier occurred as in previous cases, ending with a total $\Delta G_{D.trans}$ of ~3.3 kcal/mol. It should be noted that local minima in PG membranes are shifted toward the bilayer center relative to the PC ones, which indicates that OCT prefer to stay a bit deeper in the negatively charged membranes.

Another, much different energy profile associated with CHX behavior was reported in PC membranes (see Figure 3C). Interestingly, the molecule does not access the membrane spontaneously as OCT does. Analogous limited agent–membrane interaction was observed in our previous report [21] as several CHX molecules incorporated into membrane; however, some of them stayed in the bulk water. Here, a small barrier of ~1.9 kcal/mol accompanies molecule entry to membrane, and further at carbonyl−glycerol region strikes up to ~20 kcal/mol. This specific behavior may be related with low logP coefficient logP = 5.48, whereas for OCT logP = 9.25. This may indicate that the substance has a high tendency to

locate in the outer part of the membrane. This is in strong agreement with the results from Diptool, as a low energy barrier is at the membrane interface, with a local minimum in the membrane at hydrophilic heads. The further peak corresponds to the one observed in the ABF method; however, registered values vary a lot, as ΔG_{trans} and $\Delta G_{D.trans}$ equal ~20 and ~1.6 kcal/mol, respectively. In the case of a negatively charged PG bilayer, the agent demonstrated a distinct energy profile (see Figure 3D). A negatively charged membrane is ideal for CHX, which find the sweet spot at local minima of ~9 kcal/mol. Similar to the other cases, the biggest energy barrier occurs when facing bilayer center, ending with a total ΔG_{trans} of ~5.8 kcal/mol. Diptool results indicate a big energy barrier from negatively charged lipids at 22 Å from the bilayer center, while afterward local minimum is settled below the carbonyl−glycerol region. Here the final $\Delta G_{D.trans}$ equals ~3.5 kcal/mol, which fairly reflects the accurate energy calculations from ABF−MD. Higher Diptool energy may indicate more effective antimicrobial action. It should be noted that proposed energy analysis is one of the means of evaluating membrane−agent interactions. Because Diptool is a screening tool, extensive calculations are needed for delivering a comprehensive outcome, especially in drug-delivery studies. Given results may significantly accelerate and narrow down the group of tested compounds; however, experimental or theoretical confirmations should be delivered additionally.
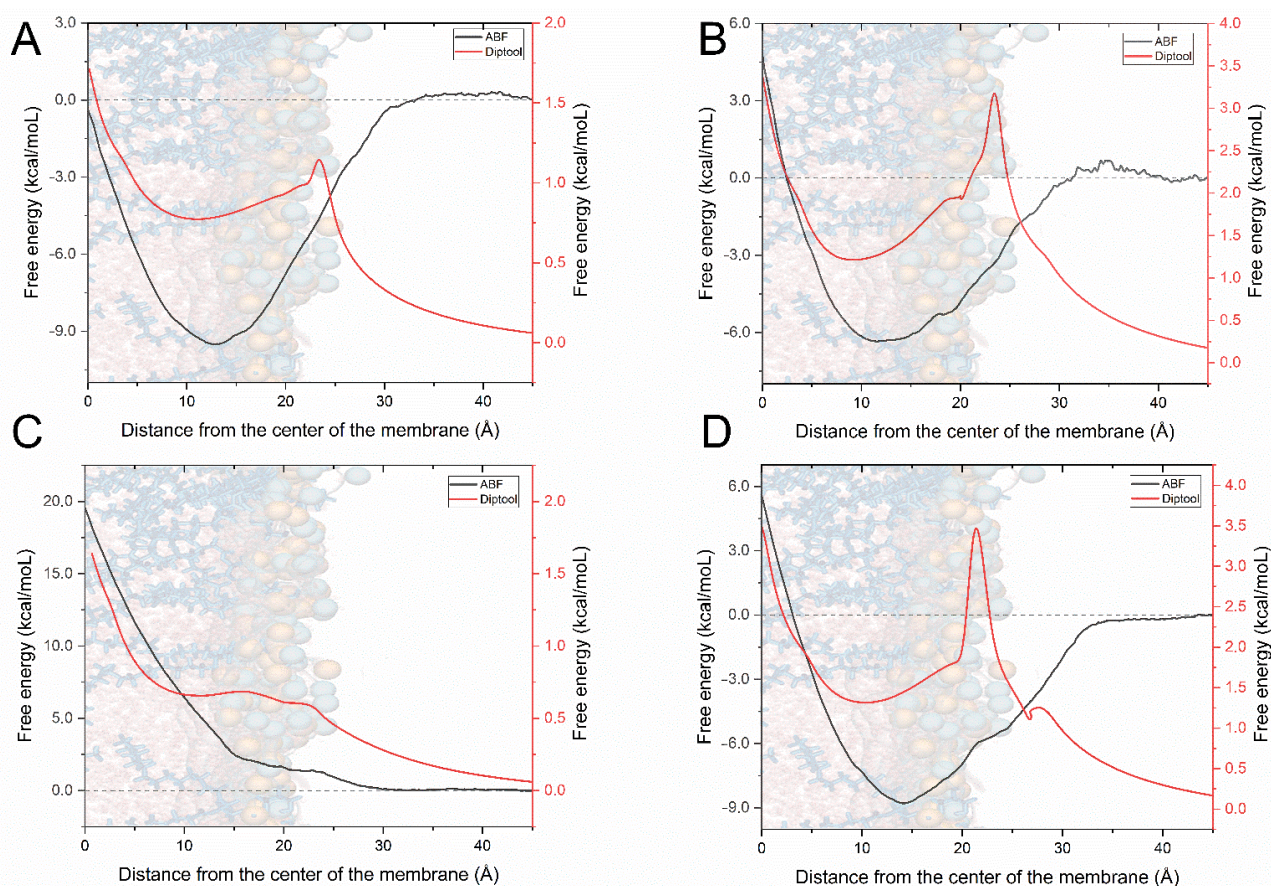

Figure 3. The comparison between MD−ABF and Diptool free energy calculation, marked in black and red, respectively. (**A**) Free energy transfer for OCT in PC membrane, (**B**) Free energy transfer for OCT in PG membrane, (**C**) Free energy transfer for CHX in PC membrane, (**D**) Free energy transfer for CHX in PG membrane.

To this end, Diptool is a screening tool whose results correspond with those derived from free energy calculations in MD. Although it is based on a modified Verlet algorithm, its capabilities and accuracy are limited and not so precise compared to a classical MD approach. The greatest advantage of the tool is its performance. Used algorithm and modifications combined in the C++ engine makes it reliable, fast, and lightweight software.

The local performance test was conducted using AMD Ryzen 5 2600 CPU (AMD Santa Clara, CA, USA) supported with 16GB DDR4 RAM. Out of 100 runs, the average computation time lasted 5 ± 1 min, whereas to provide accurate and precise calculations from the ABF method, $64,800 \pm 3527$ min were needed using a 96 Intel Xeon E5 v3 CPUs (Intel, Santa Clara, CA, USA) together on four nodes, for the single system. Estimated acceleration for one molecule screening is thus about a million times comparing to steered MD study. That gives an enormous advantage to Diptool for screening a large database to select several candidates and deliver rigorous results afterward.

4. Conclusions

In this work, we presented a novel, self−made methodology supported with a software solution named Diptool—a screening tool for a rapid determination of the Gemini agent affinity to various types of homogenous lipid membranes delivering particle trajectory visualization and free energy analysis. In the presented study we introduced from scratch the genesis and background of delivered methodology, discussed the calculation core of the Diptool software, and finally validated and tested our tool with known antimicrobial candidates: OCT and CHX. Our results indicate that Diptool is able to generate accurate free energy profiles for Gemini surfactants significantly faster than other well-known, established, and more advanced methods. We used molecular dynamics studies to verify our assumptions highlighting the estimation of the free energy perturbation. Our calculations were provided on both neutral-PC and negatively charged-PG lipids, as the latter are major components in bacterial inner bilayers. We compared computations from Diptool and the ABF method from molecular dynamics focusing on the membrane−agent interactions presenting surfactant trajectory and free energy profiles. Despite much different theories of calculation, we indicated similarities in trajectories of OCT and CHX between the tested tools. In both cases, the agents were suspended in the bulk water and afterward penetrated the membrane toward the bilayer center, which allowed us to construct the free energy profiles. Here the final results of $\Delta G_{D.trans}$ and ΔG_{trans} indicate whether a given particle prefers to stay in the water phase, anchor in hydrophilic heads, or interact with hydrophobic core, as well as the energetic cost of that displacement. Delivered results indicate that the agent behavior in various lipid environments is well reflected with mostly corresponding translocation free energies, and hence expected macroscopic biological behavior. Additionally, our results confirm that a reduction in the membrane dipole results in reduced permeability of polar compounds [57,66]. We also provided a performance test that clearly indicates that Diptool is significantly faster than classical methods, reaching a one million-fold compared to the MD approach. We would like to clearly emphasize that provided software should be considered as a screening tool for rapid determination of agent effectiveness, enabling high−throughput screening for at least antimicrobial and drug−delivery aids based on detergent molecules. In this paper, we present the first version of Diptool; however, further development is planned. In the following versions we would like to deliver various lipid mixtures implementation, apply various solvents containing ion solutions, implement additional empirical parameters in the energy calculations to better follow the particle energy fluctuations, and offer graphical user interface (GUI) for more comprehensive, rapid, and accurate solutions for surfactant analyses.

Author Contributions: Conceptualization, M.R., S.K. and M.G.-K.; methodology, M.R., S.K. and M.G.-K.; validation, M.R. and S.K.; formal analysis, M.R.; investigation, M.R., S.K. and M.G.-K.; resources, S.K. and M.G.-K.; data curation, M.R., S.K. and M.G.-K.; writing—original draft preparation, M.R. and M.G.-K.; writing—review and editing, M.R., S.K. and M.G.-K.; visualization, M.R.; supervision, S.K. and M.G.-K.; project administration, S.K. and M.G.-K.; funding acquisition, S.K., M.G.-K. and M.R. All authors have read and agreed to the published version of the manuscript.

Institutional Review Board Statement: Not applicable.

Informed Consent Statement: Not applicable.

Data Availability Statement: Most of the data are available in the main manuscript or generated by code attached to supplementary materials.

Conflicts of Interest: The authors declare no conflict of interest.

References

1. World Health Organization. *Antimicrobial Resistance: Global Report on Surveillance*; World Health Organization: Geneva, Switzerland, 2014.
2. Kramer, A. Hand Disinfection and Antiseptic of Skin, Mucous Membranes, and Wounds. In *Dermatopharmacology of Topical Preparations*; Springer: Berlin/Heidelberg, Germany, 2000; pp. 121–134.
3. Russell, A.D. Antibiotic and biocide resistance in bacteria: Introduction. *J. Appl. Microbiol.* **2002**, *92*, 1S–3S. [CrossRef]
4. Zhuang, W.; Wang, X.; Zhu, W.; Zhang, Y.; Sun, D.; Zhang, R.; Wu, C. Imidazoline Gemini Surfactants as Corrosion Inhibitors for Carbon Steel X70 in NaCl Solution. *ACS Omega* **2021**, *6*, 5653–5660. [CrossRef]
5. Heakal, F.E.T.; Elkholy, A.E. Gemini surfactants as corrosion inhibitors for carbon steel. *J. Mol. Liq.* **2017**, *230*, 395–407. [CrossRef]
6. Yang, W.; Cao, Y.; Ju, H.; Wang, Y.; Jiang, Y.; Geng, T. Amide Gemini surfactants linked by rigid spacer group 1,4-dibromo-2-butene: Surface properties, aggregate and application properties. *J. Mol. Liq.* **2021**, *326*, 115339. [CrossRef]
7. Li, Y.; Wu, P.; Lei, C.; Liu, X.; Han, X. A novel cationic surfactant synthesized from carbon quantum dots and the versatility. *Colloids Surf. A Physicochem. Eng. Asp.* **2021**, *626*, 127088. [CrossRef]
8. Zheng, L.C.; Tong, Q.X. Synthesis, surface adsorption, micellization behavior and antibacterial activity of novel gemini surfactants with morpholinium headgroup and benzene-based spacer. *J. Mol. Liq.* **2021**, *331*, 115781. [CrossRef]
9. Sarıkaya, İ.; Bilgen, S.; Ünver, Y.; Bektaş, K.İ.; Akbaş, H. Synthesis, Characterization, Antibacterial Activity, and Interfacial and Micellar Features of Novel Cationic Gemini Surfactants with Different Spacers. *J. Surfactants Deterg.* **2021**. [CrossRef]
10. Fatma, N.; Panda, M.; Beg, M. Ester-bonded cationic gemini surfactants: Assessment of their cytotoxicity and antimicrobial activity. *J. Mol. Liq.* **2016**, *222*, 390–394. [CrossRef]
11. Tawfik, S.M. Simple one step synthesis of gemini cationic surfactant-based ionic liquids: Physicochemical, surface properties and biological activity. *J. Mol. Liq.* **2015**, *209*, 320–326. [CrossRef]
12. Hübner, N.-O.; Siebert, J.; Kramer, A. Octenidine Dihydrochloride, a Modern Antiseptic for Skin, Mucous Membranes and Wounds. *Ski. Pharmacol. Physiol.* **2010**, *23*, 244–258. [CrossRef]
13. Brycki, B.E.; Kowalczyk, I.H.; Szulc, A.; Kaczerewska, O.; Pakiet, M. Multifunctional Gemini Surfactants: Structure, Synthesis, Properties and Applications. *Appl. Charact. Surfactants* **2017**. [CrossRef]
14. Lv, J.; Qiao, W.; Li, Z. Vesicles from pH-regulated reversible gemini amino-acid surfactants as nanocapsules for delivery. *Colloids Surf. B Biointerfaces* **2016**, *146*, 523–531. [CrossRef] [PubMed]
15. Black, J.W.; Jennings, M.C.; Azarewicz, J.; Paniak, T.J.; Grenier, M.C.; Wuest, W.M.; Minbiole, K.P.C. TMEDA-derived biscationic amphiphiles: An economical preparation of potent antibacterial agents Dedicated to Professor Amos B. Smith, III, in celebration of his 40 years of mentoring scientists. *Bioorg. Med. Chem. Lett.* **2014**, *24*, 99–102. [CrossRef]
16. Pernak, J.; Sobaszkiewicz, K.; Foksowicz-Flaczyk, J. Ionic liquids with symmetrical dialkoxymethyl-substituted imidazolium cations. *Chem. A Eur. J.* **2004**, *10*, 3479–3485. [CrossRef] [PubMed]
17. Bao, Y.; Guo, J.; Ma, J.; Li, M.; Li, X. Physicochemical and antimicrobial activities of cationic gemini surfactants with polyether siloxane linked group. *J. Mol. Liq.* **2017**, *242*, 8–15. [CrossRef]
18. Muslim, A.A.; Ayyash, D.; Gujral, S.S.; Mekhail, G.M.; Rao, P.P.N.; Wettig, S.D. Synthesis and characterization of asymmetrical gemini surfactants. *Phys. Chem. Chem. Phys.* **2017**, *19*, 1953–1962. [CrossRef] [PubMed]
19. Zhang, S.; Ding, S.; Yu, J.; Chen, X.; Lei, Q.; Fang, W. Antibacterial activity, in vitro cytotoxicity, and cell cycle arrest of gemini quaternary ammonium surfactants. *Langmuir* **2015**, *31*, 12161–12169. [CrossRef]
20. Negm, N.A.; Abd-Elaal, A.A.; Mohamed, D.E.; El-Farargy, A.F.; Mohamed, S. Synthesis and evaluation of silver nanoparticles loaded with Gemini surfactants: Surface and antimicrobial activity. *J. Ind. Eng. Chem.* **2015**, *24*, 34–41. [CrossRef]
21. Rzycki, M.; Drabik, D.; Szostak-Paluch, K.; Hanus-Lorenz, B.; Kraszewski, S. Unraveling the mechanism of octenidine and chlorhexidine on membranes: Does electrostatics matter? *Biophys. J.* **2021**, *120*, 3392–3408. [CrossRef]
22. Van Oosten, B.; Marquardt, D.; Komljenović, I.; Bradshaw, J.P.; Sternin, E.; Harroun, T.A. Small molecule interaction with lipid bilayers: A molecular dynamics study of chlorhexidine. *J. Mol. Graph. Model.* **2014**, *48*, 96–104. [CrossRef]
23. Sethi, A.; Joshi, K.; Sasikala, K.; Alvala, M. Molecular Docking in Modern Drug Discovery: Principles and Recent Applications. In *Drug Discovery and Development—New Advances*; IntechOpen: London, UK, 2019. [CrossRef]

24. Meng, X.-Y.; Zhang, H.-X.; Mezei, M.; Cui, M. Molecular Docking: A Powerful Approach for Structure-Based Drug Discovery. *Curr. Comput. Aided-Drug Des.* **2012**, *7*, 146–157. [CrossRef] [PubMed]
25. Tropsha, A. Best Practices for QSAR Model Development, Validation, and Exploitation. *Mol. Inform.* **2010**, *29*, 476–488. [CrossRef]
26. Paniak, T.J.; Jennings, M.C.; Shanahan, P.C.; Joyce, M.D.; Santiago, C.N.; Wuest, W.M.; Minbiole, K.P.C. The antimicrobial activity of mono-, bis-, tris-, and tetracationic amphiphiles derived from simple polyamine platforms. *Bioorg. Med. Chem. Lett.* **2014**, *24*, 5824–5828. [CrossRef] [PubMed]
27. Ator, L.E.; Jennings, M.C.; McGettigan, A.R.; Paul, J.J.; Wuest, W.M.; Minbiole, K.P.C. Beyond paraquats: Dialkyl 3,3′- and 3,4′-bipyridinium amphiphiles as antibacterial agents. *Bioorg. Med. Chem. Lett.* **2014**, *24*, 3706–3709. [CrossRef]
28. Mitchell, M.A.; Iannetta, A.A.; Jennings, M.C.; Fletcher, M.H.; Wuest, W.M.; Minbiole, K.P.C. Scaffold-Hopping of Multicationic Amphiphiles Yields Three New Classes of Antimicrobials. *ChemBioChem* **2015**, *16*, 2299–2303. [CrossRef]
29. Forman, M.E.; Jennings, M.C.; Wuest, W.M.; Minbiole, K.P.C. Building a Better Quaternary Ammonium Compound (QAC): Branched Tetracationic Antiseptic Amphiphiles. *ChemMedChem* **2016**, *11*, 1401–1405. [CrossRef]
30. Grenier, M.C.; Davis, R.W.; Wilson-Henjum, K.L.; Ladow, J.E.; Black, J.W.; Caran, K.L.; Seifert, K.; Minbiole, K.P.C. The antibacterial activity of 4,4′-bipyridinium amphiphiles with conventional, bicephalic and gemini architectures. *Bioorg. Med. Chem. Lett.* **2012**, *22*, 4055–4058. [CrossRef] [PubMed]
31. Hemmateenejad, B.; Miri, R.; Akhond, M.; Shamsipur, M. QSAR study of the calcium channel antagonist activity of some recently synthesized dihydropyridine derivatives. An application of genetic algorithm for variable selection in MLR and PLS methods. *Chemom. Intell. Lab. Syst.* **2002**, *64*, 91–99. [CrossRef]
32. Roy, K.; Ambure, P. The "double cross-validation" software tool for MLR QSAR model development. *Chemom. Intell. Lab. Syst.* **2016**, *159*, 108–126. [CrossRef]
33. Alam, S.; Khan, F. QSAR and docking studies on xanthone derivatives for anticancer activity targeting DNA topoisomerase IIα. *Drug Des. Devel. Ther.* **2014**, *8*, 183–195. [CrossRef] [PubMed]
34. Gupta, M.K.; Gupta, S.; Rawal, R.K. Impact of Artificial Neural Networks in QSAR and Computational Modeling. In *Artificial Neural Network for Drug Design, Delivery and Disposition*; Elsevier Inc.: Amsterdam, The Netherlands, 2016; pp. 153–179. ISBN 9780128015599.
35. Luo, J.; Hu, J.; Fu, L.; Liu, C.; Jin, X. Use of artificial neural network for a QSAR study on neurotrophic activities of N-p-tolyl/phenylsulfonyl L-amino acid thiolester derivatives. *Proc. Proc. Eng.* **2011**, *15*, 5158–5163. [CrossRef]
36. Montañez-Godínez, N.; Martínez-Olguín, A.C.; Deeb, O.; Garduño-Juárez, R.; Ramírez-Galicia, G. Qsar/qspr as an application of artifi cial neural networks. *Methods Mol. Biol.* **2015**, *1260*, 319–333. [CrossRef] [PubMed]
37. Dahl, G.E.; Jaitly, N.; Salakhutdinov, R. Multi-task Neural Networks for QSAR Predictions. *arXiv* **2014**, arXiv:1406.1231.
38. Lo, Y.C.; Rensi, S.E.; Torng, W.; Altman, R.B. Machine learning in chemoinformatics and drug discovery. *Drug Discov. Today* **2018**, *23*, 1538–1546. [CrossRef] [PubMed]
39. Dixon, S.L.; Duan, J.; Smith, E.; Von Bargen, C.D.; Sherman, W.; Repasky, M.P. AutoQSAR: An automated machine learning tool for best-practice quantitative structure-activity relationship modeling. *Future Med. Chem.* **2016**, *8*, 1825–1839. [CrossRef]
40. Todeschini, R.; Consonni, V. *Molecular Descriptors for Chemoinformatics*; Methods and Principles in Medicinal Chemistry; Wiley: Hoboken, NJ, USA, 2009; Volume 41, ISBN 9783527318520.
41. Andrade, C.H.; Pasqualoto, K.F.M.; Ferreira, E.I.; Hopfinger, A.J. 4D-QSAR: Perspectives in Drug Design. *Molecules* **2010**, *15*, 3281–3294. [CrossRef]
42. Gramatica, P. Principles of QSAR models validation: Internal and external. *QSAR Comb. Sci.* **2007**, *26*, 694–701. [CrossRef]
43. Lau, E. *Preformulation Studies*; Elsevier Inc.: Amsterdam, The Netherlands, 2001; Volume 3.
44. Espinosa, J.R.; Wand, C.R.; Vega, C.; Sanz, E.; Frenkel, D. Calculation of the water-octanol partition coefficient of cholesterol for SPC, TIP3P, and TIP4P water. *J. Chem. Phys.* **2018**, *149*, 224501. [CrossRef]
45. Stewart, J.P. *MOPAC 2016*; Stewart Computational Chemistry: Colorado Springs, CO, USA, 2016.
46. Stewart, J.J.P. Optimization of parameters for semiempirical methods VI: More modifications to the NDDO approximations and re-optimization of parameters. *J. Mol. Model.* **2013**, *19*, 1–32. [CrossRef]
47. Stern, H.A.; Feller, S.E. Dielectric permittivity profiles of confined polar fluids. *J. Chem. Phys.* **2003**, *118*, 926. [CrossRef]
48. Weaver, J.C.; Schoenbach, K.H. Biodielectrics. *IEEE Trans. Dielectr. Electr. Insul.* **2003**, *10*, 715–716. [CrossRef]
49. Grubmüller, H.; Heller, H.; Windemuth, A.; Schulten, K. Generalized verlet algorithm for efficient molecular dynamics simulations with long-range interactions. *Mol. Simul.* **1991**, *6*, 121–142. [CrossRef]
50. Ben-tal, N.; Honig, B.; Peitzsch, R.M.; Denisov, G.; Mclaughlin, S. Binding of Small Basic Peptides to Membranes Containing Acidic Lipids: Theoretical Models and Experimental Results. *Biophys. J.* **1996**, *71*, 561–575. [CrossRef]
51. Li, P.; Merz, K.M. Taking into account the ion-induced dipole interaction in the nonbonded model of ions. *J. Chem. Theory Comput.* **2014**, *10*, 289–297. [CrossRef] [PubMed]
52. Wu, E.L.; Cheng, X.; Jo, S.; Rui, H.; Song, K.C.; Dávila-Contreras, E.M.; Qi, Y.; Lee, J.; Monje-Galvan, V.; Venable, R.M.; et al. CHARMM-GUI membrane builder toward realistic biological membrane simulations. *J. Comput. Chem.* **2014**, *35*, 1997–2004. [CrossRef]
53. Phillips, J.C.; Braun, R.; Wang, W.; Gumbart, J.; Tajkhorshid, E.; Villa, E.; Chipot, C.; Skeel, R.D.; Kalé, L.; Schulten, K. Scalable molecular dynamics with NAMD. *J. Comput. Chem.* **2005**, *26*, 1781–1802. [CrossRef] [PubMed]

54. Klauda, J.B.; Venable, R.M.; Freites, J.A.; O'Connor, J.W.; Tobias, D.J.; Mondragon-Ramirez, C.; Vorobyov, I.; MacKerell, A.D.; Pastor, R.W. Update of the CHARMM All-Atom Additive Force Field for Lipids: Validation on Six Lipid Types. *J. Phys. Chem. B* **2010**, *114*, 7830–7843. [CrossRef]

55. Feller, S.E.; Zhang, Y.; Pastor, R.W.; Brooks, B.R. Constant pressure molecular dynamics simulation: The Langevin piston method. *J. Chem. Phys.* **1998**, *103*, 4613. [CrossRef]

56. Darden, T.; York, D.; Pedersen, L. Particle mesh Ewald: An N·log(N) method for Ewald sums in large systems. *J. Chem. Phys.* **1998**, *98*, 10089. [CrossRef]

57. Bonhenry, D.; Tarek, M.; Dehez, F. Effects of Phospholipid Composition on the Transfer of a Small Cationic Peptide Across a Model Biological Membrane. *J. Chem. Theory Comput.* **2013**, *9*, 5675–5684. [CrossRef] [PubMed]

58. Comer, J.; Gumbart, J.C.; Hénin, J.; Lelièvre, T.; Pohorille, A.; Chipot, C. The Adaptive Biasing Force Method: Everything You Always Wanted To Know but Were Afraid To Ask. *J. Phys. Chem. B* **2014**, *119*, 1129–1151. [CrossRef] [PubMed]

59. Hénin, J.; Fiorin, G.; Chipot, C.; Klein, M.L. Exploring Multidimensional Free Energy Landscapes Using Time-Dependent Biases on Collective Variables. *J. Chem. Theory Comput.* **2009**, *6*, 35–47. [CrossRef] [PubMed]

60. Humphrey, W.; Dalke, A.; Schulten, K. VMD: Visual molecular dynamics. *J. Mol. Graph.* **1996**, *14*, 33–38. [CrossRef]

61. Petrache, H.I. 5.2 Lipid Bilayer Structure. *Compr. Biophys.* **2012**, *5*, 3–15. [CrossRef]

62. Epand, R.M.; Epand, R.F. Bacterial membrane lipids in the action of antimicrobial agents. *J. Pept. Sci.* **2011**, *17*, 298–305. [CrossRef] [PubMed]

63. Malanovic, N.; Ön, A.; Pabst, G.; Zellner, A.; Lohner, K. Octenidine: Novel insights into the detailed killing mechanism of Gram-negative bacteria at a cellular and molecular level. *Int. J. Antimicrob. Agents* **2020**, *56*, 106146. [CrossRef]

64. Van Oosten, B.; Marquardt, D.; Harroun, T.A. Testing High Concentrations of Membrane Active Antibiotic Chlorhexidine Via Computational Titration and Calorimetry. *J. Phys. Chem. B* **2017**, *121*, 4657–4668. [CrossRef]

65. Wilson, M.A.; Pohorille, A. Mechanism of Unassisted Ion Transport across Membrane Bilayers. *J. Am. Chem. Soc.* **1996**, *118*, 6580–6587. [CrossRef] [PubMed]

66. Shinoda, K.; Shinoda, W. Comparative molecular dynamics study of ether-and ester-linked phospholipid bilayers. *J. Chem. Phys.* **2004**, *121*, 9648. [CrossRef] [PubMed]